UNIVERSITY OF SÃO PAULO

CHEMISTRY INSTITUTE

Graduate Program in Biological Science (Biochemistry)

RAQUEL ARMINDA CARVALHO MACHADO

Role of the CHD7 chromatin remodeler protein in glioblastoma multiforme

Versão corrigida da tese defendida

São Paulo

Data do Depósito na SPG:

26/04/2018

RAQUEL ARMINDA CARVALHO MACHADO

Role of the CHD7 chromatin remodeler protein in glioblastoma multiforme

Dissertation/Thesis presented to the Chemistry Institute of the University of São Paulo to obtain the PhD title in Science (Biochemistry)

Supervisor: Profa. Dra. Mari Cleide Sogayar
Co-Supervisor: Christian Bowman Colin

São Paulo

2018

DEDICATION

To my beloved family and friends who have always supported me along this tough,

and, at the same time, joyful path.

ACKNOWLEDGMENTS

First, I would like to thank my parents, Roberto and Heloísa, to be always the greatest example of honesty, complicity and serenity. Words cannot express how much I respect and love you. Me and my sisters could not have had better people in this life to give always unconditionally support to pursue our dreams. I also thank my fiancé, Pablo, for the incredible support in these last years. I am grateful to God to give me such a special family!

I would like to thank Prof. Dr. Mari Cleide Sogayar for her mentorship and support. Your strength, perseverance, patience and enthusiasm are admirable. You are a huge inspiration for all of us.

Christian, my thesis project was greatly influenced by your previous work on our lab and it was only possible with your help and support. Even in the distant, I have truly benefitted from having you as my mentor. I could not have found better scientist to guide me through this project.

I could not forget to thank my previous supervisor, Prof. Sebastian Jessberger, who has always given me valuable support to my scientific career. Your great words of recommendation to Prof. Michel Weller was critical for me to perform important experiments in collaboration with his team.

To Prof. Michel Weller for the opportunity and support to this project. To Hannah Schneider for your time and patient to be my mentor during my internship. Without you this period would not had been so productive and the *in vivo* experiments would not had been possible. Thanks also to Birthe Lohmann for your help with the animal experiments.

"We should consider every day lost on which we have not danced at least once. And we should call every truth false which was not accompanied by at least one laugh."

Friedrich Nietzsche

ABSTRACT

Machado, R.A.C. **Role of the CHD7 chromatin remodeler protein in glioblastoma multiforme.** 2018. Number of pages (105p). PhD Thesis - Graduate Program in Biochemistry. Chemistry Institute, University of São Paulo, São Paulo.

Chromatin remodeler proteins exert an important function in promoting dynamic modifications in the chromatin architecture, rendering the transcriptional machinery available to the condensed genomic DNA. Due to this central role in regulating gene transcription, deregulation of these molecular machines may lead to severe perturbations in the normal cell functions. Loss-of-function mutations in the *CHD7* gene, a member of the chromodomain helicase DNA-binding (CHD) family, are the major cause of the CHARGE syndrome in humans. The disease is characterized by a variety of congenital anomalies, including malformations of the craniofacial structures, peripheral nervous system, ears, eyes and heart. In this context, several studies have already shown the importance of CHD7 for proper function of the neural stem cells (NSCs). Interestingly, we found that CHD7 mRNA levels are upregulated in gliomas, when compared to normal brain tissue, therefore, we hypothesized that CHD7 might have a role in the pathogenesis of these tumors. To investigate the possible oncogenic role of CHD7 in glioblastoma (GBM), we adopted gain- and loss-of-function approaches in adherent GBM cell lines. Using CRISPR_Cas9 genome editing, we found that *CHD7* deletion suppresses anchorage-independent growth and reduces spheroid invasion in human LN-229 cells. Moreover, deletion of *CHD7* delayed tumor growth and improved overall survival in an orthotopic xenograft glioma mouse model. Conversely, ectopic overexpression of CHD7 in LN-428 and A172 cells was found to increase cell motility and invasiveness *in vitro* and LN-428 tumor growth *in vivo*. RNA-seq analysis showed that alterations of CHD7 expression levels promote changes in several molecular pathways and modulate critical genes associated with cell adhesion and locomotion. However, the mechanisms underlying the effects of CHD7 overexpression in glioma tissue are still not understood. Here, we also generated recombinant plasmid with functional CHD7 promoter activity reported by luciferase assay. This powerful tool should enable future studies to determine the direct targeting relationship between different signal transduction pathways and *CHD7* gene

expression. In summary, our findings indicate that GBM cells expressing a high level of CHD7 may exist and contribute to tumor infiltration and recurrence. Further studies should warrant important clinical-translational implications of our findings for GBM treatment.

RESUMO

Machado, R.A.C **Papel do remodelador de cromatina CHD7 em glioblastoma multiforme**. 2018. Número de páginas do trabalho (105p). Tese Doutorado - Programa de Pós-Graduação em Bioquímica. Instituto de Química, Universidade de São Paulo, São Paulo.

As proteínas remodeladoras de cromatina exercem importante papel, promovendo modificações dinâmicas na arquitetura da cromatina e dando acesso à maquinaria transcricional ao DNA genômico condensado. Devido à esta função central na regulação da transcrição gênica, a desregulação dessas máquinas moleculares pode levar a perturbações graves na função normal das células. Assim, por exemplo, mutações do tipo perda de função no gene *CHD7*, um membro da família "*chromodomain helicase DNA-binding*" (CHD), são a principal causa da síndrome de CHARGE em humanos. A doença é caracterizada por uma variedade de anomalias congênitas, incluindo malformações das estruturas craniofaciais, sistema nervoso periférico, orelhas, olhos e coração. Neste contexto, vários estudos já mostraram a importância da proteína CHD7 para o funcionamento normal de células-tronco neurais (NSCs). Curiosamente, descobrimos que os níveis de mRNA de CHD7 estão mais fortemente expressos em gliomas, quando comparados ao tecido cerebral normal, portanto, nós hipotetizamos que CHD7 poderia ter um papel na patogênese desses tumores. Para investigar o possível papel oncogênico de CHD7 em glioblastoma (GBM), utilizamos enfoques de ganho e perda de função em linhagens celulares aderentes de GBM. Utilizando a técnica de CRISPR_Cas9 para edição do genoma, demonstramos que a deleção do gene *CHD7* suprime o crescimento independente de ancoragem e reduz a invasão de esferóides em células LN-229 humanas de GBM. Além disso, a deleção de *CHD7* reduziu o crescimento do tumor e melhorou a sobrevida em modelo de injeção ortotópica xenográfica em camundongo. Por outro lado, verificou-se que a super-expressão ectópica de CHD7 nas células LN-428 e A172 aumenta não só a motilidade celular e a capacidade de invasão *in vitro*, mas, também, o crescimento do tumor de LN-428 *in vivo*. A análise de RNA-seq mostrou que o nocauteamento da sequência codificadora de *CHD7* e sua super-expressão promovem alterações em diversas vias moleculares, modulando genes críticos

associados à adesão e locomoção celular. No entanto, os mecanismos subjacentes aos efeitos da super-expressão de CHD7 em tecidos de glioma ainda não são compreendidos. Neste trabalho, geramos um plasmídeo recombinante contendo um fragmento da região promotora de CHD7, o qual se mostrou funcional em ensaios de luciferase. Esta ferramenta permitirá que estudos futuros possam identificar a relação direta entre as diferentes vias de transdução de sinal e a expressão do gene *CHD7*. Em resumo, nossos achados indicam que células de GBM expressando um alto nível de CHD7 podem existir e contribuir para a infiltração e recorrência do tumor. Estudos posteriores deverão avaliar as possíveis implicações dos resultados apresentados neste trabalho para a translação clínica no tratamento de pacientes com GBM.

Palavras-chave: CHD7 remodelador de cromatina, glioblastoma, CHD7 ganho e perda de função, motilidade celular, invasividade, atividade promotora de CHD7.

LIST OF ABBREVIATIONS

µg	Micrograms
µL	Microliters
µM	Micromolar
ARF1	ADP-ribosylation factor 1
ASH1	ASH1 Like Histone Lysine Methyltransferase
ATCC	American Type Culture Collection
ATP	Adenosine triphosphate
BLAST	Basic Local Alignment Search Tool
BLAT	BLAST-like Alignment Tool
BMP	Bone Morphogenetic Protein
cDNA	Complementary DNA r
CHARGE	Coloboma, Heart defects, Atresia choanae, Growth retardation, Genital and Ear abnormalities.
CHD	Chromodomain-helicase-DNA-binding family
CHD7	Chromodomain-helicase-DNA-binding protein 7
CNS	Central Nervous System
CRISPR	Clustered Regularly Interspaced Short Palindromic Repeats
Ct	Threshold cycle
DEGs	Differentially expressed genes
DMEM	Dulbecco's Modified Eagle's Medium
DMSO	Dimethyl sulfoxide
DNA	Deoxyribonucleic acid
DNase	Deoxyribonuclease
dNTP	Deoxyribose adenine triphosphate
DTT	Dithiothreitol
EDTA	Ethylenediaminetetraacetic acid
EGF	Epidermal Growth Factor
EGFR	Epidermal Growth Factor Receptor
EMT	Epithelial-Mesenchymal Transition
EV	Empty vector
FCS	Fetal calf serum
FDR	False discovery rate
FGF	Fibroblast Growth Factor
G418	Geneticin
GBM	Glioblastoma Multiforme
GFs	Growth Factors
GO	Gene Ontology
GICs	Glioma-initiating cells
H3K4	Histone H3 on lysine 4
HEPES	4-(2-hydroxyethyl)-1-piperazineethanesulfonic acid
HPRT1	Hypoxanthine Phosphoribosyltransferase 1
HRP	Horseradish Peroxidase
IgG	Immunoglobulin G

Kb	Kilobase
kDa	Kilodalton
KO	Knockout
LFC	Log2 fold change
LTCs	Long-term cell lines
mL	Millilitre
mM	Milimolar
mRNA	Messenger RNA
NBT	Normal brain tissue
NSC	Neural stem cells
PARP1	Poly [ADP-ribose] polymerase 1
PBSA	Phosphate-buffered saline (without cacium and magnesium)
PCR	Polymerase chain reaction
PFA	Paraformaldehyde
pH	Potential of Hydrogen
PIPES	Piperazine-N,N′-bis(2-ethanesulfonic acid)
qRT-PCR	Quantitative Reverse transcription polymerase chain reaction
RNA	Ribonucleic acid
RNA-seq	RNA sequencing
SDS	Sodium dodecyl sulfate
SDS-PAGE	SDS-Polyacrylamide Gel Eletroforesis
SEM	Standard error of the mean
sgRNA	single guide RNA
TBS	Tris-buffered saline
TCGA	The Cancer Genome Atlas
TGF-β1	Transforming growth factor beta 1
TMZ	Temozolomide
TRX	Thioredoxin
WHO	World Health Organization
WT	Wild type

SUMMARY

1. GENERAL INTRODUCTION

1.1. CHD7 protein as a member of the Chromodomain Helicase DNA-binding (CHD) family

Chromatin remodeler proteins are members of a special class of enzymes which modify chromatin structure, playing an essential role in modulating the gene expression pattern during development (Ho and Crabtree, 2010). Encoded by nine highly conserved genes, the CHD proteins are ATP-dependent chromatin remodelers which utilize the energy from ATP hydrolysis to slide nucleosomes, dissociate core histones or relocate the entire histone octamers (Li, Carey and Workman, 2007). Despite the high level of homology, it is becoming clear that ATP-dependent chromatin remodelers are involved in many aspects of cell biology in addition to their traditional role as transcriptional regulation (Ho and Crabtree, 2010). Notably, proteins involved in chromatin remodeling typically act as multiprotein complexes (Vignali et al. 2000), their actual function being associated to their interacting partner(s) (Hall & Georgel 2007). Due to this variability, the specific function of many of these proteins remains elusive.

The two defining sequence motifs of the CHD family are the centrally located ATPase region and the tandem chromo-domains, which mediate chromatin interaction in a variety of different contexts (Hall and Georgel, 2007). CHD1 and CHD7 double chromo-domains were shown to recognize lysine 4-methylated histone H3 tail (H3K4me) (Flanagan *et al.*, 2005; Schnetz *et al.*, 2009), a hallmark of active chromatin (Schneider *et al.*, 2004). In contrast, CHD3 and CHD4 chromo-domains were described to be DNA-binding modules associated with ATP-dependent nucleossome mobilization (Bouazoune *et al.*, 2002). In addition to these two regions, CHD proteins are divided into three

subfamilies, based on the presence of other conserved and less well defined carboxy-terminal domains (Figure 1) (Marfella and Imbalzano, 2007).
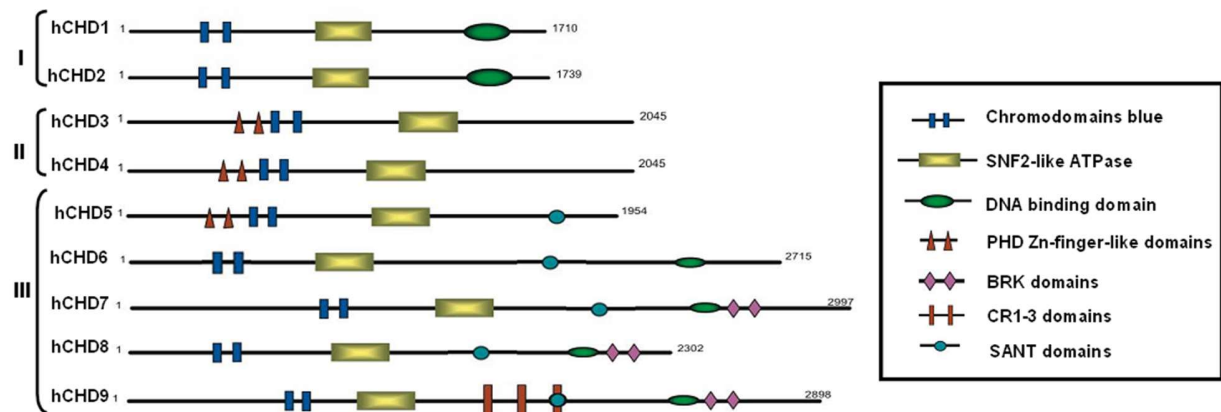
Figure 1: Schematic representation of the structural domains of the human Chromodomain Helicase DNA-binding (CHD) proteins (Modified from Marfella & Imbalzano, 2007).

CHD7 belongs to class III of the chromo-domain proteins, together with four other members. This subfamily is characterized by the presence of the SANT (SWI3, ADA2, N-COR, and TFIIB) domain, which is believed to function as a unique histone-interaction module which couples histone binding to enzyme catalysis (Boyer, Latek and Peterson, 2004). The two BRK domains, shared by CHD7, CHD8 and CHD9, is hypothesized to interact with a component which is unique to higher eukaryotes chromatin, since it is not present in yeast chromatin remodeling factors (Marfella and Imbalzano, 2007).

1.2. The *CHD7* coding gene and its expression

The complexity of gene products which may be produced from the Chd locus, due to alternative splicing events, remains largely unexplored (Marfella and Imbalzano, 2007). The *CHD7* gene comprehends 38 annotated exons in a range of approximately 200 kilobase pairs of genomic sequence (Figure 2A). Even though it is expected that such a

large gene generates several alternative transcripts, very few splice variants associated to *CHD7* have been characterized (Colin *et al.*, 2010).
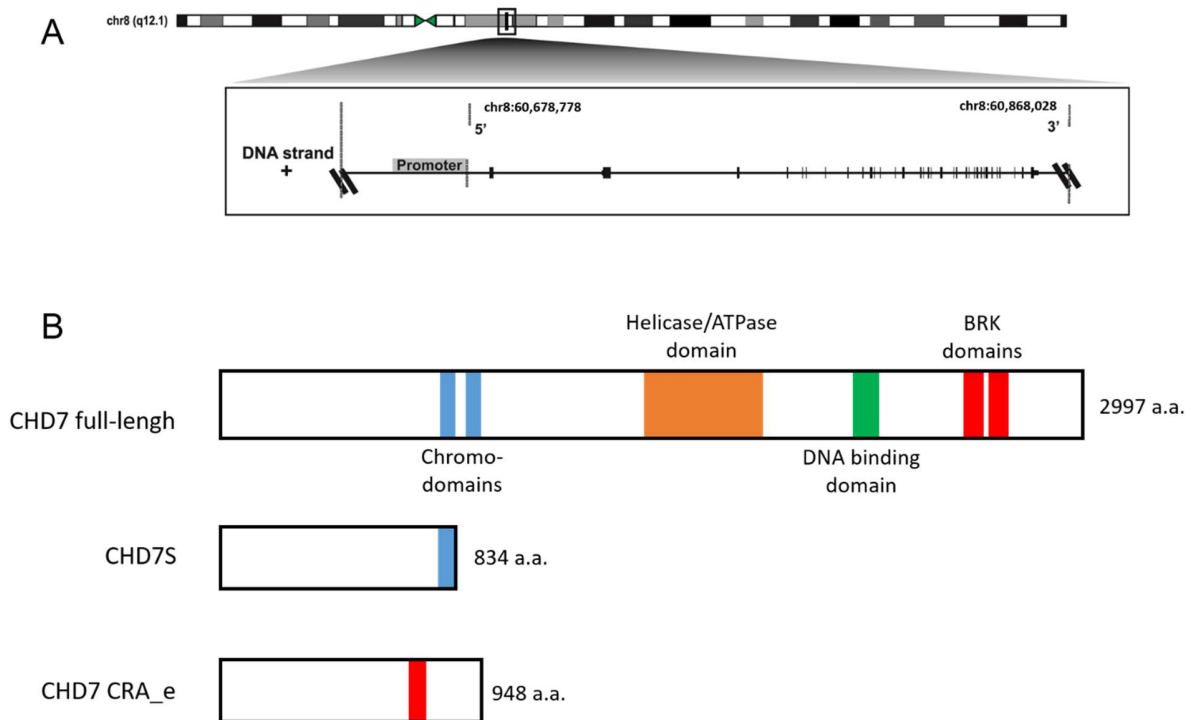
Figure 2: Organization of the human *CHD7* locus. (A) The *CHD7* gene is located at the long arm of the chromosome 8. In detail is represented the exon-intron structure of the canonical *CHD7* gene (accession number NM_017780.2) with a 8,994 bp open reading frame and a transcription start site at exon 2. (B) The full-length transcript encodes a protein of 2,997 aminoacids and molecular mass of 336 KDa. Two other transcript variants encoding different isoforms have been described for this gene (data obtained from Genome Browser - http://genome.ucsc.edu/).

Kita and collaborators characterized a *CHD7* variant transcript which was predicted to encode an approximately 100-kDa protein (designated CHD7S) which contains only the NH2-terminal chromo-domain (Kita, Nishiyama and Nakayama, 2012). The alternative splicing site of this variant occurs at intron 6 and qRT-PCR showed that it is ubiquitously expressed. Our group has also contributed to the splicing annotation of the *CHD7* gene, with the description of a novel transcript and its encoded CHD7 CRA_e protein isoform

(Colin *et al.*, 2010). The putative protein retains only one conserved domain present in the canonical CHD7 protein, the BRK domain, located at its C-terminus. This splice variant was found to be expressed in normal liver and in the DU145 human prostate carcinoma cell line. However, we speculate that alternative splicing variants associated to this gene has been underestimated and is far from being annotated (Figure 2B).

In mice, *Chd7* was shown to be expressed in specific tissues during embryogenesis, including the ear, brain, cranial nerves, olfactory epithelium, olfactory bulb, pituitary, heart, liver, eye, gut, kidney, and craniofacial structures (Layman, Hurd and Martin, 2010). *Chd7* is also expressed in the adult mouse in different cell types, such as the olfactory epithelium, olfactory bulb and in the rostral migratory stream (Layman *et al.*, 2009).

Using mass spectrometry data extracted from different samples, the Human Proteome Project also showed that *CHD7* is expressed in a wide variety of tissues, suggesting its tissue-specific and developmental stage-specific roles (Figure 3).
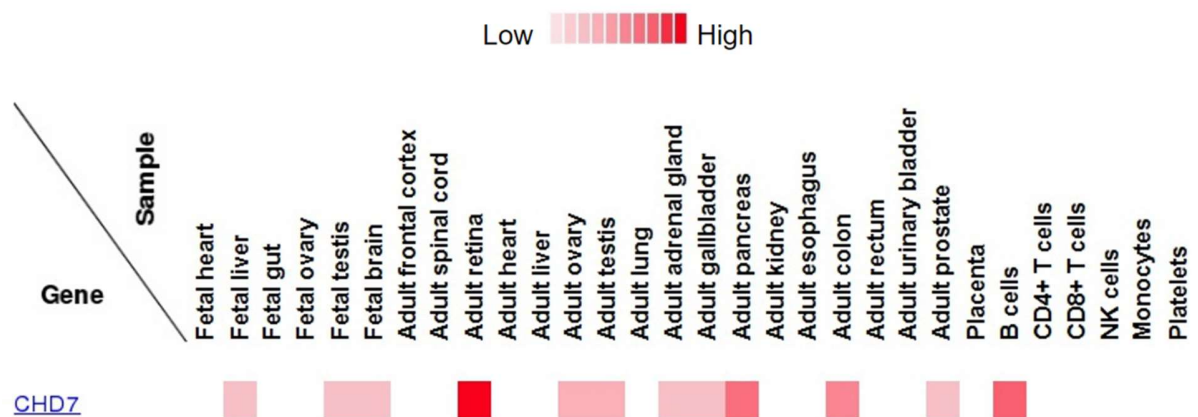
Figure 3: CHD7 protein expression across human samples. Proteomic data set in a graphical view, showing CHD7 expression in 17 adult tissues, 6 primary hematopoietic cells and 7 fetal tissues. Boxes represent expression level accordingly to the intensity of

the red color (graph generated by the Human Proteome Map portal - http://www.humanproteomemap.org/)

1.3. CHD7 biological function

Since mutations in the *CHD7* gene were reported to be a major cause of the CHARGE syndrome in human (Vissers et al. 2004), different studies have provided important insights into the role of CHD7 in regulating gene expression during tissue development and maintenance. Homozygous *Chd7* null mice are embryonic lethal by E11 (Hurd *et al.*, 2007), whereas heterozygous null animal models of mouse, Xenopus and zebrafish recapitulate many of the malformations present in CHARGE patients (Bosman *et al.*, 2005; Bajpai *et al.*, 2010; Layman, Hurd and Martin, 2010; Patten *et al.*, 2012). The disease is characterized by a variety of congenital anomalies, including malformations of the craniofacial structures, peripheral nervous system, ears, eyes and heart (Vissers et al., 2004; Wincent et al., 2008). The estimated population prevalence is around 1:10,000 (Blake *et al.*, 2011) and heterozygosity for nonsense, deletion, or missense *CHD7* mutations are found in over 90% of the patients with clinically typical CHARGE syndrome (Basson and van Ravenswaaij-Arts, 2015). The variability in CHARGE features suggests that CHD7 has a pleiotropic developmental role (Figure 4). Therefore, to identify specific mechanisms of action of CHD7 in pluripotency versus differentiation constitutes a major challenge (Martin, 2010).

CHD7 has also been implicated in Kallmann's syndrome with and without CHARGE syndrome diagnosis (Jongmans *et al.*, 2009). Kallmann syndrome is primarily characterized by idiopathic hypogonadotropic hypogonadism and anosmia (Kim *et al.*, 2008) and is genetically heterogeneous, with mutations reported in a variety of genes

including *KAL1, FGFR1, FGF8, PROKR2, PROK2*, in addition to *CHD7* (Layman, Hurd and Martin, 2010).
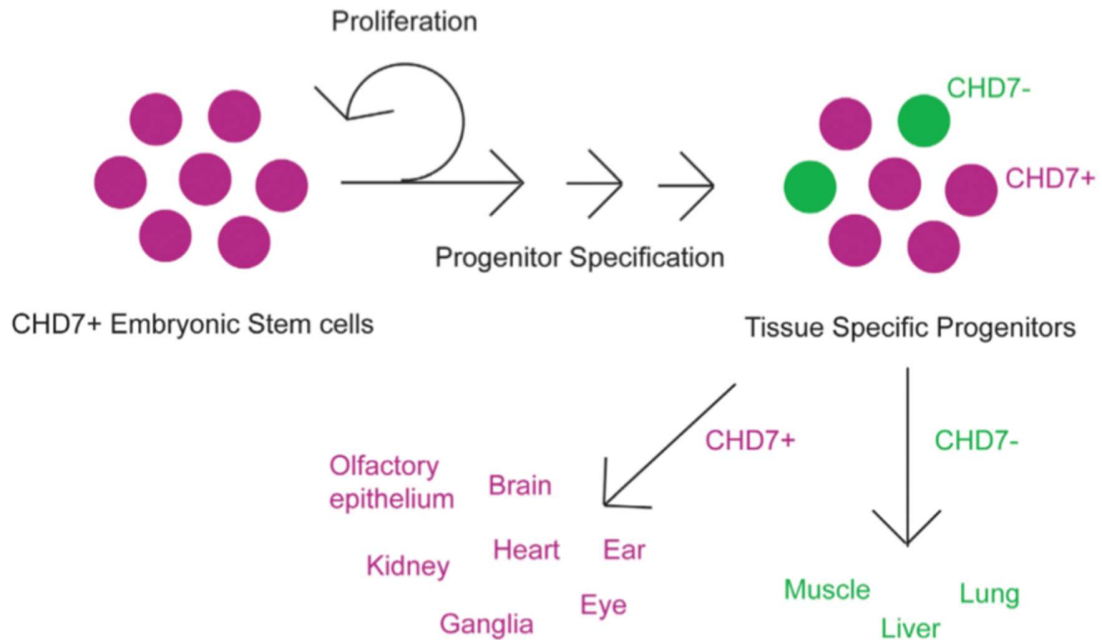
Figure 4: Schematic representation of CHD7 roles in cellular proliferation and/or differentiation. CHD7 is highly expressed in embryonic stem cells, and becomes restricted during development to tissue specific progenitor populations. These progenitors give rise to specific cell types present in the various organs which are affected in CHARGE syndrome (modified from Martin, 2010).

Kismet, the *CHD7* orthologue in *Drosophila*, is required to maintain the spatially restricted patterns of homeotic gene transcription being essential for proper larval segmentation and segment identity (Daubresse *et al.*, 1999). Later, Kis was shown to mediate transcriptional elongation by RNA polymerase II and may help maintain stem cell pluripotency by regulating methylation of histone H3 lysine 27 through recruitment of ASH1 and TRX histone methyltransferases (Srinivasan, Dorighi and Tamkun, 2008).

Functional studies suggest that CHD7 binding sites display features of enhancer elements, predominantly binding to methylated histone H3K4 in a cell type- and stage specific- manner (Heintzman *et al.*, 2007; Schnetz *et al.*, 2009, 2010) (Figure 5). Repression of gene expression has also been reported (Takada *et al.*, 2007; Yu *et al.*, 2013; Schulz *et al.*, 2014). However, it is not clear whether increased expression in CHD7-deficient cells is a secondary effect to down-regulated expression of transcriptional repressors or CHD7 acting as a direct repressor depending on the local DNA context (Basson and van Ravenswaaij-Arts, 2015).

Only in the recent years have different CHD7 interacting partners been described (Takada *et al.*, 2007; Bajpai *et al.*, 2010; Batsukh *et al.*, 2010, 2012; Engelen *et al.*, 2011). Thus, CHD7 was shown to cooperate with PBAF in Xenopus multipotent migratory neural crest cells to regulate crucial transcription factors allowing for transcriptional reprogramming, acquisition of multipotency and migratory potential (Bajpai *et al.*, 2010). Using both proteomic and genomic approaches, CHD7 was also found to be a transcriptional cofactor of the essential neural stem cell (NSC) regulator Sox2 (Engelen *et al.*, 2011), suggesting a role for CHD7 in neurogenesis.
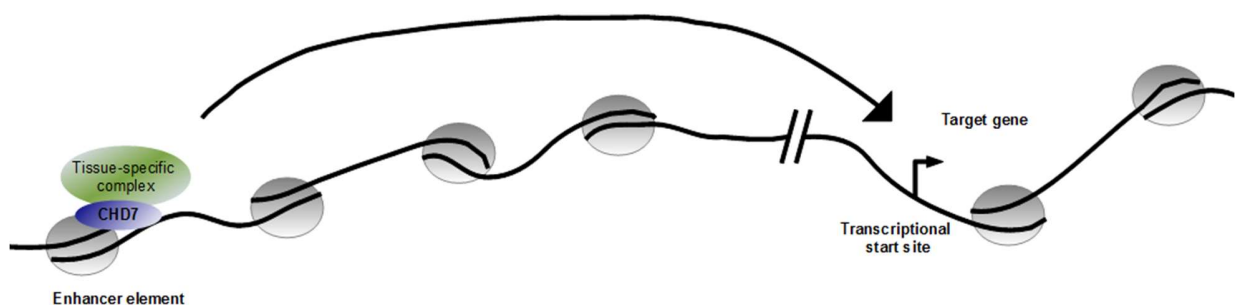
Figure 5: Proposed model for CHD7 mechanism of action. CHD7 interacts with other tissue-specific partner(s) and associates with distal gene enhancers affecting gene expression by chromatin remodeling.

In fact, Feng and colleagues demonstrated that CHD7 is selectively expressed in actively dividing NSCs and progenitors in the adult mouse brain, being critical for activation of the neural differentiation program of those cells (Feng *et al.*, 2013). Another study suggests that CHD7 is actually upregulated in type 1 NSC and that CHD7 expression levels remain high as they exit the quiescent state and progress towards a highly proliferative type 2 ASCL1+ transient amplifying state (Jones *et al.*, 2015). In addition, CHD7 inactivation resulted in loss of stem cells quiescence in the adult hippocampus and in transient increase in cell division, followed by a significant decline in neurogenesis.

Micucci and colleagues showed that CHD7 regulates pro-neuronal gene transcription in NSCs of the subventricular zone, promoting differentiation into neuroblasts, while CHD7-deficient cells display a shift toward glial fates (Micucci *et al.*, 2014). Interestingly, in the oligodendrocyte lineage, CHD7 was shown to cooperate with Sox10 to control the onset of oligodrendrocyte myelination and remyelination after injury, indicating that CHD7 could be a therapeutic target to allow myelin regeneration in patients with CHARGE Syndrome and other demyelinating diseases (He *et al.*, 2016).

Together, these studies demonstrate that altered expression and/or activity of CHD7 in different neural cell types leads to abnormal cell function which may contribute to the highly variable phenotypes observed in CHARGE patients (Figure 6).
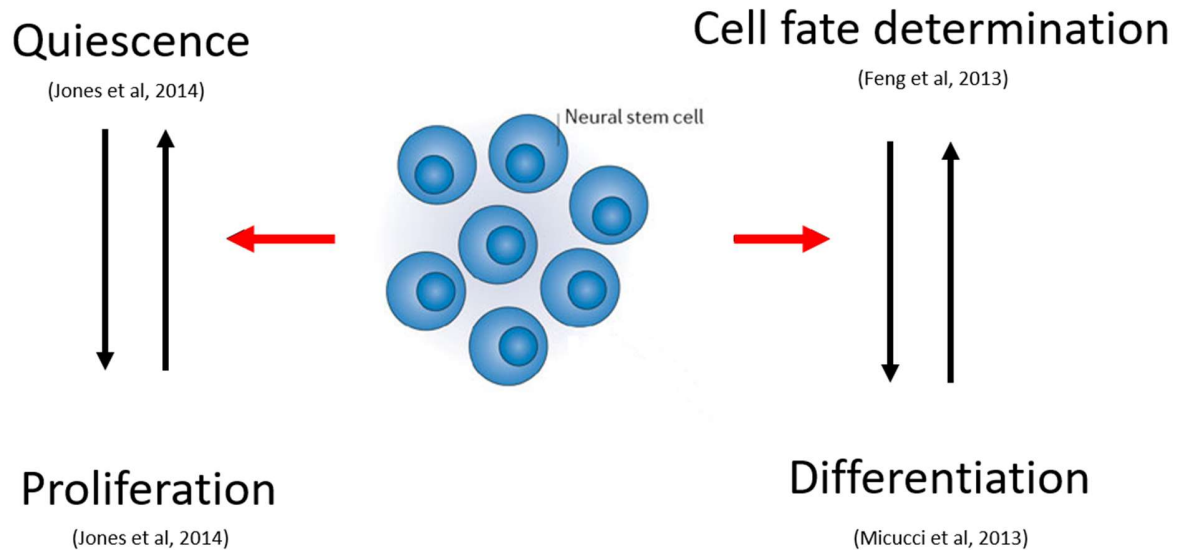
Figure 6: CHD7 is essential for the proper function of NSCs. Different studies have shown that CHD7 plays a major role in the balance between the pool of quiescent/proliferating NSCs, affecting cell fate choices and maturation.

1.4. CHD7 and cancer

A great progress has been achieved in trying to characterize the function of CHD7 in mammalian neurogenesis. On the other hand, the involvement of CHD7 in tumorigenesis has just begun to be described, gaining considerable attention in the last few years.

Initial evidences are available indicating that altered CHD7 expression may be found in different human cancers. Scanlan and colleagues reported that CHD7 (formerly known as KIAA1416) is upregulated in colon cancers (Scanlan *et al.*, 2002) and low CHD7 expression was associated with improved outcome in patients with pancreatic ductal adenocarcinoma treated with adjuvant gemcitabine (Colbert *et al.*, 2014). Additionally,

low CHD7 expression in G4 meduloblastoma subtype, was recently shown to contribute to tumor formation in combination with BMI1 overexpression (Badodi *et al.*, 2017).

Frequent mutations of *CHD7* have been reported in stomach and colon cancers (Kim *et al.*, 2011), as well as in colorectal carcinoma with CpG island methylator phenotype 1 (Tahara *et al.*, 2014). *CHD7* gene rearrangement was also suggested to be a driver mutation identified in small-cell lung cancer (Pleasance *et al.*, 2010).

Consistent with these findings, *in silico* analysis of 32 tumor types, revealed that *CHD7* is the most commonly gained/amplified and mutated gene between the nine CHD members. This study also showed that overexpression of *CHD7* was more prevalent in aggressive subtypes of breast cancer and was significantly correlated with high tumor grade and poor prognosis (Chu *et al.*, 2017).

Supporting the idea that CHD7 functions in a tissue-specific and developmental stage-specific manner, its tumor-suppressive or oncogenic roles has also been shown to be particular to each cancer type. Yet, recent genetic and functional studies have provided significant evidence for the contribution of CHD7 to tumorigenesis in a broad range of cancers. However, the possible involvement of CHD7 in brain tumor development and/or maintenance remains to be investigated (Ohta *et al.*, 2016).

1.5. Glioblastoma

Gliomas are tumors which arise from glial or precursor cells, constituting the most common primary central nervous system (CNS) type of tumor, with an estimated incidence of 6.6 per 100,000 individuals every year in the United States (Ostrom *et al.*, 2017). Glioblastoma (GBM) accounts for nearly half of the total patients diagnosed with gliomas, being the most malignant primary brain tumor variant (Reifenberger *et al.*, 2016). The

World Health Organization (WHO) classifies the tumors of the CNS into different grades, according to their histological subtype, malignant potential, response to treatment, survival and, more recently, molecular landscape (Louis *et al.*, 2016). The diffuse astrocytic and oligodendroglial tumor category comprises several diverse glioma identities (Figure 7). New insights into the molecular subtypes have led to unprecedented discoveries of potential prognostic and predictive markers (Reifenberger *et al.*, 2016).

Tumour classification	WHO grade
Diffuse astrocytic and oligodendroglial tumours	
Diffuse astrocytoma, IDH-mutant • Gemistocytic astrocytoma, IDH-mutant	II
Diffuse astrocytoma, IDH-wild-type*	II
Diffuse astrocytoma, NOS	II
Anaplastic astrocytoma, IDH-mutant	III
Anaplastic astrocytoma, IDH-wild-type*	III
Anaplastic astrocytoma, NOS	III
Glioblastoma, IDH-wild-type • Giant-cell glioblastoma • Gliosarcoma • Epithelioid glioblastoma*	IV
Glioblastoma, IDH-mutant	IV
Glioblastoma, NOS	IV
Diffuse midline glioma, H3-K27M-mutant	IV
Oligodendroglioma, IDH-mutant and 1p/19q-codeleted	II
Oligodendroglioma, NOS	II
Anaplastic oligodendroglioma, IDH-mutant and 1p/19q-codeleted	III
Anaplastic oligodendroglioma, NOS	III
Oligoastrocytoma, NOS‡	II
Anaplastic oligoastrocytoma, NOS‡	III

Figure 7: The 2016 WHO classification of tumors of the CNS. The new classification uses molecular parameters in addition to histology to define many tumor entities. In detail, is highlighted the updated defined diffuse astrocytic and oligodendroglial tumor, including GBM. All diffusely infiltrating gliomas have been grouped together, based not only on their growth pattern and behavior, but, also, more pointedly, on the shared genetic driver mutations in the IDH1 and IDH2 genes (modified from Reifenberger et al. 2016).

The major change incorporated in the new classification of the disease subtypes is the isocitrate dehydrogenase 1 or 2 mutation status (IDHmt) (Figure 8). IDH mutation causes aberrant DNA and histone methylation, eventually leading to widespread hypermethylation of CpG islands, a phenomenon termed the 'glioma CpG-island methylator phenotype' (G-CIMP) (Noushmehr *et al.*, 2011).
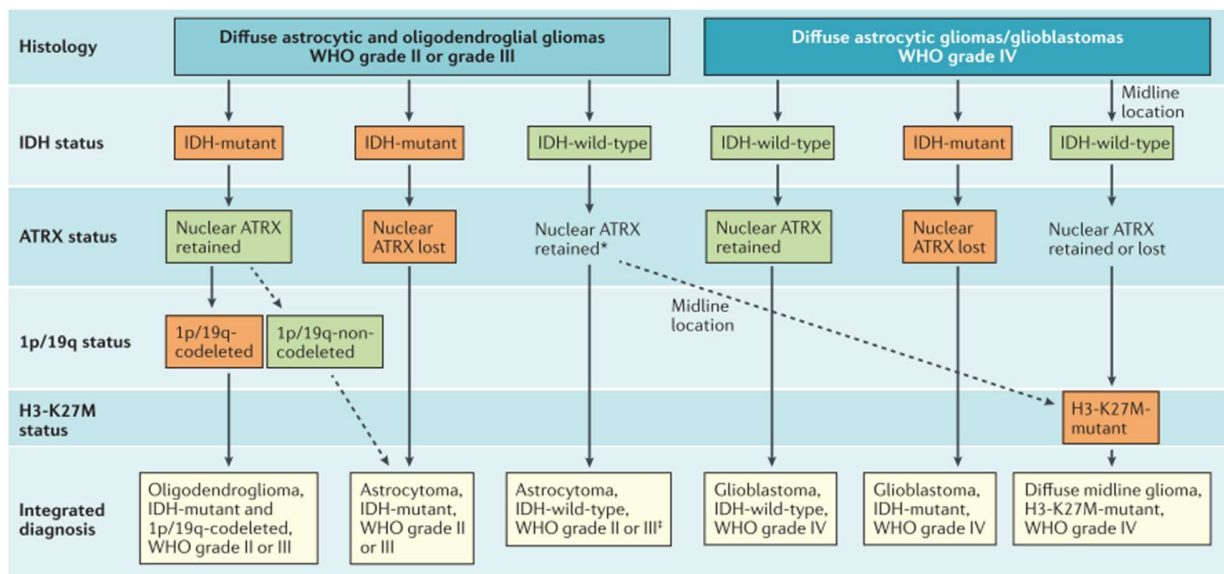
Figure 8: Integrated histological and molecular classification of diffuse gliomas according to the 2016 WHO Classification. In addition to histological typing and grading, diffuse gliomas are evaluated for IDH mutation status and other relevant genetic markers (modified from Reifenberger et al. 2016).

The presence of these mutations distinguishes among gliomas displaying different characteristics and clinical behaviors. IDHmt, 1p/19q co-deleted tumors, with mostly oligodendroglial morphology, are associated with better prognosis; IDHmt, 1p/19q non-co-deleted tumors, with mostly astrocytic histology, are associated with an intermediate outcome; and the wild-type *IDH*, classified mostly as higher WHO grades (III or IV) tumors are associated with poor prognosis (Weller *et al.*, 2015). In GBM, *IDH* mutations are infrequent (<10%) (Yan, Parsons and Jin, 2009) and are usually observed in younger

patients whose tumors may have progressed from lower grade gliomas (Gusyatiner and Hegi, 2017).

Additionally, distinct genetic and epigenetic profiles have been used to stratify GBM subtypes. Based on mRNA genetic profile and genomic data, GBM has been classified as: classical, neural, proneural and mesenchymal (Verhaak *et al.*, 2010). The mesenchymal expression signature has been linked with radio-resistance and low survival rate (Bhat *et al.*, 2013), whereas the proneural signature has been reported to be benefitted by anti-angiogenic treatment in patients with wild-type IDH GBM (Sandmann *et al.*, 2015). However, given the highly heterogeneous nature of these tumors, a more complex clinical classification has been suggested (Figure 9).

Besides different genetic aberrations, another prominent epigenetic marker which is routinely tested for GBM diagnosis, is the promoter methylation status of the DNA repair gene O6-methylguanine DNA methyltransferase (*MGMT*) (Thon, Kreth and Kreth, 2013). MGMT removes alkyl groups from the O6 position of guanine, an important site of DNA alkylation. Therefore, gene silencing mediated by promoter methylation, is known to be associated with longer overall survival of patients receiving alkylating chemotherapy with carmustine or temozolomide, in addition to radiotherapy (Hegi *et al.*, 2005).

Still, the poor prognosis of GBM patients is associated to multiple characteristics, including constitutive or acquired resistance to cytotoxic therapy, deep infiltration of tumor cells into the normal brain parenchyma, angiogenesis and establishment of an immune-suppresive environment, thereby reducing the immune surveillance and allowing escape from the immune system (Tabatabai and Weller, 2011). In this context, identifying the molecular mechanisms regulating the maintenance and developmental steps of the tumor

mass is critical to identify the cellular pathways and gene networks associated with this type of cancer.

Glioblastoma group	PXA-like	LGG-like	H3-K27[‡]	H3-G34	IDH-mutant	RTK I	RTK II (classic)	Mesenchymal
Genetic aberrations	• BRAF-V600E mutation • CDKN2A/B deletion	• BRAF-V600E mutation* • Rare copy-number aberrations / • H3-K27M mutation • TP53 or PPMD1 mutation • PDGFRA amplification • ACVR1 mutation[§] • ATRX mutation[‖]		• H3F3A-G34 mutation • ATRX mutation • DAXX amplification • TP53 mutation • DNA hypomethylation	• IDH1/IDH2 mutation • G-CIMP • TP53 mutation • ATRX mutation • CDKN2A/B deletion • Chr. 10q loss	• PDGFRA amplification • TERT-promoter mutation • Chr. 7 gain • Chr. 10 loss	• EGFR amplification • CDKN2A/B deletion • PTEN mutation • TERT-promoter mutation • Chr. 7 gain • Chr. 10 loss	• TERT-promoter mutation • Chr. 7 gain • Chr. 10 loss
MGMT-promoter methylated (%)	~15	20–25	<5	~75	~90	~40	~40	~40
Age group	Children (predominantly)			Children–young adults	Young adults		Older adults	
Location	Predominantly hemispheric		Midline	Predominantly hemispheric				
Median OS (months)	>36		~12	~24	~30	~12–14		

Figure 9: Molecular subgroups of glioblastoma, as defined by distinct genetic and epigenetic profiles. Several markers have been used to improve the diagnostic accuracy and guide decision making for individualized therapies (modified from Reifenberger et al. 2016).

Previous experiments performed in our laboratory by Dr. Christian Colin during his PhD thesis (Colin, 2006)[1] suggest that the *CHD7* gene is highly expressed, at the mRNA level, in glioma cell lines, as well as in patient samples of different malignancy grades, when compared to samples of normal brain. Given this evidence, we hypothesized that CHD7 plays an important role in human brain tumor cells. Here, we aim to validate these preliminary results and to perform functional analysis in order to better characterize the impact of this chromatin remodeler in brain tumor cells.

---

[1] Colin C. (2006) Identificação de genes diferencialmente expressos em linhagens de glioma de rato e sua potencialidade como novo salvos terapeuticos para gliomas humanos. PhD thesis. University of São Paulo.Instituto de Química. Supervised by Prof. Mari Cleide Sogayar.

GBM is a complicated pathological process characterized by highly intra- and inter-individual heterogeneity (Inda, Bonavia and Seoane, 2014). Successful future treatment will most likely include multimodal therapy. Therefore, it is of great interest to evaluate whether CHD7 regulates specific signaling pathways during tumorigenesis and, in this case, whether those pathways may be manipulated by molecular intervention. No information is yet available on the potential roles of CHD7 in GBM.

In Chapter 1, I describe our results from gain and loss-of function experiments, *in vitro* and *in vivo*, using GBM cell lines.

In Chapter 2, I detail the preliminary results on analysis of the *CHD7* promoter. In this part of the work, we aimed to clone and characterize the *CHD7* promoter region to test possible signaling pathways, which might be involved in the regulation of the gene expression in GBM cells.

Our study is not only relevant to understand the implication of CHD7 in brain tumor, but it may also provide important insights into how CHD7 functions in specific tissues and cell types.

2. AIMS

2.1. General Aim

To investigate the role of the chromodomain helicase DNA-binding protein 7 in human glioblastoma cells.

2.2. Specific Aims

- To characterize *CHD7* gene expression at both the mRNA and protein levels in human brain tumor cell lines and in human glioma patient samples of different malignancy grades.

- To assess the function of CHD7 in two different GBM cell lines by overexpression and down-regulation of this gene.

- To analyze possible CHD7 downstream effectors by RNA-seq of the modified cell lines.

- To compare brain tumor development of mice stereotactically injected with GBM cell lines in which *CHD7* has been deleted or overexpressed.

- To identify possible mechanisms which may regulate CHD7 expression in GBM cells.

Chapter 1: Functional impact of CHD7 chromatin remodeler protein in glioblastoma

Abstract

Chromatin remodeler proteins have emerged as critical regulators of chromatin structure, playing critical roles during development. Since CHD7 mutations were found to be the major cause of the CHARGE syndrome in humans, this gene has been further studied from the functional point of view. However, no reports are yet available demonstrating a role for CHD7 in the pathogenesis of glioblastoma (GBM). To investigate the possible oncogenic role for CHD7, we analyzed mRNA expression and protein levels in glioma tissues. TCGA interrogation and qRT-PCR showed that CHD7 is upregulated in samples of glioma tumor patients, being predominantly expressed in the proneural GBM subtype. Using CRISPR_Cas9 genome editing, we found that CHD7 deletion suppresses anchorage-independent growth and reduces spheroid invasion in human LN-229 GBM cells. Moreover, CHD7 knockout delayed tumor growth and improved overall survival in an orthotopic xenograft glioma mouse model. Conversely, ectopic overexpression (OE) of CHD7 was found to increase cell motility and invasiveness capacity in LN-428 and A172 cells. Additionally, LN-428 OE promoted tumor growth *in vivo*. RNA-seq analysis of the modified cell lines showed that alterations in CHD7 expression levels promote changes in several molecular pathways, with significant enrichment for GO terms associated with "cell adhesion", "locomotion" and "cell migration". Our findings indicate that GBM cells overexpressing CHD7 are naturally present in these tumors and may contribute to

infiltration and recurrence. Further studies may warrant important clinical-translational implications for GBM treatment.

Introduction

The chromatin remodeler proteins are members of a special class of enzymes which modify the chromatin structure, thereby playing an essential role in modulating gene expression patterns during development (Ho and Crabtree, 2010). Encoded by nine highly conserved genes, the CHD proteins are ATP-dependent chromatin remodelers which utilize the energy from ATP hydrolysis to slide nucleosomes, dissociate core histones and/or relocate the entire histone octamers (Li, Carey and Workman, 2007). Since mutations of the CHD7 gene were reported to be a major cause of the CHARGE syndrome in humans (Vissers L M *et al.*, 2004), significant progress has been made in understanding the role of this protein in regulating gene expression during tissue development and maintenance. Homozygous *Chd7* null mice are embryonic lethal by E11 (Hurd *et al.*, 2007), whereas heterozygous null animal models of mouse, Xenopus and zebrafish recapitulate many of the malformations present in CHARGE patients (Bosman *et al.*, 2005; Bajpai *et al.*, 2010; Layman, Hurd and Martin, 2010; Patten *et al.*, 2012).

Abnormal activity of chromatin remodeler proteins may result in a multitude of deregulated cellular programs, affecting cell survival, cell death, or malignant transformation, in different ways, depending on the cell type (Yaniv, 2014). Frequent mutations of *CHD7* and/or altered gene expression have been reported in different human cancers (Kim *et al.*, 2011; Tahara *et al.*, 2014; Badodi *et al.*, 2017; Chu *et al.*, 2017). Thus, *CHD7* gene rearrangement was suggested to be a driver mutation identified in small-cell lung cancer (Pleasance *et al.*, 2010) and low CHD7 expression was associated with

improved outcome in pancreatic ductal adenocarcinoma patients treated with adjuvant gemcitabine (Colbert *et al.*, 2014). However, the functional contribution of the chromatin remodeler CHD7 to malignant brain tumor biology remains unclear.

Functional studies showed that CHD7 binding sites display features of enhancer elements, predominantly binding to methylated histone H3K4 in a cell type- and stage-specific manner (Heintzman *et al.*, 2007; Schnetz *et al.*, 2009, 2010). Using both proteomic and genomic approaches, CHD7 was also found to be a transcriptional cofactor of the essential neural stem cell (NSC) regulator Sox2 (Engelen *et al.*, 2011), suggesting a role for CHD7 in neurogenesis. In fact, CHD7 was shown to be critical for activation of the neural differentiation program of NSC and progenitors in the adult mouse brain (Feng *et al.*, 2013). Moreover, CHD7 inactivation resulted in loss of stem cells quiescence in the adult hippocampus and a transient increase in cell division, followed by a significant decline in neurogenesis (Jones *et al.*, 2015). Given the pivotal role of CHD7 for NSC function, the aim of this study was to investigate the possible involvement of CHD7 in GBM tumorigenesis.

Material and Methods

Gene expression and patient survival analysis using The Cancer Genome Atlas (TCGA) dataset

Genetic alteration analysis in 33 human tumor types in provisional TCGA studies were carried out using the cBio Cancer Genomics Portal (http://www.cbioportal.org). Overall expression analysis within the TCGA database (http://cancergenome.nih.gov) was undertaken using the single gene expression analysis module of the R2: microarray analysis and visualization platform (http://www.r2.amc.nl) CHD7 expression clusters were

generated across 284 samples (MAS5.0 - u133p2 dataset) and analyzed with k-means algorithm and 2Log transformation of gene expression. Analysis of CHD7 expression relative to the GBM subtype (Verhaak *et al.*, 2010) was carried out using 435 samples classified into these groups within the subtype track mode and z-score transformation.

Kaplan-Meier survival curves and log-rank tests were constructed to evaluate eventual differences in the overall survival time of predicted good or poor prognosis groups determined by CHD7 gene expression. Patients were classified into the good and poor prognosis groups (low and high risk, respectively) using the median cutoff of the CHD7 expression value.

To better evaluate the association between CHD7 gene expression and survival outcome, we used a Cox regression model to minimize the influence of clinical variables. Patient data such as age at diagnosis, gender, chemotherapy, and tumor subtype were included as covariates. We only considered individuals presenting all information regarding these covariates (i.e., 446 individuals out of 558). For survival probability, the gene expression data were normalized to zero mean and unit variance. All computations were carried out in the R statistical environment (https://www.r-project.org/). For Cox regressions we used the R package survival.

Patient samples

Brain tissue samples from temporal lobectomy epileptic patients and from resected astrocytoma specimens were macro-dissected and immediately snap-frozen in liquid nitrogen, as previously described (Oba-Shinjo *et al.*, 2005). The specimens were categorized according to the 2007 WHO classification (Louis *et al.*, 2007). This project has the approval of the Ethical Committee of the University of São Paulo School of

Medicine (CAPPesq, 691/05), and informed consents were obtained from all patients. The CD133^{pos} and CD133^{neg} cells were isolated from freshly resected human GBM tumor tissue (ZH-496, ZH-525, ZH-445, ZH-464, ZH-456 and ZH-419) after written informed consent of the patients and approval by the Institutional Review Board of the University Hospital Zurich. Briefly, tumor tissues were dissociated with 10 mg/mL collagenase/dispase (Roche, Basel, Switzerland) and gentle rotation in MACS C-tubes (Miltenyi biotech, Cologne, Germany). Discrimination of cell populations was achieved using MicroBeads conjugated to the mouse anti-human CD133/1 epitope antibody (clone AC133) (Miltenyi Biotec), followed by depletion of CD45+ cells utilizing MACS LS columns (Miltenyi Biotec). Cells were immediately lysed after magnetic sorting and total RNA for qRT-PCR was prepared using the NucleoSpin System (Macherey-Nagel) and complementary DNA transcribed using SuperScript® II reverse transcriptase (Invitrogen). Differential CD133 expression was confirmed by analyzing CD133 mRNA levels in both cell populations, using Arf1 transcript levels as a house-keeping reference for relative quantification.

Cell lines and reagents

The human A172, U87MG and T98G long-term cell lines (LTCs) were purchased from the American Type Culture Collection. The LN-18, LNT-229, LN-308, LN-319 and LN- 428 cell lines were kindly provided by Dr. N. de Tribolet (Lausanne, Switzerland). LTCs were maintained in Dulbecco's modified Eagle's medium (DMEM, Invitrogen, Life Technologies, Carlsbad, CA), containing 10% fetal calf serum (FCS) (VWR Lonza, Leighton Buzzard, UK) and supplemented with 2 mM glutamine (Invitrogen, Life Technologies), in a 5% CO_2 incubator at 37°C. The S-24, T-269, T-325, ZH-161 and ZH-

305 glioma-initiating cells (GICs) were generated and cultured as described (Weiler *et al.*, 2013). Briefly, GICs were maintained as sphere cultures in Neurobasal A medium (Invitrogen, Life Technologies) supplemented with EGF (10 ng/mL), FGF (10 ng/mL) (Peprotech, Rocky Hill, NJ), heparin (31.5 U/mL) (Sigma Aldrich, St. Louis, MO), 1% Glutamax (Invitrogen, Life Technologies) and 2% B27 (Invitrogen, Life Technologies).

Quantitative Real time PCR (qRT-PCR)

For mRNA expression analysis, total RNA was transcribed into cDNA using the iScript cDNA Synthesis Kit (Bio-Rad Laboratories, Hercules, CA). cDNA amplification was monitored using SYBRGreen chemistry and the ViiA™ 7 Real-Time PCR System (Applied Biosystems, Foster City, CA). Conditions for PCR reactions were: 40 cycles of 95°C/15 sec, 60°C/1 min, using the specific primers listed in below (Table 1).

Table 1: Primer sequences used in qRT-PCR.

Gene	Forward (5' to 3')	Reverse (5' to 3')
Arf1	GACCACGATCCTCTACAAGC	TCCCACACAGTGAAGCTGATG
CD133	TGGATGCAGAACTTGACAACGT	ATACCTGCTACGACAGTCGTGGT
HPRT1	TGAGGATTTGGAAAGGGTGT	GAGCACACAGAGGGCTACAA
CHD7	CAGAACACCCCGCAGAAAGTGCCTGT	AGCATTCGGTCCACTAACCTGAGTCAT
CADM2	CCCTCCCTTACCACTGCAA	GCCAGCCAAAGCATTAGGA
RIMS1	CAGCCGAGCCGAGAGTCTA	CAGCCGAGCCGAGAGTCTA
COL3A	AAAACCCCGCTAGAAACTGC	GCATCCAATTTGCATCCTTG
KCNK13	CTTCCTCCGCCACTACGAG	TCCTACTGTCGCCGGAGTT
BMP5	TGTGCAGAAACAGGGGATG	TTTGTTGGCTGCTCTCACG
XIRP1	GTCAGTGCAACTCGCTGGA	GATGCTGCTGCTGCTGAAC
CHI3L1	TTCCGAGGTCAGGAGGATG	CACCAGCTTACTGGCAGGAG
CNTN1	AGCAACCCTGAGCTTTGGA	GGGGGTCACAGAGAAGCAC
PAK3	ATCGCACCAAGACCAGAGC	TTCAGCAGAGGGTGGTGTG
NCAM2	TCGTATGTGATGCGGAAGG	ATGCTGCCCTTTGACTTCG
AIF1L	GAGGTGACAGGAGGGGTCA	TGCTCTCGTTGGCTTTTCC
ADAM33	CTGGCCTGGTGTTGCTACC	CCAACTCCATGGGGTGAAC
MYO10	TATGGCTCGACGCTGTTTG	CTTCCCTCTCCACGCTTGT

ZNF502	TCTGCATCAGTGGGAAACAA	TGGGTAAGGGATGAGCTCTG
SIRPA	CATCCACAGCACAGCCAAG	TCCAAGGTGGGTGGAACTC
MAGED4B	CAACAGCAACCCACCTGAG	TTCTGATTCTGGGCGATGA
WNT10B	CTGGTGAGCTGTGGCTGTG	TTGTGGATTCGCATTCGTG
KCNA2	GTGGGGTGACCTTCCACAC	GCTGGGACAGGCAAAGAAC
GCSAML	TCCTCCCTGAGCTCCAATG	ATCATGCTCATGGGTGCAG
CADM3	TACCTCTACGCCCCACGAG	GCAGTTCGCACAGGCATAG
ATP1A3	GCCTTCCAGAATGCCTACC	TCACAGTCGAAGGCAAAGC
NKX2-2	CGAGGGCCTTCAGTACTCC	GTCATTGTCCGGTGACTCG
VIT	CATGGCTGCCCATCTGAAG	GGGGTGAGTGGCAATGACT
PLPPR4	GCGGGCTAACACGGATAAC	TTCCCCACAGCATACAAGC
SATB1	GTGACAGATGCCCCTGATG	GTTCGGGAGGCAAGTCTTC
SFMBT2	CCCCAGAGAGGACACGAAG	TCCTCCTCCTCCTGTTTCG
PRDM9	CCAGTGTCCCCTTCTGGAG	GGCTCGCTGACCTCTTTGT
MAF	ATCCGGCTGAAGCAGAAGA	TGAGGTGGTCGACTTGCTG
FOXO1	AGCGTGCCCTACTTCAAGG	TGGATTGAGCATCCACCAA
FOXD3	TGCGAGTTCATCAGCAACC	GGGGATCTTGACGAAGCAG
CCND2	TGTTCCTGGCCTCCAAACT	GTTCCCACTCCAGCAGCTC
CXCL12	ATGCCGATTCTTCGAAAGC	TGTTCTTCAGCCGGGCTAC
NPY4R	TCCCACTGGGCTTCATCTT	CACCAGCACCACATTGACC
CCBE1	CTCTGCTCCCCAACAATGC	TCCCTTTGGTCCTGGTGAG
FBN1	CCTTACCTGGCGGAAATCA	CTGGAGCCACAGGAAGGAG
HTRA1	ACGGTGCCACTTACGAAGC	GATGGCGACCACGAACTCT
PBX1	CAGCAACCCTTACCCCAGT	CCGGATTCGCTTATTTCCA
EMILIN2	CTGTGCCTGGAACCAGATG	AGGACAGCACCTCCATTCC
NRCAM	CTCCAGAAGGCAATGCAAG	TGGGTAGCATTCCATCTTCC
CEACAM1	CGTCACCCAGAATGACACAG	TCCTCCACAGGGTTGGAGT

CRISPR/Cas9 knockout clones

CHD7 knockout clones were generated according to the protocol described in Ran and colleagues (Ran *et al.*, 2013). Briefly, small guide RNAs (sgRNAs) were designed, using an online CRISPR Design Tool (http://tools.genome-engineering.org) and then cloned (Table 2) into the pSpCas9(BB)-2A-Puro plasmid (Addgene, Massachusetts, US). Lipofectamine 2000 (Life Technologies) was used for transient co-transfection of two guide RNAs at a 1:1 ratio. Cells were selected with Puromycin (Life Technologies) for 48h

and genomic DNA from cell populations was extracted using QIAamp DNA Kit (Qiagen, Venlo, Netherlands) for detection of the CHD7 deletion by PCR (Table 3). Transfected cells were then isolated by single cell sorting in 96 well plates. Cell clones were further expanded for nuclear protein extraction and tested by immunoblotting.

Table 2: Primer sequences used to clone the sgRNAs targeting CHD7.

Guide	Forward (5' to 3')	Reverse (5' to 3')
sgCHD7-5'	CACCGACACCCTTACTAACGTCAGG	AAACCCTGACGTTAGTAAGGGTGTC
sgCHD7-3'	CACCGGTTCTTCGCATCGCCTCCGG	AAACCCGGAGGCGATGCGAAGAACC

Table 3: Primer sequences used in genomic PCR to detect the CHD7 deletion.

Primer	5' to 3'
Forward	CTATTGAAGATACGTGTGTACCTCTGCCCTTATAGT
Reverse	ACTGCACAATACTTAATGACCAAGATACCTTTTGAC

CDH7 Overexpression

A 9Kb cDNA, comprising the ORF of the human *CHD7* gene (GenBank Accession #NM_017780.3) was amplified from the OVCAR8 human ovarian cancer cell line, using long RT-PCR and standard molecular cloning techniques. Briefly, total RNA was purified from OVCAR8 cells (RNeasy RNA Purification Kit, Qiagen) and 1 μg RNA was used as the template for reverse transcription with SuperScriptIII® (Life Technologies), according to the manufacturer's instructions. PCRs were carried out using Phusion® High Fidelity DNA Polymerase (New England Biolabs, Ipswich, MA). Long PCR primers were designed to amplify the CHD7 coding sequence as three overlapping fragments flanking the unique *AflII* and *MfeI* restriction sites of the CHD7 cDNA. A Kozak consensus sequence was also added, in juxtaposition to the initial ATG codon, in order to boost CHD7 expression levels in mammalian cells. The full-length cDNA was assembled using a combination of TOPO®

cloning and Gibson® cloning. The cloned sequence was thoroughly verified by Sanger sequencing of both strands. The final full-length 9Kb CHD7 fragment was cloned into the pCXN2-DEST expression vector (Hitoshi, Ken-ichi and Jun-ichi, 1991) using the Gateway®-assisted sub-cloning.

LN-428 and A172 cells were transfected with the pCXN2_CHD7 construct or with the empty vector using Lipofectamine 2000 (Life Technologies). Transfected cells were selected with 750 μg/mL and 200 μg/mL of Geneticin G418 Sulfate (Gibco, Thermo Scientific).

Immunohistochemistry of patient samples

For immunohistochemistry, de-paraffinized and rehydrated tumor tissue sections were boiled in EDTA buffer, pre-treated with 1% H_2O_2 and blocked in blocking solution (Candor Biosciences, Germany). Sections were incubated with primary anti-CHD7 antibodies (ab31824, 1/200) (Abcam, Cambridge, UK) at 4°C overnight. The secondary antibody conjugated to diaminobenzidine was obtained from Dako and used according to standard procedures.

Immunoblotting and immunofluorescence

Total cellular extracts were obtained by lysing cells with RIPA buffer (150 mM, NaCl, 1% NP-40, 0.5% SDS, 50 mM Tris pH 8.2, 1 mM EDTA). Cytoplasm and nuclear protein lysates were prepared with the NE-PER Nuclear and Cytoplasmic Extraction kit (Thermo Scientific). Proteins (30 μg per lane) were resolved on a 3 to 7% Tris-acetate gel (Life Technologies) and transferred to a nitrocellulose membrane (Life Technologies). After blocking with 0.5% non-fat milk in TBS containing 0.5% Tween 20 (TBST), the membrane was incubated in blocking solution overnight at 4°C with the following primary antibodies:

anti-β-actin (csc-1616, 1/2,000) (Santa Cruz Biotechnology, Dallas, TX), anti-CHD7 (ASB453, 1/500) (Millipore, Billerica HQ, MA), anti-LaminB1 (Ab 16048, 1/2,000) (Abcam, Cambridge, UK), anti-PARP (556494, 1/2,000) (BD Biosciences, Franklin Lakes, NJ). After washing and incubation with the HRP-conjugated secondary antibody (1/5,000, Sigma Aldrich), the protein bands were detected with enhanced chemoluminescence (ECL, Thermo Scientific).

For immunofluorescence, cells were washed with PHEM buffer (2 mM HEPES, 10 mM EGTA, 2 mM $MgCl_2$, 60 mM PIPES – pH 6.9) and fixed for 30 min with cold PFA 4%. Cells were permeabilized with 0.1% Triton X-100 for 10 min, blocked with 3% goat serum (DY005, R&D Systems, Minneapolis, US) for 1h, and then incubated with rabbit anti-CHD7 (ab 176807, 1:1000) (Abcam) or Tubulin (T5168, 1/2000) (Sigma Aldrich) overnight at 4°C. After PHEM washing (3x), the cells were incubated with the fluorescent dye, namely: AlexaFluor 594 goat anti-rabbit IgG (A11012, 1/1000) or goat anti-mouse IgG (A21203, 1/1000) (Thermo Fisher Scientific, Waltham, MA) and Alexa fluor 488-Phalloidin (A12379, 1/1,000) (Thermo Fisher Scientific) at room temperature for 1h. Coverslips were mounted using VECTASHIELD Anti-fade Mounting Medium with DAPI (H-1200, Vector Laboratories, CA) and images were acquired with a confocal Zeiss LSM 780-NLO microscope.

Anchorage-independent clonal growth in semi-solid medium

Anchorage-independent clonal growth was assessed using the soft-agar assay, as previously described (Trombetta-Lima *et al.*, 2015). Briefly, $1x10^4$ cells/well were seeded on top of the 0.6% agarose (Fisher Scientific, Leicestershire, UK) solution in 10% FCS-DMEM in a 24 well plate. Cells were plated onto the 0.6% agarose layer and allowed to

stand for about 10 min before the addition of 500 µL of melted 0.3% agarose in 10% FCS-DMEM. Finally, 500 µL of liquid 10% FCS-DMEM were added. This liquid medium was renewed every two days and cells were allowed to grow for about 14 days, forming large colonies, which were then quantified using the AMG EVOS FL Inverted Microscope.

Migration and Invasion assays

Cells were washed in phosphate buffered saline (PBSA) and ressuspended in serum-free medium. A cell suspension containing 50,000 cells was added to the upper well of transwell migration inserts (pore size: 8 µm, BD Biosciences) or to BD BioCoatTM MatrigelTM invasion chambers (pore size: 8 µm, BD Biosciences). In the lower well, 700 µL of complete medium were used as chemo-attractant. The cells were maintained for 16h at 37°C and 5% CO_2, followed by fixation in cold methanol for 10min and staining with Mayer's alum haematoxylin for 20 min. Inserts were mounted in glass slides and six fields per sample were counted, with duplicates for each treatment.

For the spheroid invasion assays, LN-229 and A172 spheroids were generated by incubating 1,000 cells for 72h in 96-well plates pre-coated with 1% Noble Agar (Difco Laboratories, Detroid, US). Spheroids with a diameter of 200 µm were embedded into a collagen matrix containing collagen type I (Invitrogen), 10% FCS and 10% $NaHCO_3$ in a 96-well plate. Sprouting of spheroids was monitored daily by photographs. For quantitation, the area covered by sprouting cells was assessed using the ImageJ 1.40g software (NIH). For measurement of the invasion area, the area covered by the spheroid at Day 0 was subtracted from the overall area, which was covered on subsequent days.

For wound-healing scratch assay, $2x10^5$ LN-428 cells were plated in 24 well plates in triplicates. On the following day, the cell layers were scratched using a 200 µl sterile

pipette tip. The wound location was marked and images of the same field were captured to record the wound width at 0, 8 and 24 h.

RNA-seq experiment and data analysis

The next-generation sequencing (NGS) libraries were prepared according to Illumina TruSeq Stranded mRNA LT protocol. Quality control of the amplified products before and after fragmentation and labeling was analyzed using the Agilent Bioanalyzer. Samples were sequenced on Illumina NextSeq 550 (2 x 76 bp paired-end sequencing) operated by the Biomedical Institute Facility Center CEFAP of the University of São Paulo (USP). All calculations were carried out using Linux Scripts and R-Studio IDE (R language). To map and quantify the transcripts, we used the Subread (Liao, Smyth and Shi, 2013) aligner package. Samples were then normalized and the Differentially Expressed Genes (DEGs) were calculated using EdgeR (Robinson, McCarthy and Smyth, 2009) package. The mean transcription counts were determined through the biological coefficient of variation, using a negative binomial distribution, resulting in counts per million (CPM) estimation. DEG between Overexpressed (case) and Empty Vector (control) samples; and Knockout (case) and Wild Type (control) samples were calculated. DEGs are defined as genes with absolute value of log2 fold change (LFC) > 1, p-value < .05 and false discovery rate (FDR) < .05 between case and control. The levels of gene expression of selected targets were validated by qRT-PCR. Differential gene set analysis was carried out using the Panther Classification System and String-db.

Animal studies

All experiments were carried out according to the Swiss Federal Law on the Protection of Animals, the Swiss Federal Ordinance on the Protection of Animals, and the guidelines of

the Swiss confederation (permission #ZH062/15). FoxN1 nu/nu mice (Charles River) aged between 6–12 weeks were anaesthetized and placed in a stereotaxic fixation device. A burr hole was drilled in the skull 2 mm lateral and 1mm posterior to the bregma. The needle of a Hamilton syringe was introduced into a depth of 3 mm (Tabatabai *et al.*, 2007). LN-229 (7.5×10^4) and LN-428 (1×10^5) cells were ressuspended in PBSA and then injected into the right striatum. Animals were clinically assessed three times per week and sacrificed upon developing neurological symptoms, justifying euthanasia (score 2).

Statistics

Analysis of the relative mRNA expression between different glioma grades and GBM samples were carried out by a non-parametric analysis of variance (Kruskal-Wallis test) with Dunn test for post-hoc comparison. *In vitro* experiments were performed in biological and technical replicates. Results are expressed as the mean and SEM of triplicate determinations. The statistical analyses were performed by unpaired Student's t-test or ANOVA for multiple comparison tests. Animal survival statistics was assessed using Gehan-Breslow-Wilcoxon test. All statistical analyses were carried out using Prism 5 (GraphPad Software, La Jolla, CA).

Results

CHD7 expression is upregulated in gliomas

To investigate the relevance of CHD7 for the malignant glioma phenotype, we first examined CHD7 mRNA expression across all glioma grades using the Cancer Genome Atlas Project (TCGA) database. Even though no significant alteration in genetic copy number was found in GBM (Figure 10A), microarray analysis revealed that CHD7 is up-

regulated in the tumor samples, when compared to normal brain tissue (NBT) (Figure 10B).

Moreover, upon comparing the four glioblastoma subtypes (Verhaak *et al.*, 2010) with higher levels in the proneural tumor samples (Figure 10C) we found that CHD7 exhibited different expression patterns. Consistent with the TCGA interrogation, we confirmed increased CHD7 expression levels in glioma tissue samples by qRT-PCR and immunohistochemistry (Figure 10D, E). These results show that CHD7 is up-regulated in gliomas, indicating a potential contribution to the malignant phenotype of these tumors.

CHD7 expression is highly heterogeneous in human GBM-derived cell lines *in vitro*

To further characterize CHD7 expression, we used the CD133 cell surface marker to enrich for the glioblastoma-initiating cell (GIC) population (Brescia *et al.*, 2013) from freshly dissected tumors. As measured by qRT-PCR, we did not detect consistent difference in CHD7 mRNA levels between the CD133^{pos} and CD133^{neg} sub-populations (Figure 11A).

We next analyzed CHD7 mRNA and protein levels in a panel of eight human long-term glioblastoma cell lines (LTCs) and five GIC lines. We found that CHD7 is expressed in the vast majority of human GBM-derived cell lines *in vitro* (Figure 11B). To better detect CHD7 protein levels, we optimized immunoblotting with fractionated cytoplasmic and nuclear cell extracts, confirming CHD7 protein localization in the nucleus (Figure 11C). Among the LTCs, highest CHD7 protein levels were found in LN-229 cells and in T-269 cells among the GICs (Figure 11D). Taken together, these results suggest that CHD7 is, in fact, up-regulated in gliomas and its expression is not particularly enriched in GICs.

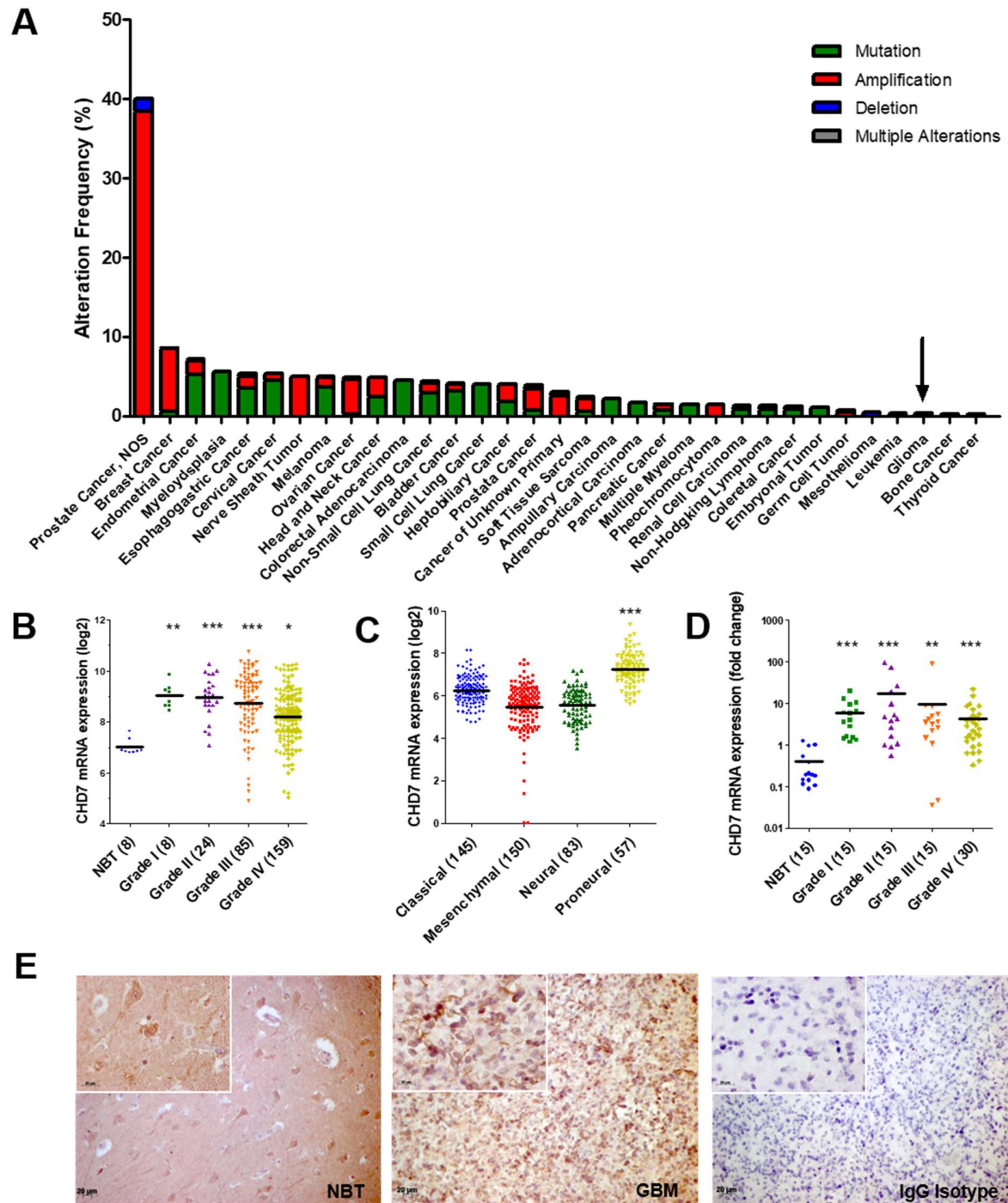Figure 10: CHD7 is up-regulated in gliomas. (A) Frequencies of *CHD7* genetic alterations across 33 human cancers. Mutations in *CHD7* were found in 0.29% (7 cases) of 2,454 GBM samples. The TCGA database was analyzed via cBioportal. (B) CHD7 expression in 284 human brain tissue samples from the TCGA microarray database. (C) Relative CHD7 expression in GBM subtypes according to the Verhaak classification. (D) CHD7

mRNA expression of macro-dissected brain tissue samples from normal brain tissue (NBT) and from resected glioma specimens was assessed by qRT-PCR. (E) Representative CHD7 immunohistochemistry in NBT and in glioma patient samples. Values are presented as k-means algorithm and 2Log transformation gene expression. (P < 0.05). Scale bar = 20 μm.
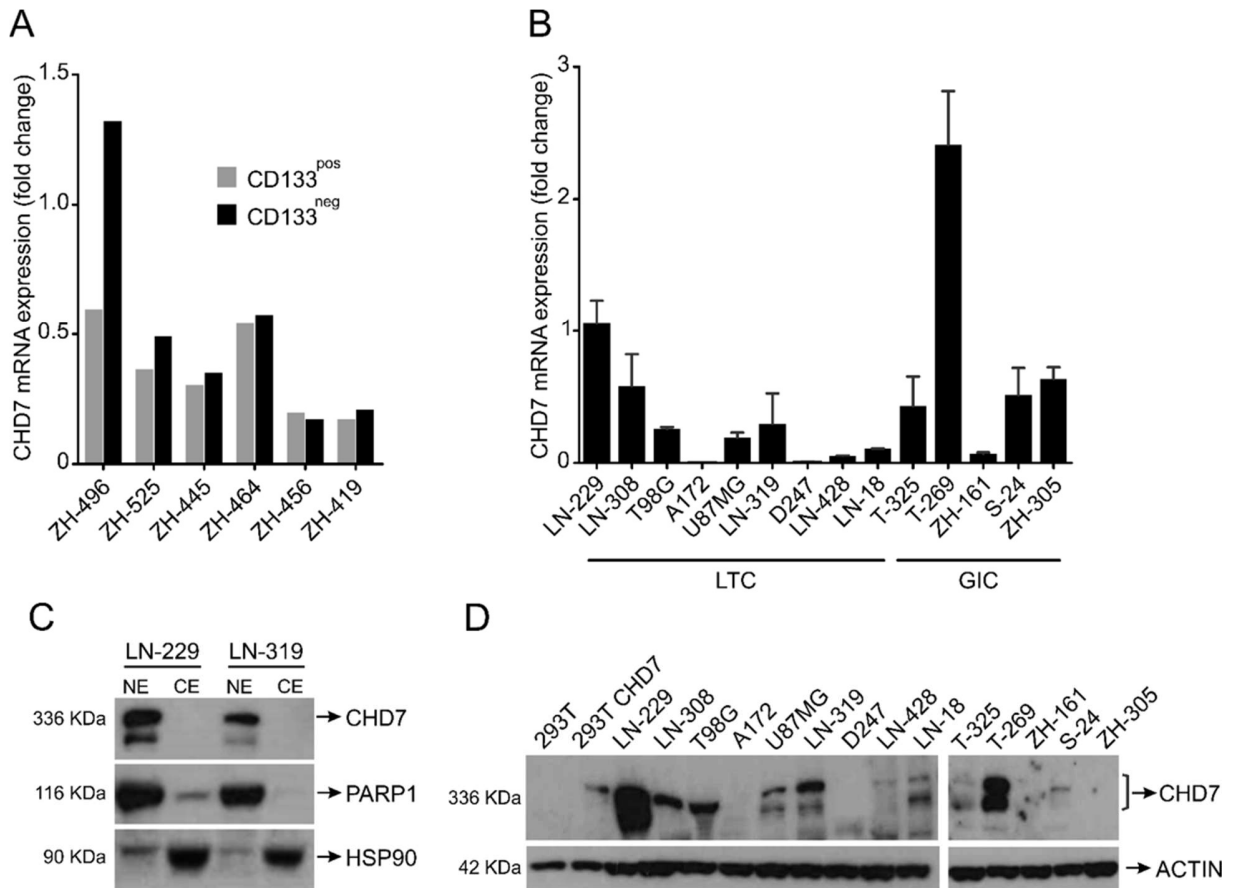
Figure 11: CHD7 expression levels in freshly dissected tumor tissue and in human-GBM derived cell lines. (A) CHD7 mRNA expression of freshly dissociated CD133^{pos} and CD133^{neg} tumor cells was assessed by qRT-PCR. Cell fractions represent matched sub-populations from the same patient. (B) CHD7 expression in different LTCs and GICs, determined by qRT-PCR. The results represent mean ± SEM from two independent experiments. (C) CHD7 immunoblotting of fractionated nuclear extracts (NE) and cytoplasmic extracts (CE) of LN-229 and LN-319 cell lines. PARP1 and HSP90 were used as nuclear and cytoplasmic markers, respectively. (D) CHD7 immunoblotting of nuclear extracts of human-GBM derived cell lines. Actin was used as the loading control and total protein extract of 293T cells transfected with the empty vector and CHD7 overexpression plasmids were used as negative and positive controls, respectively.

CHD7 expression is not correlated to prognosis of GBM patients

Next, we aimed to investigate whether high CHD7 expression in GBM samples might be directly associated with poor survival. We examined the distribution of CHD7 RNA expression and median patient survival across all GBM samples from TCGA. We found that survival was not significantly changed in tumors displaying high CHD7 expression, when compared to those showing low expression (**Erro! Fonte de referência não encontrada.**A).

		HR	Lower 95% CI	Upper 95% CI	P-value
Age		1.0025	1.0018	1.0033	<3.00E-11
Gender		1.0745	0.8668	1.3319	0.5121
Subtype					
	Mesenchymal	1.2883	0.9741	1.7038	0.0758
	Neural	1.1741	0.8529	1.6164	0.3250
	Proneural	1.5368	1.1081	2.1313	0.0100
Treated		0.4567	0.3668	0.5686	<2.40E-12
CHD7		0.9786	0.8560	1.1187	0.7511
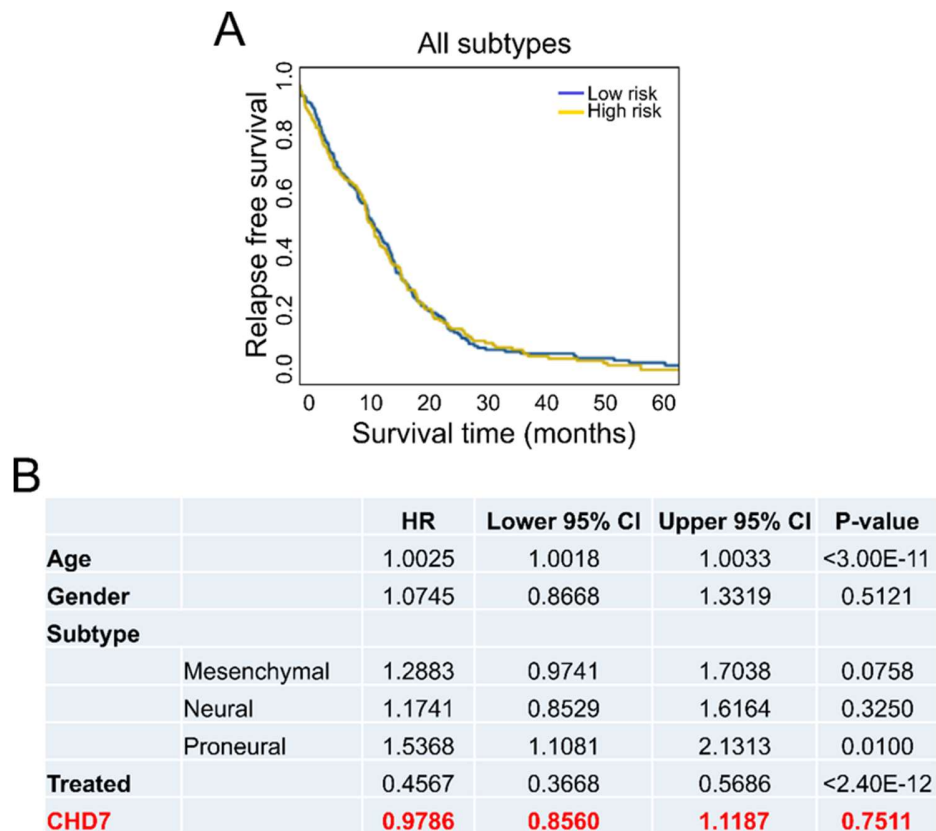
C

		HR	Lower 95% CI	Upper 95% CI	P-value
Age		1.0025	1.0017	1.0032	<9.08E-11
Gender		0.9915	0.7998	1.2292	0.9383
Subtype					
	Mesenchymal	1.2988	0.9803	1.7206	0.0684
	Neural	1.2703	0.9169	1.7599	0.1502
	Proneural	1.5383	1.0980	2.1553	0.0122
TMZ		0.5423	0.4387	0.6703	<1.53E-08
BCNU		0.9062	0.6593	1.2455	0.5439
Irinotecan		0.4099	0.2694	0.6239	<3.16E-05
Lumustine		0.7012	0.4669	1.0531	0.0872
CHD7		0.9739	0.8507	1.1149	0.7020

Figure 12: CHD7 expression is not directly correlated to patient survival. (A) Kaplan-Meier analysis of CHD7high and CHD7low in glioblastoma patients from TCGA. Analysis for all glioblastoma samples (p= 0.77). (B) Cox regression analysis. "Subtype" contrasts individuals from different glioblastoma subtypes to individuals classified as "Classical". "Treatment" contrasts individuals treated with any chemotherapy drug from those without chemotherapy. (C) Cox regression analysis. Subtype contrasts individuals from different glioblastoma subtypes to individuals classified as "Classical". Temozolomide (TMZ), carmustine (BCNU), irinotecan and lomustine are dichotomous variables, indicating whether the patient was treated (or not) with that drug. CHD7 gene expression, on log2 scale, is normalized to zero mean and unity variance. HR - Hazard Ratio, CI - Confidence Interval.

To obtain a more detailed relationship between patient prognosis and CHD7 expression levels, we used Cox regression analysis (Figure 12B, C). The Cox proportional hazards model allows the analysis of correlation between different variables with the survival time. Here, we used Cox regression to correlate CHD7 expression to survival time considering the patients' clinical and genetic data as co-variates, including: age, gender, subtype and treatment. As expected, in our analysis, we confirmed that age, subtype and type of treatment have a significant correlation to the risk factor. Yet, no significant correlation of CHD7 expression and patient survival was found.

CHD7 was efficiently deleted in LN-229 cells

Although CHD7 was not significantly correlated to patient prognosis, the great heterogeneity within GBM tumors prompted us to further examine the functional impact of CHD7 on GBM cells. To investigate the effect of CHD7 depletion, we used the CRISPR_Cas9 genome editing technique to completely abrogate its expression in the LN-229 cells. Cells were transiently transfected with a combination of two guide RNAs, targeting the initial and the final coding region of the *CHD7* gene, aiming to obtain whole fragment excision or eventual frame shift mutation. After confirming the deletion by PCR of genomic DNA in the cell population, we undertook single cell sorting in order to isolate cell clones (Figure 12A, B). A total of 50 clones were expanded and CHD7 immunoblotting showed that several samples did not express the canonic transcript of the CHD7 protein (Figure 12C).
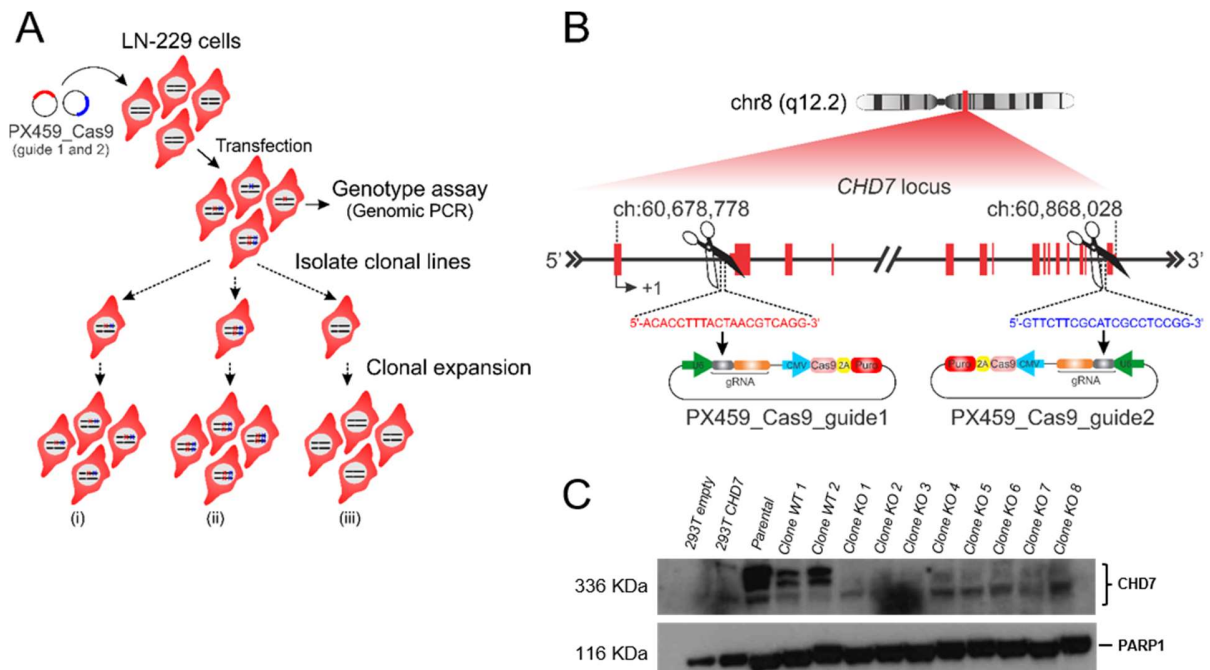

Figure 12: LN-229 CRISPR-Cas9 CHD7 mediated knockout (KO) cell clones. (A) Protocol used to generate CHD7 KO cell clones. LN-229 cell line was co-transfected with two sgRNAs and selected with Puromicin for 48h. After confirmation of genomic editing by

PCR, we performed clonal isolation. (i-ii) indicate possible mutations present in the different clones, which may lead to abrogation of CHD7 expression, or not (iii). (B) Scheme indicating the sgRNA sequences, targeting the initial and final region of the *CHD7* gene. (C) Screening of cell clones by immunoblotting of nuclear extracts. PARP1 was used as loading control and total protein extract of 293T transfected with empty vector and CHD7 overexpression plasmids were used as controls.

CHD7 deletion attenuates anchorage-independent growth and spheroid invasion in

LN-229 GBM cell clones *in vitro*

To examine the effect of CHD7 deletion in GBM cells in more detail, we randomly selected two LN-229 cell clones that still showed CHD7 expression, designating them as wild type clones (WT), and another two clones, which did not show CHD7 expression, which were named knockout clones (KO) (Figure 13A).

The culture expansion was successful, with equivalent growth rates being displayed by both cell clone types (Figure 13B). Only KO1 cell clone showed significant reduction in cell number after nine days, however, this reduction was not sufficient to drastically impact cell culture maintenance over time. Similarly, no apparent morphological differences were noted between the cell clones, as indicated by phalloidin and tubulin staining (Figure 13C).

Next, we analyzed anchorage-independent growth in a soft-agar colony formation assay. The total number of colonies greater than 50 µm of diameter, was consistently decreased in the KO cell clones, when compared to the WT clones (Figure 14A). Since anchorage-independent cell growth is associated with neoplastic transformation and metastatic potential, we asked whether the invasion capacity would be affected in the LN-229 KO clones. To that end, we used a 3D collagen invasion assay to assess invasion in the LN-229 multicellular spheroids, at 24, 48 and 72h culturing in a serum-containing collagen matrix (Figure 14B). The area covered by the invading cells was reduced by

about two-fold in the KO clones after 24h, when compared to the CHD7 expressing clones. The invaded area remained significantly reduced over time, indicating that the invasive potential of the cells was impaired upon CHD7 deletion. Therefore, we demonstrated that CHD7 is not essential for LN-229 cell survival *in vitro*, however, its deletion affects their anchorage-independent growth and invasiveness capacity.
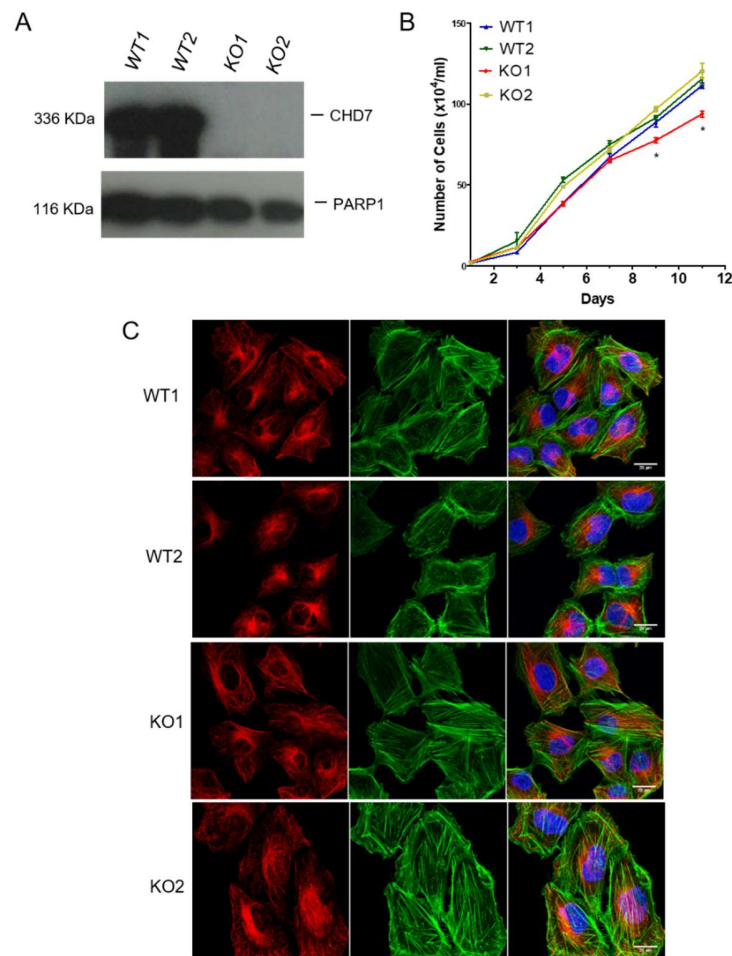

Figure 13: LN-229 CRISPR-Cas9 CHD7 mediated KO cell clones. (A) Immunoblotting of nuclear extracts from two WT and two KO isolated clones. PARP1 was used as the loading control. (B) Growth curves of LN-229 clones. 1×10^4 cells were plated in 12 well plates in triplicates for each time point. At least three independent experiments were performed. The graph represents mean ± SEM for three wells. Analysis of significance was performed using one-way ANOVA followed by Dunnett´s test in comparison with WT1. * $P < 0.05$. (C) Immunofluorescence of cell clones. Images were captured using a confocal microscope. Actin filaments (green), Tubulin (red) and nuclei (blue). Bar: 100 μm.
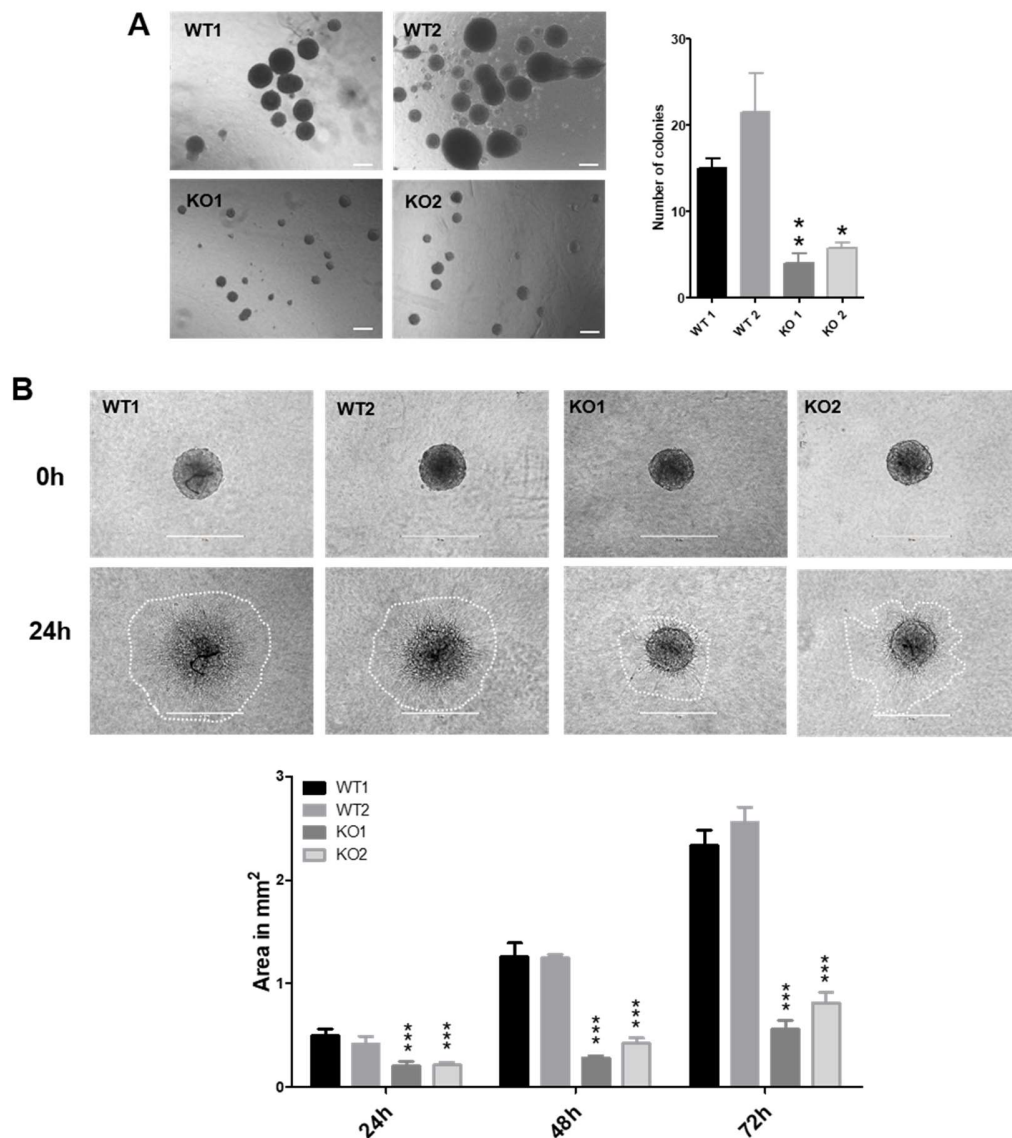
Figure 14: CHD7 deletion inhibits anchorage-independent cell growth and spheroid invasion in LN-229 cells. (A) 1×10^4 LN-229 cells suspended in soft agar were layered onto the bottom agar in 24-well plates in triplicates. Cells were grown in culture medium for two weeks. The graph represents total number of colonies per well, greater than 50 µm in diameter. The results are expressed as means ± SEM from three independent experiments. Analysis of significance was performed using one-way ANOVA followed by Dunnett´s test in comparison with WT1. Scale bar: 100 µm. (B) Spheroids of WT and KO clones were placed in a 3D collagen I matrix and the area covered by invading cells was measured for quantitation after 24, 48 and 72h. Experiments were performed three times in quadruplicates for each cell clone. Results from a single representative experiment are presented. Values are means ± SEM. Analysis of significance was performed using two-way ANOVA followed by Bonferroni test in comparison with WT1. *P<0.05, **P<0.01, *** P<0.001. Scale bar: 400 µm.

Ectopic CHD7 overexpression elicits LN-428 cell migration and invasion *in vitro*

To determine whether the reduced cell invasion capacity observed in LN-229 KO cell clones might originate from a direct effect of CHD7 deletion, we selected the LN-428 cell line, which expresses low level of endogenous CHD7 protein, to generate a cell population that constitutively overexpresses CHD7 (OE). To this end, the full-length CHD7 was amplified and cloned into the pCXN2-DEST expression vector (Figure 15A). LN-428 cells were transfected with the empty vector (EV) or the CHD7 expressing construct and the G418-resistant cells were selected and expanded for analysis. Quantification by qRT-PCR and immunoblotting confirmed OE in LN-428 (Figure 15B).
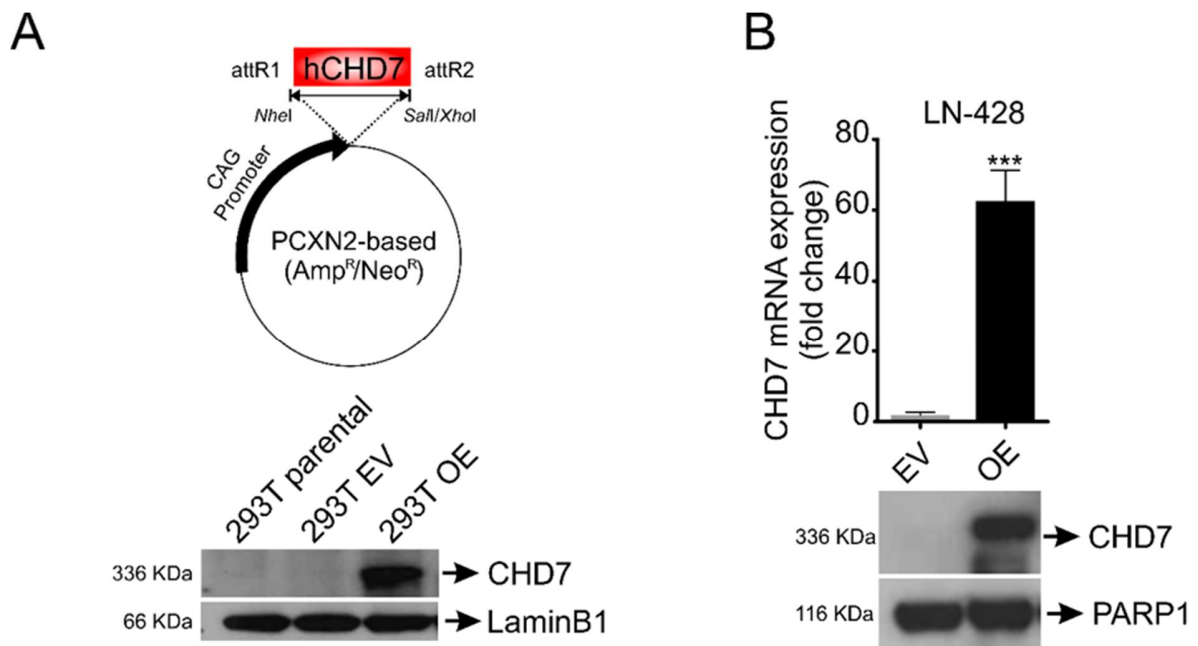
Figure 15: Generation of LN-428 cell population overexpressing CHD7. (A) Full-length CHD7 cDNA was amplified, as described in methods, and cloned into the pCXN2-DEST using the Gateway®-assisted sub-cloning system. Plasmids were transfected into 293T cells and protein expression was assessed by immunoblotting of total protein cell extracts. LaminB1 was used as loading control. (B) LN-428 cells were transfected with either the EV or OE vectors and selected with 750 µg/mL G418. CHD7 expression levels were assessed by qRT-PCR and immunoblotting of nuclear cell lysates. PARP1 was used as loading control. Values are the means ± SEM.

We next examined the migration and invasion potential of these cells *in vitro.* We first performed a scratch wound healing assay and we observed that OE cells possessed approximately 30% increased migration potential compared to EV (Figure 17A). We also found that CHD7 ectopic expression increased, by almost two fold, the transwell migration capacity of LN-428 cells (Figure 17B). We further investigated the role of CHD7 in modulating tumor cell invasion using the Matrigel invasion assay. CHD7 significantly enhanced, by about six fold, the invasion capacity of LN-428 cells across the transwell chamber, when compared to cells transfected with the EV (Figure 17C).
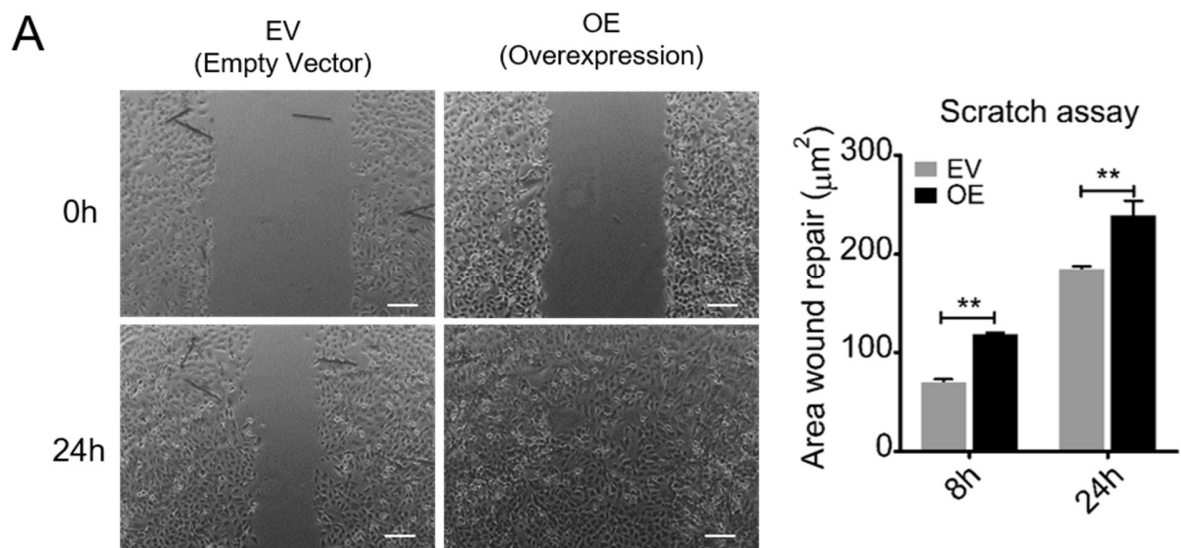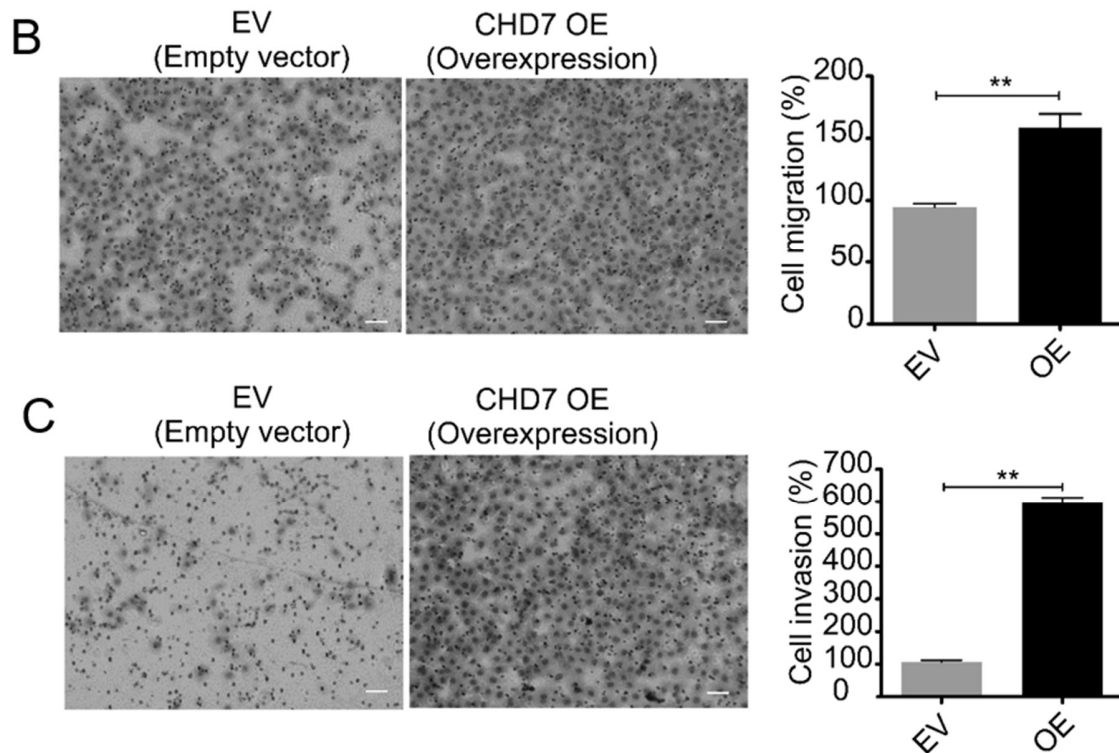
Figure 16: CHD7 overexpression promotes migration and invasion of LN-428 cells in vitro. (A) Wound-healing scratch assay: 2x105 cells were plated in 24 well plates in triplicates. Representative images are shown with the quantified data of a single experiment. Results are means ± SEM. **p < 0.01; 2-way ANOVA. (B) Representative images and statistical plots of transwell migration assays. (C) Representative images and statistical plots of transwell Matrigel coated invasion assays. The number of cells which transversed the membrane was assessed after 16h incubation and six fields at 10x magnification objective were counted for each well. Three independent experiments using duplicates were performed for each assay. Analysis of significance was performed using unpaired Student's t-test. **p<0.01.

Additionally, immunofluorescence staining of actin filaments was used to evaluate whether the differences in cytoskeletal alterations were associated with cell motility (Figure 18). We observed increased stress fiber formation in OE cells, which could be correlated to enhanced cell motility in these cells. Together, these data strongly indicate that CHD7 plays an important role in GBM cell migration and invasion.
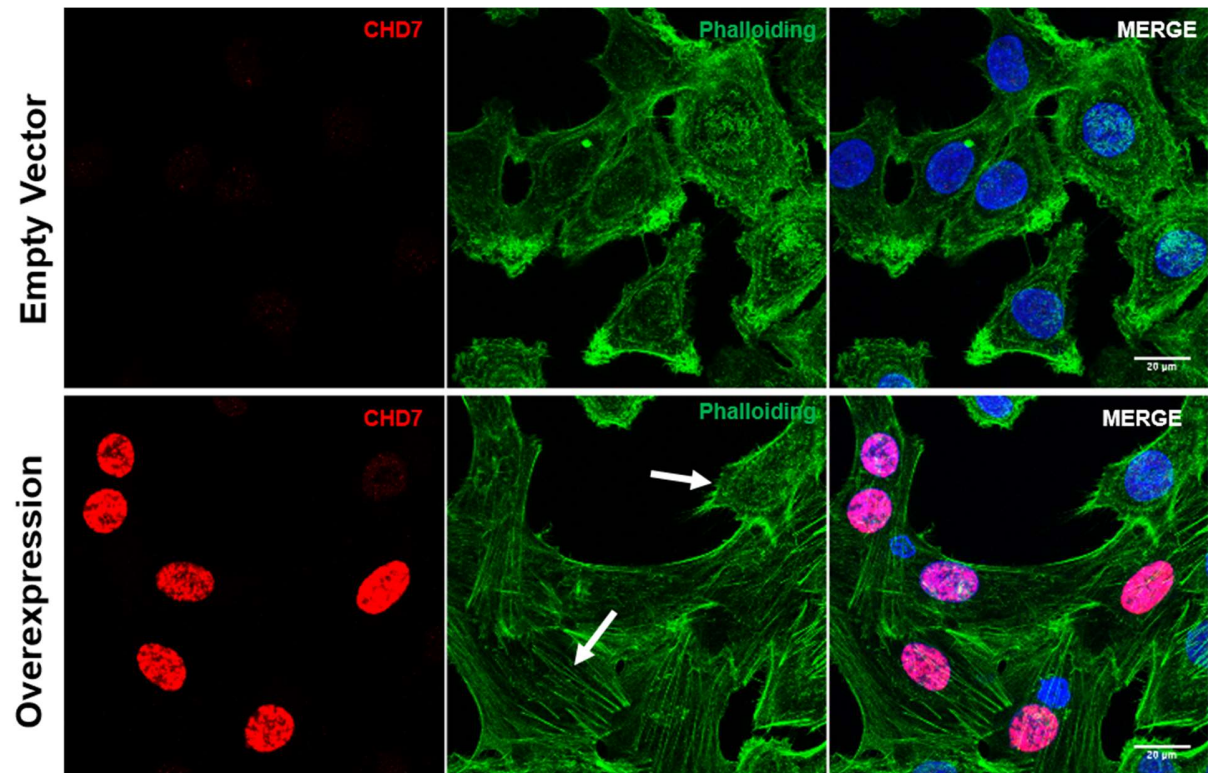
Figure 17: CHD7 overexpression promotes changes in LN-428 cytoskeleton. The upper panel shows LN-428 EV and the lower panel shows LN-428 OE. White arrows indicate differential cytoskeleton organization in a cell that does not display high CHD7 protein expression, in comparison with OE cells. Images were captured using confocal microscope. CHD7 (red), Actin filaments (green) and nuclei (blue). Bar: 20 µm.

CHD7 modulates tumor growth in orthotopic xenograft mouse glioma models

To investigate whether CHD7 is relevant for tumor development and progression, we analyzed whether modulation of CHD7 protein expression affects the tumorigenic potential of GBM cells in an orthotopic xenograft murine glioma model. Athymic nude mice were used for stereotactical implantation of cells derived from one LN-229 WT clone and two KO clones (n=8). To measure tumor volume, three pre-randomized mice of each group were sacrificed on the day when the first animal developed neurological symptoms. Analysis of brain sections showed that animals bearing tumors of KO cell clones,

developed smaller tumors, when compared to the WT clone, but with no statistical significance (Figure 19A and B). Thus, mice inoculated with the KO1 clone experienced a significant survival benefit, whereas animals injected with Clone KO2 cells showed a similar effect, although the differences were not statistically significant, when compared to the WT clone (Figure 19C).
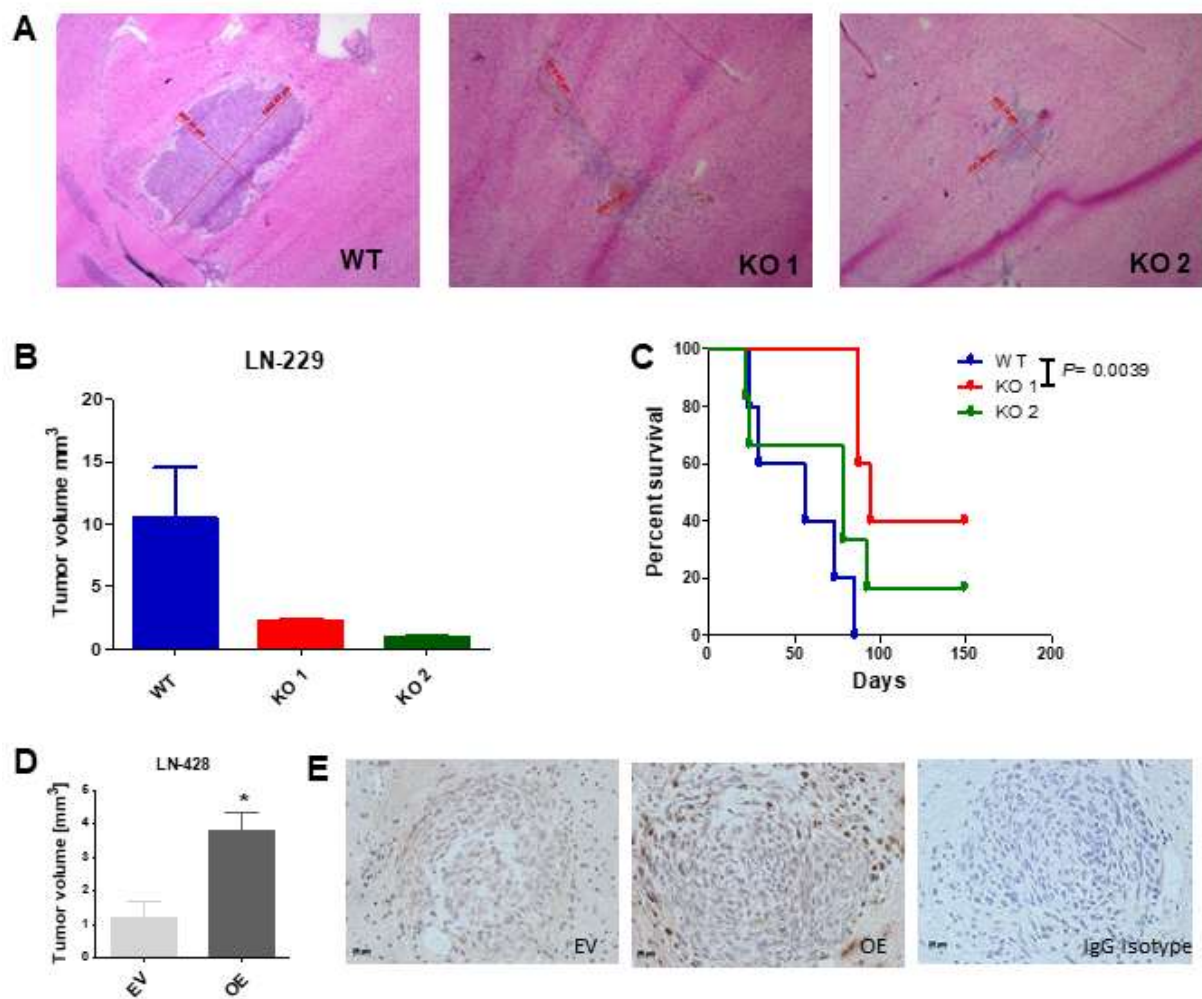
Figure 18: Effect of altered CHD7 expression in tumor development *in vivo*. (A) 75,000 human LN-229 cells were orthotopically implanted into the right striatum of nude mice (n=8). For histological analysis, three animals per group were sacrificed on the same day when the first animal(s) became symptomatic. Brain sections were examined and tumor sizes were assessed on H&E-stained sections. Results are means ± SEM (n=3; one-way ANOVA followed by Bonferroni test compared with WT clone, P>0.05). (C) Kaplan–Meier

survival curves (n=5; Gehan-Breslow-Wilcoxon test, considered significant for p<0.05). Animals were maintained until the onset of clinical grade 2 symptoms. (D) Four animals per group were inoculated with 100,000 human LN-428 GBM cells stably expressing EV and OE vectors. For histological analysis, animals were sacrificed on the same day when the first animal(s) became symptomatic. LN-428 tumor size was assessed on H&E-stained sections (n=4; unpaired Student's t-test, *p<0.05). (E) Representative CHD7 immunohistochemistry in LN-428 EV and in LN-428 OE tumors. Bar: 20 µm.

Additionally, animals were inoculated with LN-428 OE and EV and the tumors volume was measured (n=4). The tumor size was significantly increased in OE tumors, when compared to EV (Figure 19D). Immunohistochemistry of brain sections showed that cells displaying high protein expression, within the LN-428 OE cell population, are located at the border of the tumor (Figure 19E). These data suggest that ectopic CHD7 overexpression also enhances migration and invasion of LN-428 cells *in vivo*.

Our results demonstrate that genetic deletion of CHD7 in LN-229 decreases tumorigenicity, whereas ectopic expression enhances tumor growth and increases cell invasiveness of LN-428 cells *in vivo.*

Modulation in CHD7 levels altered the expression of adhesion proteins

Due to the previously described function of CHD7 in enhancer mediated transcription (Schnetz *et al.*, 2009, 2010; Engelen *et al.*, 2011), we performed deep transcriptome sequencing analysis via RNA sequencing (RNA-seq), on LN229 cell clones and LN-428 OE cells, to further assess how CHD7 might contribute to GBM pathogenesis.

This analysis identified 307 differentially expressed genes (DEGs) whose expression was commonly altered between three distinct WT cell clones and three isolated KO LN-229 cell clones. In LN-428 cells, we identified 869 DEGs in OE when compared to EV transfected cells (Figure 20).
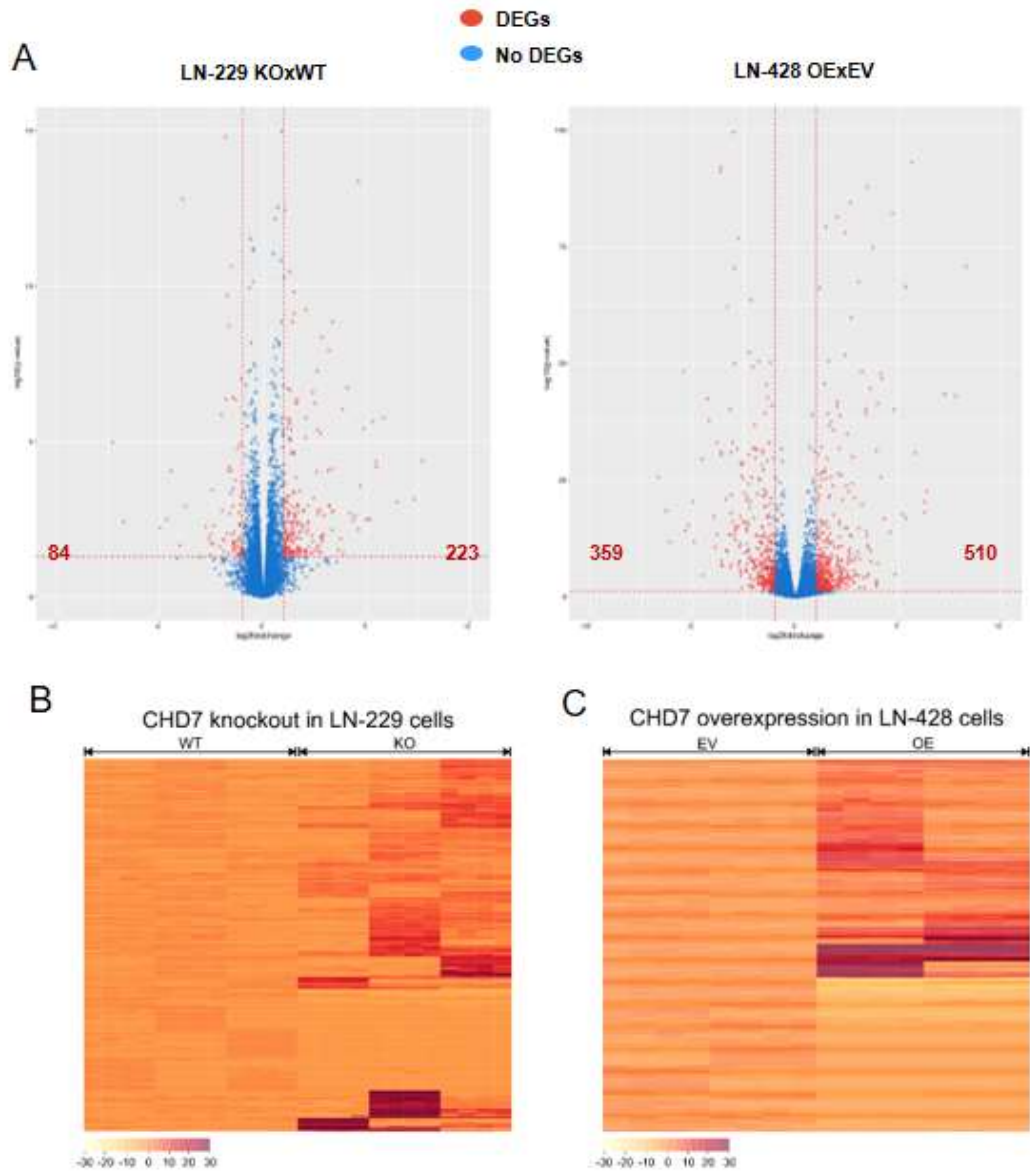
Figure 19: Differential transcriptome analysis of LN-229 cell clones and LN-428 OE cell population. (A) Volcano plot representation of the RNA-seq data, indicating the genes which are significantly and differentially expressed between KO x WT and OE x EV conditions. Each red dot indicates a gene significantly modulated. The x-axis shows the log2 fold change and the y-axis shows the p value expressed in − log10 scale. CHD7 deletion altered the expression of 307 genes (84 down and 223 up) in LN-229 cells and CHD7 OE modified the expression of 869 genes (359 down and 510 up) in LN-428 cells (cut-off of + /− 1 in the log2 scale over the control, $p < 0.05$). (B) Unsupervised hierarchical clustering of whole-transcriptome RNA-seq data of three independent KO and WT clones. (C) Unsupervised hierarchical clustering of whole-transcriptome RNA-seq data of two independent samples of LN-428 EV and OE cell populations.

Notably, only 58 transcripts were commonly regulated in both cell lines, whereas 18 presented alterations in opposite directions in the expression levels, between these two groups (Table 4).

Symbol	Name	LN-229 KO	LN-428 OE
COL3A1	Collagen Type III Alpha 1 Chain	2,05	6,51
ANGPTL4	Angiopoietin Like 4	1,18	3,98
CHD7	**Chromodomain Helicase DNA Binding Protein 7**	**-1,76**	**2,75**
PCDH7	Protocadherin 7	1,33	2,64
NXF3	Nuclear RNA Export Factor 3	5,46	2,61
FGF5	Fibroblast Growth Factor 5	1,42	2,52
PRSS3	Protease, Serine 3	3,76	2,39
FOSB	FosB Proto-Oncogene, AP-1 Transcription Factor Subunit	1,81	2,31
TYRP1	Tyrosinase Related Protein 1	1,32	2,25
SOD3	Superoxide Dismutase 3	7,32	2,22
LYPD3	LY6/PLAUR Domain Containing 3	1,08	2,19
HPX	Hemopexin	1,27	2,09
CDH19	Cadherin 19	1,08	2,06
SLC9A9	Solute Carrier Family 9 Member A9	1,49	1,83
TDO2	Tryptophan 2,3-Dioxygenase	2,22	1,74
CD226	CD226 Molecule	1,28	1,72
AP003486.1	Uncharacterized LOC103611081	1,68	1,70
CTGF	Connective Tissue Growth Factor	1,26	1,65
COLEC12	Collectin Subfamily Member 12	1,28	1,62
CACNA1G	Calcium Voltage-Gated Channel Subunit Alpha1 G	1,39	1,55
AIF1L	**Allograft Inflammatory Factor 1 Like**	**-1,83**	**1,52**
RNA5-8S4	RNA, 5.8S Ribosomal N1	1,67	1,51
STK32A	Serine/Threonine Kinase 32A	3,22	1,50
RNA5-8S5	RNA, 5.8S Ribosomal N5	1,73	1,48
AL133346.1	Uncategorized	1,39	1,45
RNA5-8S5	RNA, 5.8S Ribosomal N5	1,73	1,43
IGFN1	Immunoglobulin-Like And Fibronectin Type III Domain Containing 1	4,45	1,42
RNA5-8S5	RNA, 5.8S Ribosomal N5	1,73	1,39
IL11	Interleukin 11	1,71	1,36
RNA5-8S5	RNA, 5.8S Ribosomal N5	1,68	1,30
ITGA11	Integrin Subunit Alpha 11	2,87	1,24
ADPRHL1	ADP-Ribosylhydrolase Like 1	1,02	1,22
SEMA3F	Semaphorin 3F	1,67	1,21

RNA5-8S5	RNA, 5.8S Ribosomal N5	1,64	1,17
BDKRB2	Bradykinin Receptor B2	6,48	1,16
ACTBL2	Actin, Beta Like 2	2,20	1,15
PINLYP	Phospholipase A2 Inhibitor And LY6/PLAUR Domain Containing	1,04	1,11
IL7R	Interleukin 7 Receptor	1,47	1,00
ZNF502	**Zinc Finger Protein 502**	**-5,01**	**1,00**
C4orf26	**Odontogenesis Associated Phosphoprotein**	**4,79**	**-1,16**
FRMPD4	**FERM And PDZ Domain Containing 4**	**1,20**	**-1,17**
MSC-AS1	**MSC Antisense RNA 1**	**2,40**	**-1,18**
APLN	Apelin	-1,54	-1,26
ABCA1	**ATP Binding Cassette Subfamily A Member 1**	**1,01**	**-1,30**
CCL5	**C-C Motif Chemokine Ligand 5**	**3,32**	**-1,31**
KIF26B	**Kinesin Family Member 26B**	**1,46**	**-1,38**
SEMA3G	Semaphorin 3G	-1,10	-1,41
PXYLP1	**2-Phosphoxylose Phosphatase 1**	**1,04**	**-1,59**
SLCO1A2	**Solute Carrier Organic Anion Transporter Family Member 1A2**	**1,18**	**-1,63**
CHMP1B2P	**Charged Multivesicular Body Protein 1B2, Pseudogene**	**1,98**	**-1,71**
MYH16	**Myosin Heavy Chain 16 Pseudogene**	**1,92**	**-2,06**
RN7SL2	**RNA, 7SL, Cytoplasmic 2**	**1,36**	**-2,08**
RN7SL3	**RNA, 7SL, Cytoplasmic 3**	**1,24**	**-2,17**
HAPLN1	**Hyaluronan And Proteoglycan Link Protein 1**	**2,73**	**-2,68**
BMPR1B	**Bone Morphogenetic Protein Receptor Type 1B**	**1,20**	**-2,99**
ZNF618	**Zinc Finger Protein 618**	**2,85**	**-3,13**
CA9	Carbonic Anhydrase 9	-1,87	-3,14
MSR1	Macrophage Scavenger Receptor 1	-3,36	-3,33
MGAM	Maltase-Glucoamylase	-2,16	-4,51

Table 4: Commonly regulated DEGs between LN-229 KO x WT and LN-428 OE x EV. Altered genes in both experiments are shown. Values of expression level changes in opposite directions are represented in bold, with fold change values expressed as log2 scale over the control. Negative and positive values indicate down-regulation and up-regulation of gene expression, respectively. Red indicates genes with decreased expression in KO and increased expression in OE. Blue indicates genes displaying increased expression in KO and decreased expression in OE. Significant changes were included for $p < 0.05$.

Even though CHD7 seems to regulate distinct genes in LN-229 and LN-428, differential gene set analysis revealed strong enrichment for molecules with functions related to binding in both KO and OE (Figure 20A). Consistently, the altered genes were

highly associated with pathways such as "biological adhesion", "cell adhesion" and "locomotion" in gene ontologies (GO) analysis (Figure 20B).

Genes encoding proteins involved in cell–cell adhesion, including several integrins (*Itga11*, *Itgbl1*, *Itgb2*, and *Itgb3*) and protochaderins/cadherins (*Pcdh7*, *Pcdh10*, *Pcdh15*, *Cdh7*, *Cdh19* and *Cdh15*), as well as other cell binding molecules, such as *Cadm2*, *Cadm3*, *Nrcam*, *Ncam2*, *Emilin2* and *Cntn1*, were modulated upon changes in CHD7 expression. Interestingly, none of the master regulators of epithelial-mesenchymal transition, such as, *Zeb1*, *Zeb2*, *Snai1*, *Snai2*, and *Twist1*, were significantly altered.

The heat-maps indicate the top 30 DEGs in both groups (Figure 21A). To independently validate these results, changes in the expression of 40 genes associated with tumorigenesis, cell motility or invasiveness, were analyzed by qRT-PCR (Figure 21B).

Next, we asked whether the altered genes constituted direct targets of CHD7 activity. To that end, we compared our results, obtained by RNA-seq, with previously described Chd7 localization determined by chromatin immunoprecipitation, followed by DNA sequencing (ChIP-seq) in NSCs (Engelen *et al.*, 2011). These authors revealed approximately 16,000 binding sites near or in the genes sequences. We found that 28% (85 genes) of the DEGs in KO and 30% (259 genes) of the genes modulated in OE, overlap with Chd7 binding sites in NSCs, suggesting a direct control of gene transcription.
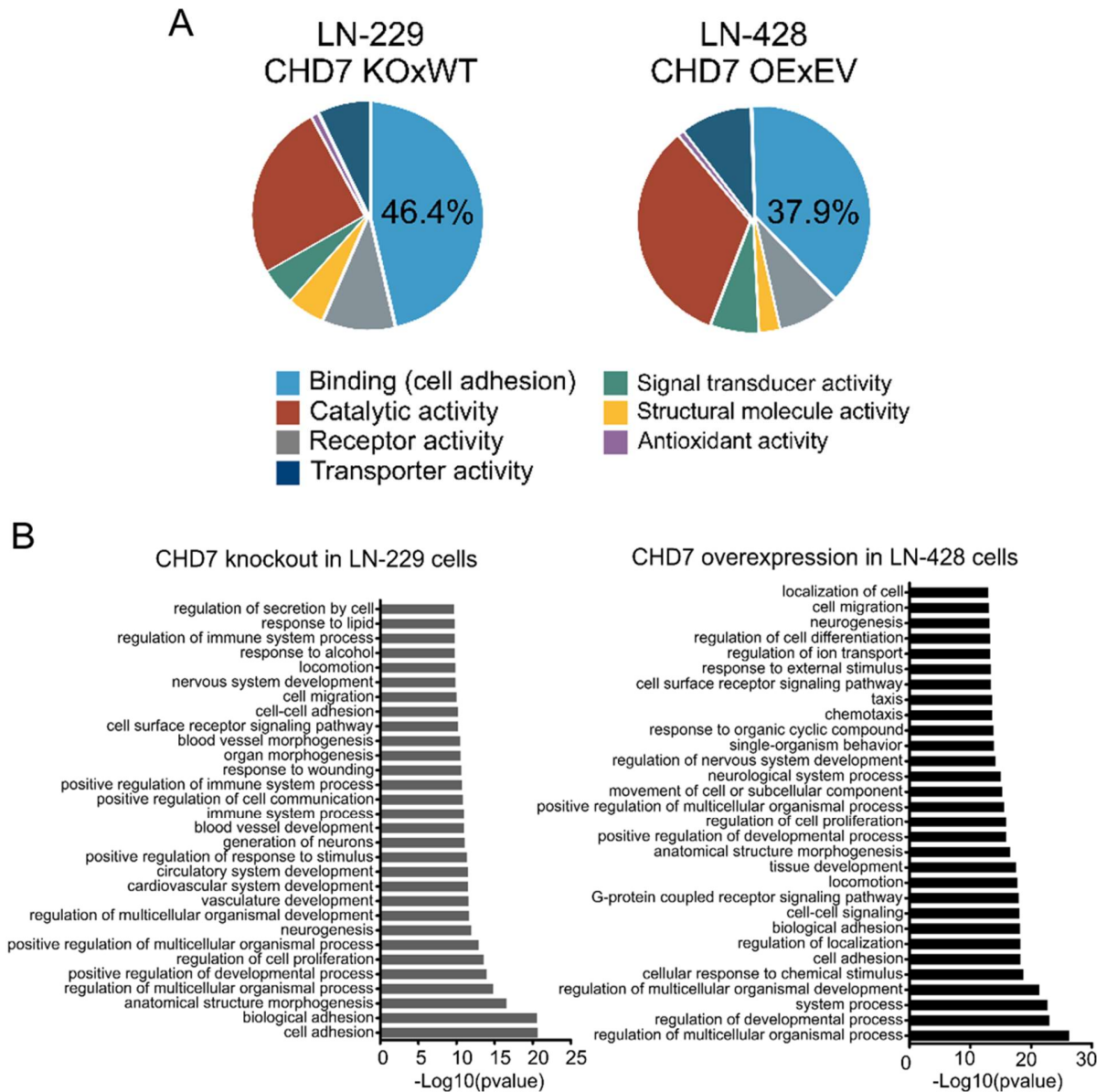
Figure 20: CHD7 regulates the expression of binding proteins promoting cell motility and invasiveness in GBM cells. (A) Pie chart depicts distribution of top molecular functions in the set of DEGs, analyzed using the PANTHER database. (B) Gene ontology analysis indicating the 30 most enriched pathways for the significantly altered genes in the modified cell lines, defined by STRING database.
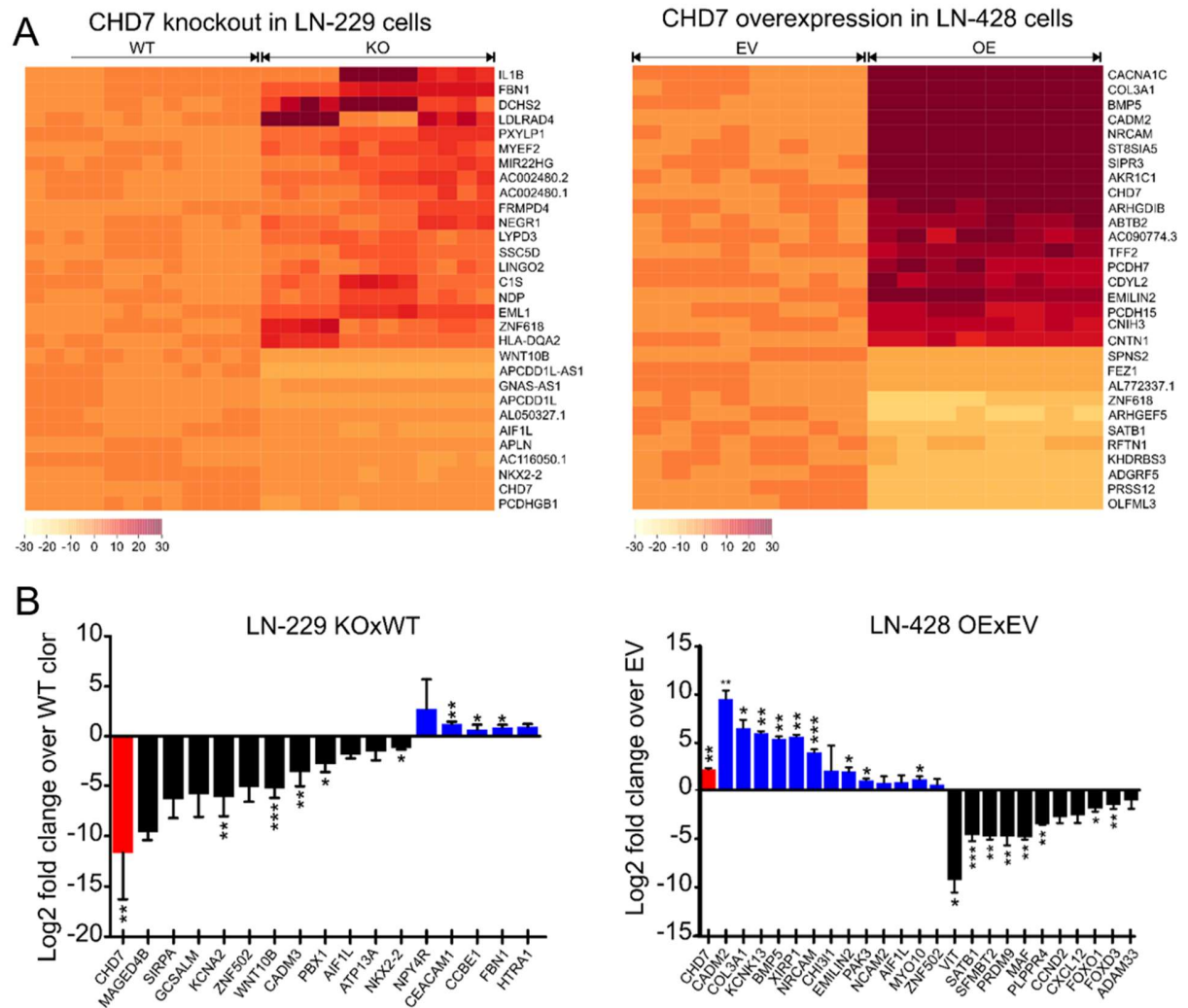
Figure 21: Altered genes in LN-229 CHD7 knockout and in LN-428 CHD7 overexpression (A) Heat-maps indicating the shortlisted genes which are most significantly modulated under both comparative conditions. (B) Validation of gene expression by qRT-PCR in down-regulated (black) and up-regulated (blue) genes related to tumorigenesis, cell migration or cell invasion. Values are the means ± SEM (n = 3 independent experiments, unpaired Student's t-test).

CHD7 OE also promotes cell motility and invasiveness in A172 cells

Given the phenotypically heterogeneous nature of GBM-derived cells (Soeda *et al.*, 2015), we aimed to test the consistency of CHD7 OE phenotype in another cell line.

Therefore, we generated A172 cells overexpressing CHD7 to investigate whether the migration and invasion capacity of these cells were altered.

Using transwell assays, we found that migration was significantly increased upon CHD7 expression while invasion, in Matrigel coated inserts, indicated a slight increase, even though, not statistically significant (Figure 22A). To better investigate the invasion ability of these OE cells, we used the 3D collagen spheroid invasion assay, assessing invasion after 24h in a serum-containing collagen I matrix. The area covered by the invading cells was increased by about two-fold in OE cells, when compared with the EV cells (Figure 22B). Changes in cytoskeleton are not so evident in OE cells due to the elongated shape of A172 (Figure 22C).

In order to investigate whether the mechanisms of enhanced cell motility and invasiveness regulated by CHD7 in GBM cells are similar between both cell lines studied, we analyzed the expression of target genes identified in LN-428 by qRT-PCR. Few targets were found to be commonly regulated in the same direction, including *AIF1L* and *SATB1* (Figure 22D).
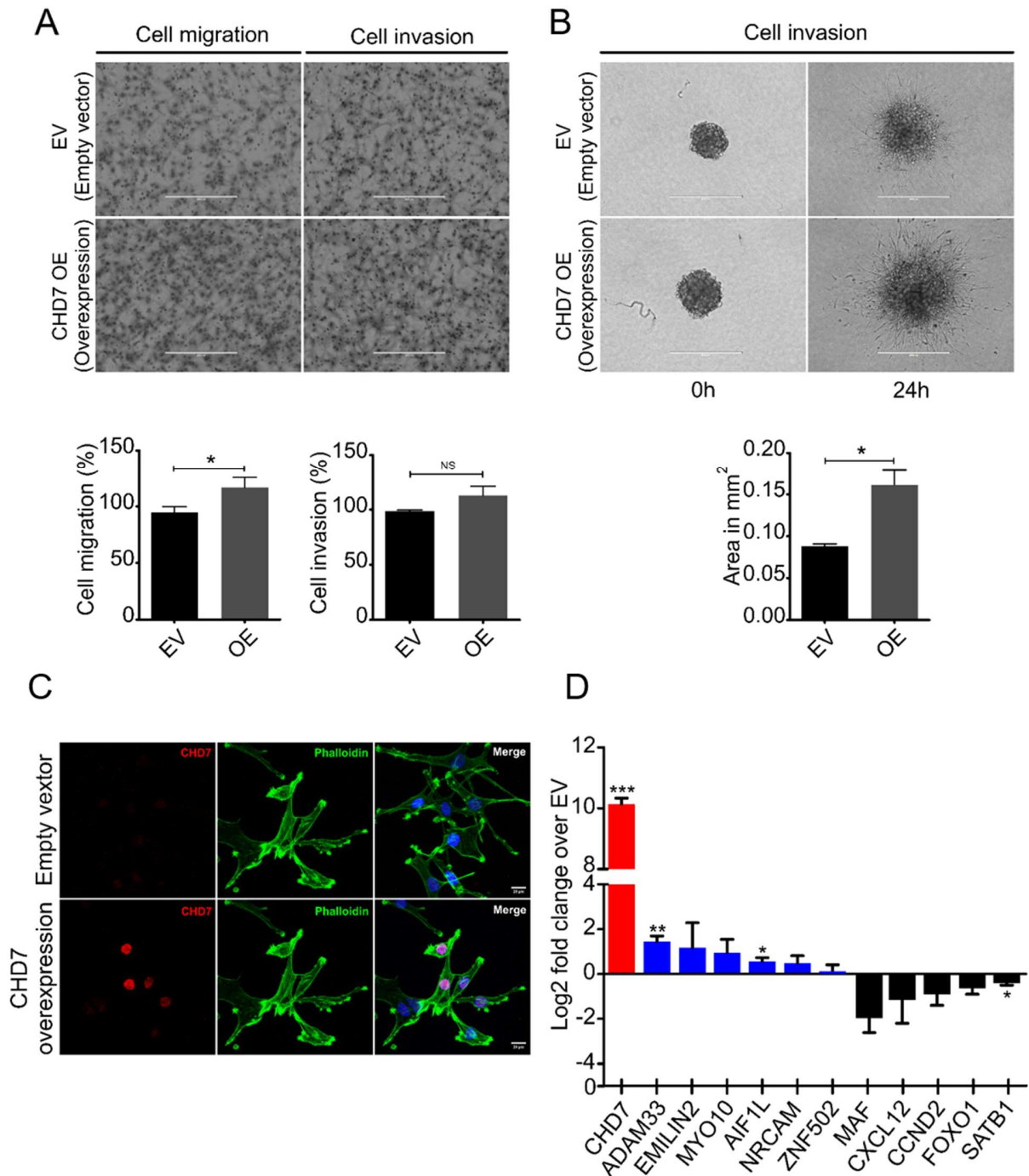
Figure 22: CHD7 modulates A172 cell motility and invasiveness. (A) Representative images and statistical plots of transwell migration and transwell Matrigel coated invasion assays. The number of cells which transversed the membrane was assessed after 16h incubation and six fields were counted for each well using a 10x magnification objective. Three independent experiments using duplicates were performed for each assay. For significance analysis, we used unpaired Student's t-test. **p<0.01. (B) Multicellular

spheroids of EV and OE clones were placed in a 3D collagen I matrix and the area covered by invading cells was quantified after 24h. Experiments were performed three times in triplicates. Results from a single representative experiment are presented. Values are means ± SEM. Significance was analysed using unpaired Student's t-test. *p<0.05. Scale bar: 400 μm. (C) Immunofluorescence of A172 EV and OE cell lines. Images were captured using Zeiss LSM 780-NLO confocal microscope. CHD7 (red), Actin filaments (green) and nuclei (blue). Bar: 20 μm. (D) qRT-PCR of target genes modulated in OE cells. Down-regulated (blue) and up-regulated (black) genes compared to EV. Values are the means ± SEM (n = 3 independent experiments, unpaired Student's t-test).

Discussion

Current evidence indicates that formation of combinatorial tissue-specific complexes underlies refinement and specificity of chromatin remodelers' activity (Ho and Crabtree, 2010). Due to this variability, the individual function of many of these proteins remains elusive. CHD7 is known to be essential for the normal development of the organism (Feng *et al.*, 2017). Over 90% of the patients displaying clinically typical CHARGE syndrome carry mutations in *CHD7* (Basson and van Ravenswaaij-Arts, 2015). The disease is characterized by a variety of congenital anomalies, including malformations of the craniofacial structures, peripheral nervous system, ears, eyes and heart (Vissers L M *et al.*, 2004; Wincent *et al.*, 2008).

In the non-pathological brain, CHD7 was shown to be crucial for NSC function (Engelen *et al.*, 2011; Feng *et al.*, 2013; Micucci *et al.*, 2014; Jones *et al.*, 2015). On the other hand, the involvement of CHD7 in tumorigenesis has just begun to be described, gaining considerable attention in the last few years. Initial evidence is available indicating that altered CHD7 expression may be found in different human cancers. Scanlan and colleagues reported that CHD7 (formerly known as KIAA1416) is up-regulated in colon cancers (Scanlan *et al.*, 2002) and low CHD7 expression was associated with improved outcome in pancreatic ductal adenocarcinoma patients treated with adjuvant gemcitabine

(Colbert *et al.*, 2014). Additionally, low CHD7 expression in the G4 meduloblastoma subtype, in combination with BMI1 overexpression, was recently shown to contribute to tumor formation (Badodi *et al.*, 2017).

Frequent *CHD7* mutations have been reported in stomach and colon cancers (Kim *et al.*, 2011), as well as in colorectal carcinoma with CpG island methylator phenotype 1 (Tahara *et al.*, 2014). *CHD7* gene rearrangement was also suggested to be a driver mutation identified in small-cell lung cancer (Pleasance *et al.*, 2010). Consistent with these findings, *in silico* analysis of 32 tumor types, revealed that *CHD7* is the most commonly gained/amplified and mutated gene among the nine CHD members. This study also showed that overexpression of *CHD7* was more prevalent in aggressive subtypes of breast cancer, being significantly correlated with high tumor grade and poor prognosis (Chu *et al.*, 2017).

In this present study, we provide evidence that CHD7 may play an important role in GBM pathogenesis. GBM is the most common and most malignant primary brain tumor (Huse, Holland and Deangelis, 2013). Despite the multimodality treatment, which typically includes surgery, ionizing radiation, and cytotoxic chemotherapy, the average overall survival rate remains at only ~15 months, highlighting the urgent need for more effective targeted therapeutics (Weller *et al.*, 2014, 2015).

Our results indicate that CHD7 is highly expressed in glioma patient samples, as previously suggested (Otha et al, 2016). However, we found no evidence that CHD7 is particularly up-regulated in GICs. Here, we demonstrated that CHD7 deletion not only inhibited anchorage-independent growth in LN-229 cells, but also reduced cell invasion capacity (Figure 14). Conversely, ectopic CHD7 expression enhanced migration and

invasion potential of LN-428 cells and, to a lesser extent, in A172 cells, by regulating stress fiber assembly and adhesion dynamics (Figure 16 and Figure 17). Actin stress fibers formation is one of the critical steps associated with cell invasion (Tavares *et al.*, 2017), but the precise mechanism by which CHD7 promotes reorganization of the cell cytoskeleton remains to be elucidated. We were unable to explore the role of CHD7 in GICs using the same approach.

A recent study using iPS-derived neural crest cells from CHARGE patients, also found that CHD7 mutations lead to defective cell migration (Okuno *et al.*, 2017). This study showed modulation of several genes related to cell adhesion and migration, such as CTGF, COL3A1, SERPINE1 and THBS1, all of which we found to be modulated in GBM cells. CHD7 has also been implicated in regulation of neural crest cell migration during embryogenesis in *Xenopus* (Bajpai *et al.*, 2010). In this model, CHD7 was shown to cooperate with PBAF to modulate Slug, Sox9 and Twist1 gene expression, which are essential for proper cell migration in this cell type. We did not observe significant changes in those genes in our study, indicating that CHD7 may regulate cell motility by different mechanisms, possibly by association with cell-specific interaction partners.

CHD7 binding sites show a high degree of cell type specificity and binding itself is context dependent (e.g., embryonic cell in differentiation state showed only 30% overlap in the binding sites) (Schnetz *et al.*, 2009). Our analysis also demonstrates the complexity of CHD7 targets. Only 18 genes were commonly regulated in opposite directions in LN-229 and LN-428 cell lines. Importantly, the large majority of the DEGs were related to adhesion molecules in both groups, showing about 30% overlap with genome-wide Chd7 localization in NSCs (Engelen *et al.*, 2011).

Our data are relevant to transduce diversity of CHD7 targets which occurs in different cell types, though it suggests a broader function for CHD7 as a master regulator of cell migration and invasion. It will be of great interest to investigate, for example, the underlying mechanism regulating differential CHD7 expression in GBM cells and whether these pathways are amenable to manipulation by molecular intervention, aiming at clinical therapeutic protocol.

Conclusions

The invasive behavior of malignant gliomas is one of the most important characteristics which contribute to tumor recurrence after surgery (Tabatabai and Weller, 2011). Given the variability in the CHD7 binding sites, its tumor-suppressive or oncogenic effect is likely to be particular to each cancer type. Our data provide functional and molecular evidence for a novel oncogenic role of CHD7 as a transcriptional regulator of pro-invasive and motility factors in GBM cells (Figure 23). Further studies may warrant important clinical-translational implications for GBM treatment.

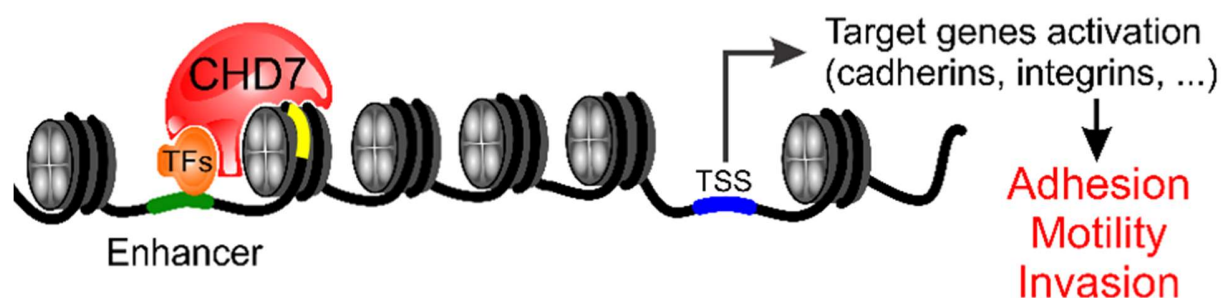Figure 23: Proposed model of CHD7 regulation of GBM cell motility and invasiveness. CHD7 is recruited to binding sites through interactions with cell type-specific transcription factors (TFs) and histone modifications. The energy provided from the ATP hydrolysis enables nucleosome translocation revealing extra TF-binding sites (yellow rectangle). Binding of additional TFs, associated with co-activators, results in further histone

modifications (H3K27ac) promoting DNA accessibility favoring transcription. In GBM cells, CHD7 modulates the expression of several adhesion molecules, such as integrins and cadherins, stimulating cell motility and invasiveness.

Chapter 2: Molecular cloning and analysis of the CHD7 promoter region

Abstract

GBM is the most common, aggressive and fatal type of cerebral tumor. The average patients' survival rate is 12-15 months, highlighting the urgent need for more effective targeted therapeutics. CHD7 is an ATP-dependent chromatin remodeler protein, acting in enhancer-mediated transcription, therefore, abnormal CHD7 expression may result in aberrant transcription of tissue-specific genes. Previous results from our laboratory suggest that the CHD7 gene is highly expressed in glioma patient samples, when compared to normal brain tissue, however, the mechanism underlying its expression is still not understood. In this study, we aimed to identify the CHD7 promoter region and test different signaling pathways which may directly modulate the expression of this gene in GBM cells. Using the luciferase reporter gene assay, we validated a regulatory sequence with promoter activity between -1149 and +619. This fragment greatly stimulated luciferase activity by 15-fold in 293T cells, when compared to the empty vector. Importantly, the antisense sequence did not show significant activity, indicating that CHD7 expression is regulated by an unidirectional promoter. Our construct constitutes a valuable tool to determine the direct targeting relationship between different signal transduction pathways and CHD7 gene expression. We believe that this work will be important for better understanding of the molecular mechanisms underlying greater CHD7 expression in brain tumor tissue, when compared to the normal counterpart.

Introduction

Deregulated gene expression is often related to different types of cancer. Altered *CHD7* expression has been reported in colon cancer (Scalan et al, 2002) and low *CHD7* expression was associated with improved outcome in patients with pancreatic ductal adenocarcinoma treated with adjuvant gemcitabine (Colbert et al, 2014). However, the mechanisms which lead to modulation of CHD7 expression in tumor cells are not yet understood.

CHD7 is a positive regulator of pro-neuronal gene transcription in neural stem cells (NSCs), promoting their differentiation into neuroblasts, while CHD7-deficient cells display a shift towards glial fates (Micucci *et al.*, 2014). In the oligodendrocyte lineage, CHD7 cooperates with Sox10 to control the onset of oligodendrocyte myelination and remyelination after injury (He *et al.*, 2016), suggesting that altered CHD7 expression might disrupt the behavior of other neural populations.

Our laboratory has previously shown that CHD7 mRNA levels are upregulated in glioma samples, when compared to normal brain tissue. Moreover, as an oncogene candidate, we found that *CHD7* deletion delayed tumor growth and improved overall survival in an intracranial xenograft glioma mouse model (Chapter 1, data not published). Therefore, modulation of CHD7 expression could possibly have therapeutic implications for GBM tumor treatment. Here, we aimed to establish a gene reporter assay as a versatile and powerful tool to investigate CHD7 promoter activity under a variety of conditions.

Material and Methods

Cell lines and reagents

The human 293T cell was purchased from the American Type Culture Collection (ATCC).

The LNT-229 and LN- 428 cell lineages were kindly provided by Dr. N. de Tribolet

(Lausanne, Switzerland). Cells were maintained at 37°C in Dulbecco's modified Eagle's

medium (DMEM, Invitrogen, Life Technologies, Carlsbad, CA), containing 10% fetal calf

serum (FCS) (VWR Lonza, Leighton Buzzard, UK) and supplemented with 2 mM

glutamine (Invitrogen, Life Technologies), in a 5% CO_2 incubator. The following peptide

growth factors were used: EGF (10 ng/mL), FGF1 (10 ng/mL) and TGF-β1 (10 ng/mL)

(Peprotech, Rocky Hill, NJ).

Plasmids construction

A 1.7Kb genomic DNA fragment, containing the upstream region of the *CHD7* gene (-

1149/+619), was synthesized and cloned by the GenScript company (Nova Jersey, USA)

into the pUC57 plasmid vector. The fragment was excised with restriction enzymes

(Thermo Fisher Scientific, Waltham, MA) and inserted into the multiple cloning site of the

pGL3 Basic vector (Promega, Madison, USA), located immediately upstream of the

luciferase reporter gene, in either the sense or the anti-sense orientation.

Luciferase assay

Cells were plated at a density of 4×10^4 cells/well in 24-well platesand, 24h later, they

were transfected with the plasmids described above using Lipofectamine 2000 (Thermo

Fisher) according to the manufacturer's instructions. The medium containing the

transfection reagent was changed 3h after initial incubation to fresh medium. For promoter

induction analysis, growth factors were added at the concentration of 10 ng/mL. At 48h

after transfection, the monolayer cultures were washed with PBSA and total lysates were prepared using passive lysis buffer (Promega). Luciferase activity was measured using the Dual Reporter assay system (Promega) and Falcon™ Solid Opaque 96-Well Plates (Thermo Scientific). The luminescence was measured using TECAN, infinite M200PRO. The level of firefly luciferase activity was normalized to Renilla luciferase activity and expressed as arbitrary units.

Quantitative Real time RT-PCR (qRT-PCR)

For mRNA expression analysis, total RNA was transcribed into cDNA using the iScript cDNA Synthesis Kit (Bio-Rad Laboratories, Hercules, CA). cDNA amplification was monitored using SYBRGreen chemistry on the ViiA™ 7 Real-Time PCR System (Applied Biosystems, Foster City, CA). Conditions for PCR reactions were: 40 cycles at 95°C/15 sec and 60°C/1min, using the specific primers listed below:

Gene	Forward (5' to 3')	Reverse (5' to 3')
HPRT1	TGAGGATTTGGAAAGGGTGT	GAGCACACAGAGGGCTACAA
CHD7	CAGAACACCCCGCAGAAAGTGCCTGT	AGCATTCGGTCCACTAACCTGAGTCAT

Immunoblotting

Total cellular extracts were obtained by lysing cells with RIPA buffer (150 mM, NaCl, 1% NP-40, 0.5% SDS, 50 mM Tris pH 8, 2 mM EDTA). Cytoplasmic and nuclear protein lysates were prepared with the NE-PER Nuclear and Cytoplasmic Extraction kit (Thermo Scientific). Proteins (30 µg per lane) were resolved on a 3 to 7% Tris-acetate gel (Life Technologies) and transferred to a nitrocellulose membrane (Life Technologies). After blocking with 0.5% non-fat milk in TBS containing 0.5% Tween 20 (TBST), the membrane was incubated in blocking solution overnight at 4°C with the following primary antibodies:

anti-β-actin (csc-1616, 1/2000) (Santa Cruz Biotechnology, Dallas, TX), anti-CHD7 (ASB453, 1/500) (Millipore, Billerica HQ, MA), anti-LaminB1 (Ab 16048, 1/2000) (Abcam, Cambridge, UK), anti-PARP (556494, 1/2000) (BD Biosciences, Franklin Lakes, NJ). After washing and incubation with HRP-conjugated secondary antibody (1/5000, Sigma Aldrich), the protein bands were detected with enhanced chemoluminescence (ECL, Thermo Scientific).

Statistics

In vitro experiments were performed in both biological and technical replicates. The results are expressed as the mean ± SEM. Unpaired Student's t-test was used for statistical analyses, with Prism 5 (GraphPad Software, La Jolla, CA). P values of <0.05 were considered statistically significant.

Results

Prediction of the CHD7 promoter

The 1.7 Kbp CHD7 gene sequence was analyzed using the NCBI database. To predict the region with promoter activity, we investigated the presence of the following elements: (i) CpG island, sequences which are rich in cytosine and guanine, and can be methylated, thereby inhibiting transcription (Deaton and Bird, 2011); (ii) regions which have been associated to transcription factors and (iii) regions which have previously been described as displaying histone modifications (Figure 24).
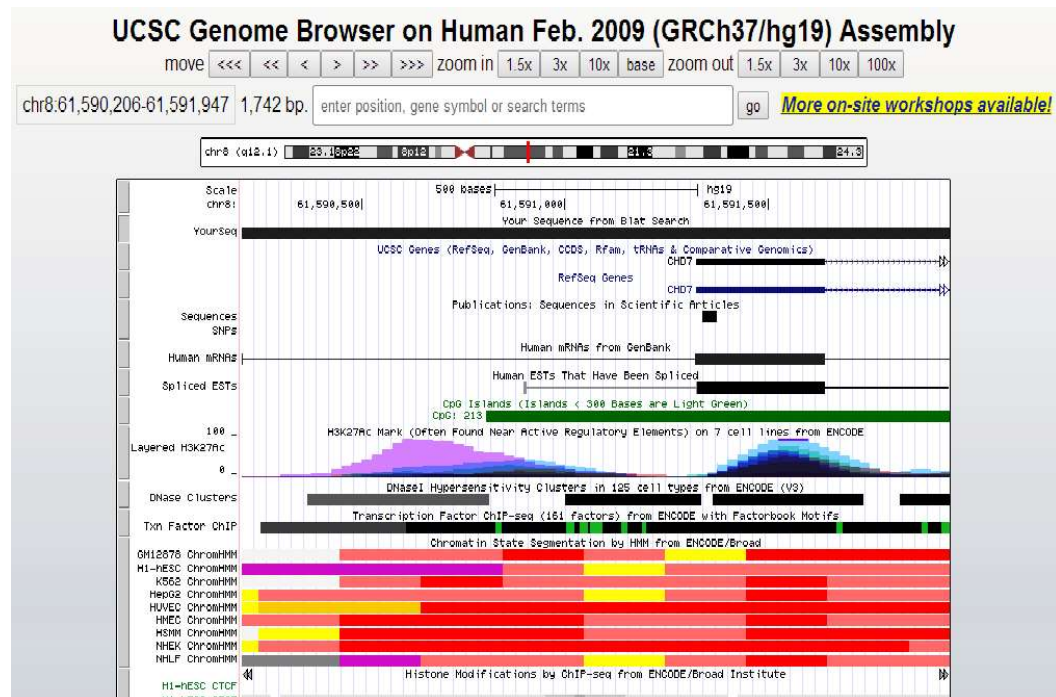
Figure 24: *In silico* analysis of the CHD7 promoter region. Image showing identification of the CHD7 fragment on chromosome 8, which displays transcriptional activity, obtained by BLAT alignment. The black boxes in the upper portion represent the hypothetical promoter region (1,769 bp) indicated as "YourSeq. The bars in the lower portion indicate the reference sequences corresponding to CHD7, ESTs, CpG islands, potential binding regions for transcription factors and histone modifications.

Subcloning the *CHD7* promoter into the pGL3_Basic vector

Based on the Bioinformatics results and on characteristics of the promoter region, we selected a fragment of 1,769 bp as a candidate for the CHD7 core promoter region (Figure 25A). Due to difficulties encountered in amplifying this highly C-G-rich fragment, we ordered the fragment sequence from the GenScript Company. The putative promoter fragment was synthesized and cloned into the pUC57 vector by this Company. We released the insert from the pUC57 plasmid, by double digestion, using the restriction enzymes *MfeI* and *HindIII* (Figure 25).
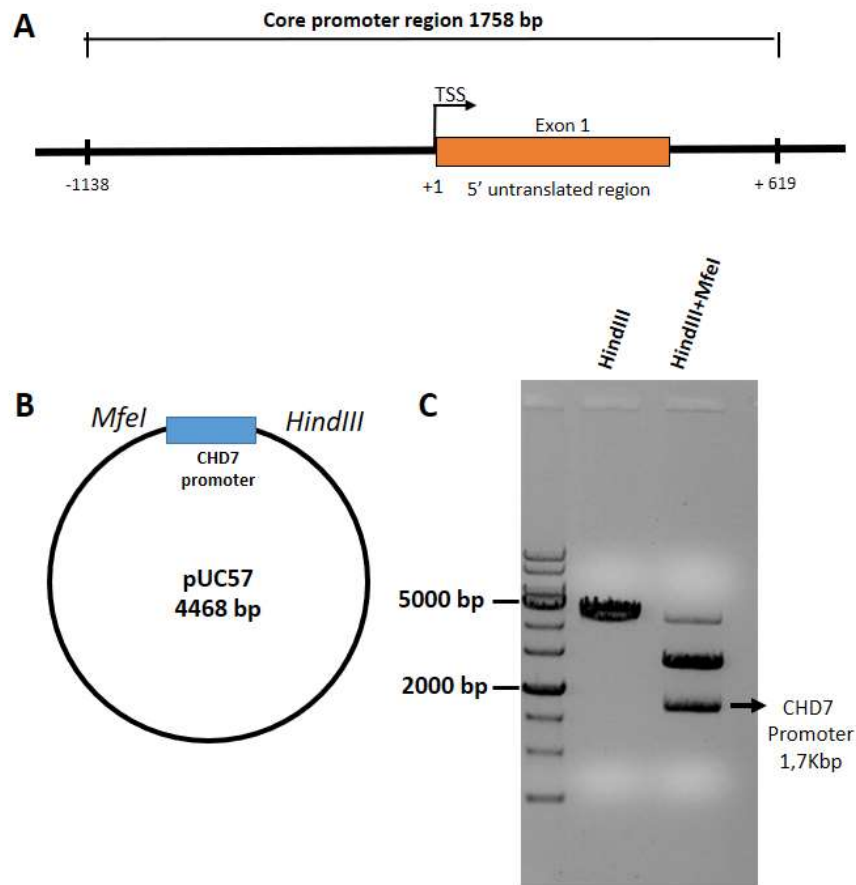
Figure 25: Excision of the 1.7Kbp CHD7 promoter fragment from the pUC57 construct. (A) Schematic illustration of the CHD7 core promoter region (-1149/+619). (B) Scheme of the recombinant pUC57 vector. (C) Agarose gel (0.8%) showing the linearized vector, prepared by HindIII digestion, and the fragment of interest obtained by double digestion with HindIII and MfeI.

After extraction and purification of the CHD7 5' end 1.7Kbp regulatory sequence, we proceeded to a three-fragment ligation in order to construct the recombinant plasmid of the firefly luciferase reporter gene, as detailed in Figure 5. The bacteria clones containing the pGL3_CHD7 promoter construct were screened by *HindIII* digestion and the positive clones were sequenced to confirm the correct insertion (Figure 26).
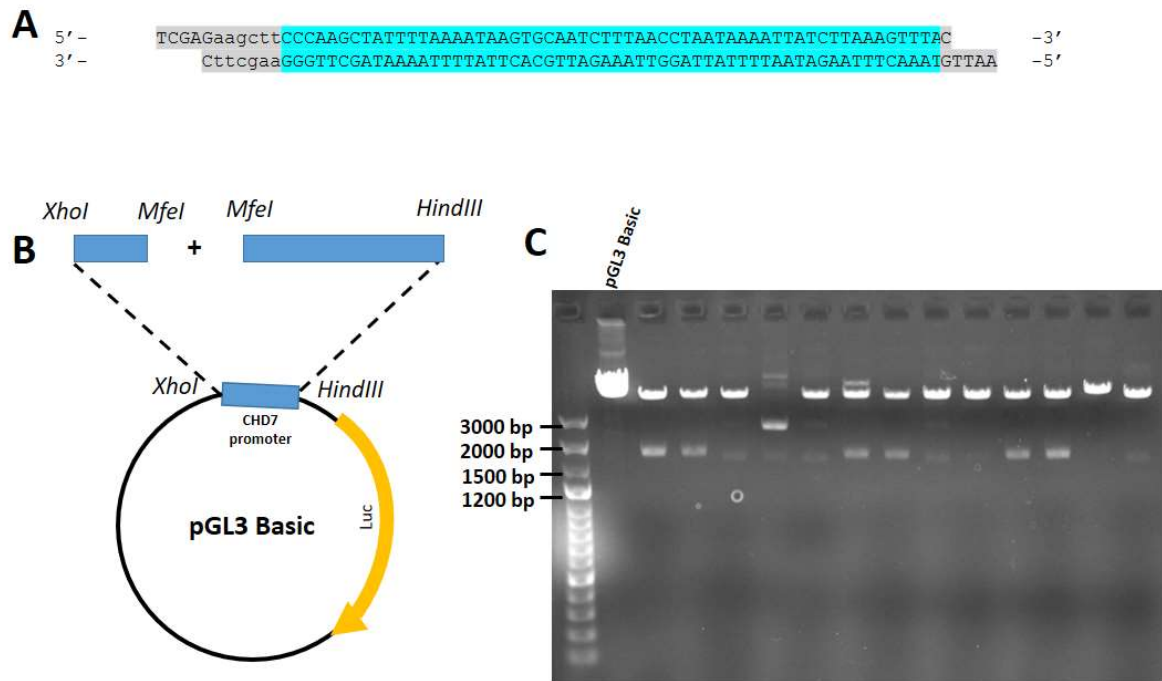
Figure 26: Construction of the pGL3_CHD7 recombinant vector. (A) Annealed primers designed to allow CHD7 fragment ligation into pGL3 Basic vector. (B) Schematic illustration of the recombinant pGL3_CHD7 vector. The pGL3 Basic was linearized by double digestion with the *XhoI* and *HindIII* restriction enzymes. The CHD7 promoter fragment (1,769bp) was introduced into the pGL3 vector by a three-fragment ligation. (C) Screening of the positive bacteria clones was preceded by *HindIII* plasmid digestion. The pGL3 Basic empty vector was used as a negative control. The positive clones show two fragments of 4.8 and 1.7kbp.

The antisense pGL3_CHD7 promoter vector was also constructed to be used as an appropriate control for the luciferase assay. The recombinant plasmid was digested with *HindIII* to extract the promoter fragment. The purified fragment was then inserted into the pGL3 Basic, which had also been linearized with *HindIII*. The correct clone, containing the antisense direction of the promoter sequence, was then screened by *XbaI* digestion and the combination of *XbaI* and *ApaI* digestion. The positive clones were sequenced to confirm the correct insertion of the fragment (Figure 27).
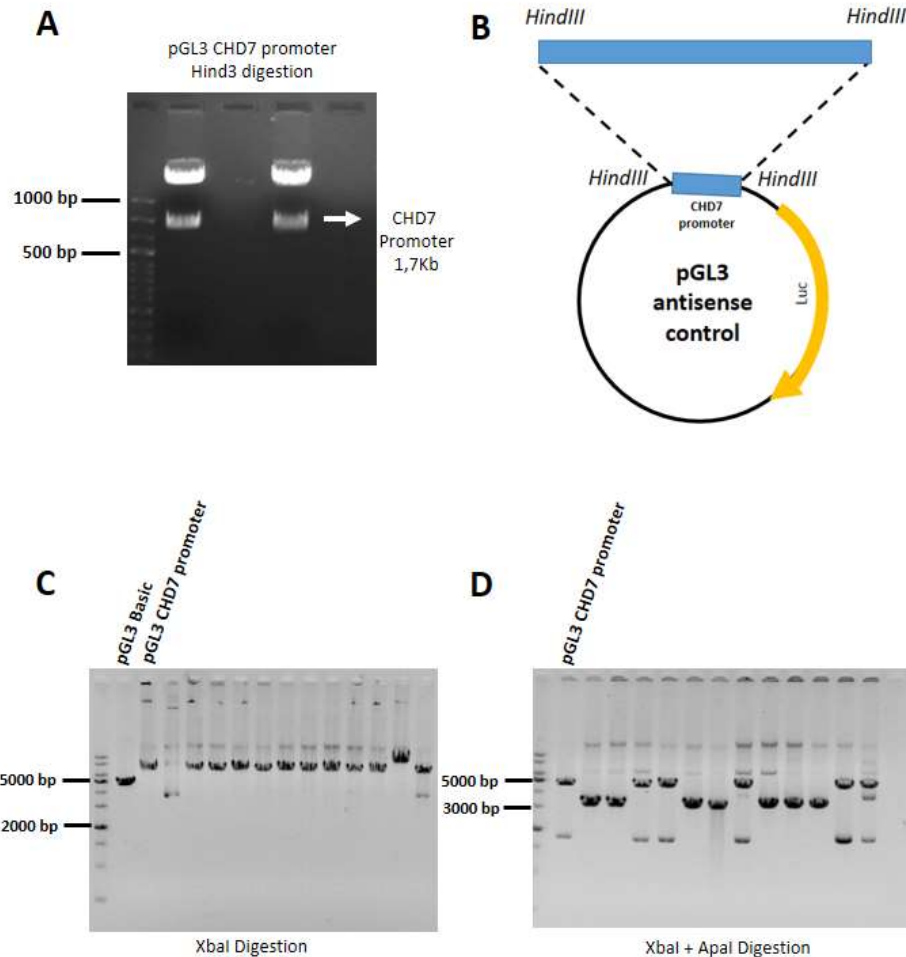
Figure 27: Construction of the antisense control vector. (A) The CHD7 promoter region was obtained by *HindIII* digestion of the recombinant pGL3_CHD7 vector. (B) The fragment (1.7kbp) was fused, in frame, with the luciferase gene, into the promoter-deficit pGL3-Basic vector, which had also been linearized upon *HindIII* restriction enzyme digestion. (C) Positive clones were screened by *XbaI* digestion. The pGL3 Basic was used as a negative control (4.8kbp) and the pGL3_CHD7 was used as a positive control (6.5kbp), confirming ligation of the fragment. (D) Double digestion with *XbaI* and *ApaI* indicates the direction of the fragment. The pGL3_CHD7 was used as a negative control, resulting in two fragments of 4.8kbp and 1.7kbp. Positive clones show only one band, of approximately 3.2kbp, corresponding to the two resulting fragments.

Validation of the *CHD7* promoter region activity

To test the recombinant vectors, we transiently transfected 293T cells and analyzed

luciferase activity using the reporter gene assay. The fragment selected greatly stimulated

luciferase activity, by 15-fold, in 293T cells, when compared to the empty vector.

Importantly, the antisense sequence did not show significant activity, indicating that *CHD7*

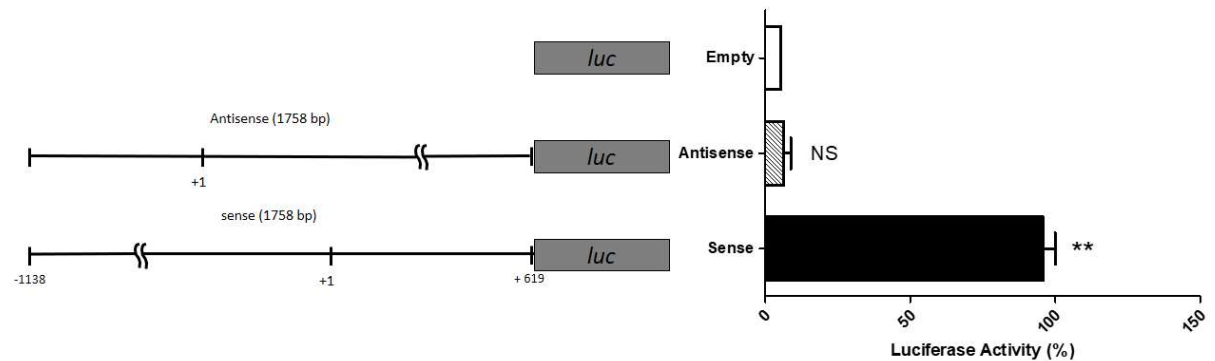expression is regulated by an unidirectional promoter (Figure 28).

Figure 28: CHD7 promoter activity in 293T cells. (A) Schematic representation of the luciferase gene reporter construcs. (B) Luciferase nomalized values obtained in two independent experiments. Each pGL3 vector was co-transfected with the renilla expressing vector (pRL-CMV) in 293T cells. Cell lysates were collected 72h after transfection. T-student test was used to compare the promoter activity displayed by the sense and antisense vectors with respect to that of the empty vector. (NS = not significant, **$P < 0.01$).

Next, we aimed to validate the recombinant vectors using GBM cells. To that end,

we selected two cell lines, namely, LN-229 and LN-428, characterized as displaying high

and low *CHD7* endogenous expression, respectively. As expected, pGL3_CHD7 showed

distinct luciferase activity between these two cell lines, indicating reliable functionality of

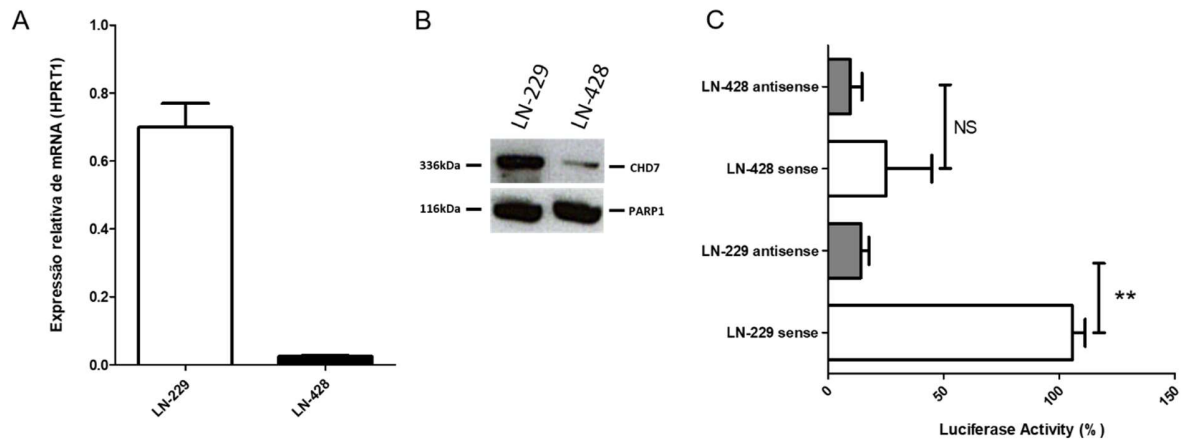the pGL3 system in our model (Figure 29).

Figure 29: Validation of CHD7 promoter activity in the human GBM cell lines LN-229 and LN-428. (A) CHD7 expression level was assessed by qRT-PCR and (B) immunoblot of nuclear extracts. PARP1 was used as the loading control. (C) Luciferase assays. The results are expressed as the mean ± SEM in arbitrary units, based on the firefly luciferase activity, normalized relative to the renilla expressing vector for a single transfection. The data shown are representative of two independent experiments. Cell lysates were collected 48h after transfection. T-student test was used to compare the promoter activity of the sense and antisense vectors. (NS = not significant, **P < 0.01).

EGF stimulation suppresses CHD7 protein expression

To test the possible inhibition of CHD7 promoter activity by EGF, FGF or TGF-β1 signaling, we transiently transfected LN-229 cells with the recombinant pGL3 plasmids, supplemented the culture media with these growth factors (GFs) and assessed luciferase activity 48h after transfection.

In our model, these treatments did promote significant changes in the promoter activity (Figure 30A). To certificate that the luciferase reporter assay matches to CHD7 mRNA transcripts level, we performed qRT-PCR 12h after treatment. Consistently, we found that GFs treatments did not alter significantly mRNA expression levels in LN-229 cells, suggesting that those pathways does not directly modulate gene transcription (Figure 30B).
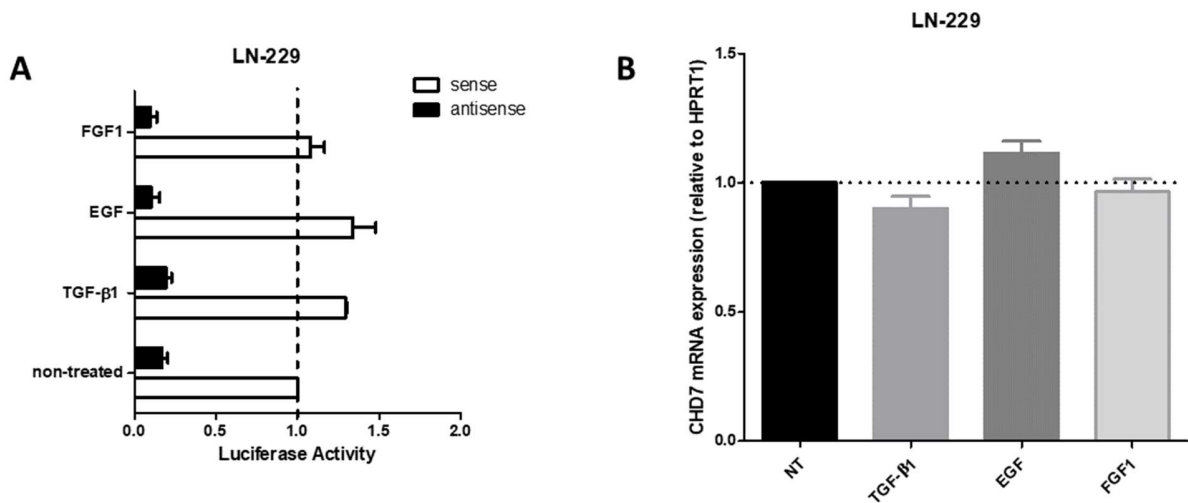
Figure 30: Effect of GFs treatment on CHD7 expression in the LN-229 GBM cell line. (A) Luciferase reporter assay upon medium supplementation with different peptide growth factors (GFs). Cells were transfected with the pGL3_CHD7 promoter plasmid or the antisense vector, as the control. Each pGL3 vector was co-transfected with the pRL-CMV renilla expressing vector. Cell lysates were collected 48h after transfection. (B) CHD7 mRNA levels were assessed by qRT-PCR after 12h in the presence and absence of growth factors supplemented media. All GFs, at the concentration of 10 ng/mL, were added to the complete medium.

Discussion

Our results demonstrate the existence of functional promoter activity in the −1149/+619 region of the *CHD7* gene. Differential promoter activity between the LN-229 and LN-428 cell lines confirmed the presence of regulatory elements within the selected fragment. It will be interesting to determine which binding sites are essential to modulate endogenous *CHD7* expression in these cell lines.

The highly mutated genome of GBM tumors lead to deregulation of many key signaling pathways involved in cell proliferation, survival, and apoptosis (Mao *et al.*, 2013). We have previously shown that increased CHD7 expression is not due to genetic amplification in glioma tissues and, also, that GBM cells overexpressing high CHD7 levels

acquire greater motility and invasive ability (Chapter 1). However, the signaling pathways affecting CHD7 expression in GBM are still unknown.

Epidermal growth factor receptor (EGFR) gene amplification and overexpression are a particularly striking feature of GBM, observed in approximately 40% of tumors (Hatanpaa *et al.*, 2010). Therefore, EGFR-mediated oncogenic signaling is of interest and different EGFR inhibitors have already been tested in clinical trials, with disappointing results so far (Seystahl, Wick and Weller, 2016).

Fibroblast Growth Factors (FGF) has also been implicated in tumor growth (Korc and Friesel, 2009). Studies have shown that FGF can act synergistically with vascular endothelial growth factor (VEGF) to amplify tumor angiogenesis, therefore, targeting both pathways may be more effective in suppressing tumor growth and angiogenesis than targeting either factor alone (Casanovas *et al.*, 2005). Moreover, FGF signaling has also been associated with Epithelial-Mesenchymal Transition (EMT) by promoting Slug expression and decreasing E-cadherin expression (Savagner, Yamada and Thiery, 1997).

TGF-β signaling is deregulated in many different types of cancers and its aberrant signaling has been shown to contribute, at least in part, to initiation and progression of the tumors, including GBM (Han *et al.*, 2015). Importantly, TGF-β is known as a key player in tumor invasion and metastasis (Massagué, 2008).

Using the recombinant vectors generated here, we investigated the effect of treatment with these three GFs on CHD7 promoter activity, with no evidence that the activation of these pathways by GFs treatment directly modulates CHD7 transcript levels in LN-229 cells. It should be noted that the luciferase assay represents an artificial model to monitor promoter activity, which may not necessarily correspond to the *in vivo*

dynamics. Therefore, we proceeded to confirm these results by qRT-PCR, demonstrating that the luciferase assay greatly corresponds to the endogenous mRNA levels. Whether these conditions affect CHD7 protein levels requires further investigation.

Fujita and collaborators (Fujita *et al.*, 2014) showed that BMP/Wnt signaling induced CHD7 expression, maintaining the multipotency of mouse neural crest cells. Additionally, CHD7 was shown to be a downstream effector of macrophage migration inhibitory factor (MIF) in murine neural stem/progenitor cells, playing an important role in modulating cell proliferation (Ohta *et al.*, 2016). The effect of these two pathways in our cellular model is currently under investigation.

Conclusions

Although further studies, using other GBM cell lines and different conditions, are warranted to elucidate the mechanisms modulating CHD7 expression during tumor development and cancer cell metastasis. Cloning of the 1.7Kbp promoter region of the CHD7 gene, achieved here, constitutes a very powerful tool which should greatly contribute to a better understanding of the molecular mechanisms underlying the role of CHD7 chromatin remodeler protein and provide valuable insights into the cellular pathways and gene networks associated with different cancer types, particularly GBM.

3. GENERAL CONCLUSIONS

The involvement of CHD7 in development and disease has just begun to be elucidated. In the non-pathological brain, CHD7 was shown to be essential for NSC function and it has previously been implicated in cancer. However, the precise mechanisms by which CHD7 regulates stem cells proliferation, quiescence, fate and differentiation or which binding partners and genomic targets it associates with and whether these mechanisms vary between developmental and postnatal stages, remain to be determined (Micucci et al. 2015). Cooperative, detailed studies using high-throughput approaches and different model organisms will be necessary in order to address these questions.

Here, we show that CHD7 is relevant to GBM pathogenesis by modulating cell adhesion–related genes. This finding may indirectly explain how CHD7 promotes migration and invasion of GBM cells, regulating cytoskeleton rearrangement and focal adhesion dynamics. Nevertheless, the mechanism underlying these biological functions still requires further studies.

CHD7 was shown to regulate crucial transcription factors allowing for acquisition of migratory potential in Xenopus neural crest cells (Bajpai *et al.*, 2010). A recent study also found that CHD7 mutations lead to defective cell migration using iPS-derived neural crest cells from CHARGE patients (Okuno *et al.*, 2017). Interestingly, *CHD7* duplications have been suggested to be a driver mutation identified in small-cell lung cancer, one of the most highly metastatic and aggressive types of cancer (Pleasance *et al.*, 2010). One could argue that each cell type in a given tissue might have unique CHD7 binding sites and protein complexes, which vary over time (Martin, 2010). These data and our results

suggest that it is likely that common factors, targets, and molecular pathways are modulated by CHD7 to promote cell motility and invasiveness in different types of cells. It will be of great interest to know, for example, what are the mechanisms regulating CHD7 expression in tumor cells and whether those pathways may be manipulated by molecular intervention.

Stratification of patients according to prognostic markers may improve future therapeutic strategies to treat recurrent GBM (Seystahl, Wick and Weller, 2016). Appropriate combination of novel targeted and immunotherapeutic approaches will hopefully lead to more durable responses in GBM patients (Szopa *et al.*, 2017). Targeting CHD7 activity could be useful for inhibiting cancer cells migration, however a number of issues still need to be addressed. For example, does CHD7 regulate other signaling pathways which are associated with tumorigenesis? How consistent is this overexpression phenotype between GBM cells from different genetic backgrounds? Or between different tumor types? How can CHD7 be targeted for clinical cancer treatment? The findings described in the present work may not only lead to a new understanding of CHD7's role in CHARGE syndrome, but, also, suggests that CHD7 may be involved in the migration and invasion potential of tumor cells. With the development of new research and technologies to study epigenetics and remodeler proteins, the relationship between CHD7 and tumor metastasis may be uncovered.

4. REFERENCES

Badodi, S. et al. (2017) 'Convergence of BMI1 and CHD7 on ERK Signaling in Medulloblastoma', Cell Reports. ElsevierCompany., 21(10), pp. 2772–2784. doi: 10.1016/j.celrep.2017.11.021.

Bajpai, R. et al. (2010) 'LETTERS CHD7 cooperates with PBAF to control multipotent neural crest formation', Nature. doi: 10.1038/nature08733.

Basson, M. A. and van Ravenswaaij-Arts, C. (2015) 'Functional Insights into Chromatin Remodelling from Studies on CHARGE Syndrome', Trends in Genetics. Elsevier Ltd, 31(10), pp. 600–611. doi: 10.1016/j.tig.2015.05.009.

Batsukh, T. et al. (2010) 'CHD8 interacts with CHD7, a protein which is mutated in CHARGE syndrome', Human Molecular Genetics, 19(14), pp. 2858–2866. doi: 10.1093/hmg/ddq189.

Batsukh, T. et al. (2012) 'Identification and Characterization of FAM124B as a Novel Component of a CHD7 and CHD8 Containing Complex', PLoS ONE, 7(12), pp. 1–12. doi: 10.1371/journal.pone.0052640.

Bhat, K. P. L. et al. (2013) 'Mesenchymal Differentiation Mediated by NF-κB Promotes Radiation Resistance in Glioblastoma', Cancer Cell. Elsevier Inc., 24(3), pp. 331–346. doi: 10.1016/j.ccr.2013.08.001.

Blake, K. et al. (2011) 'Clinical utility gene card for: CHARGE syndrome', European Journal of Human Genetics. Nature Publishing Group, 19(9), p. 1016. doi: 10.1038/ejhg.2011.45.

Bosman, E. A. et al. (2005) 'Multiple mutations in mouse Chd7 provide models for CHARGE syndrome', Human Molecular Genetics, 14(22), pp. 3463–3476. doi: 10.1093/hmg/ddi375.

Bouazoune, K. et al. (2002) 'The dMi-2 chromodomains are DNA binding modules important for ATP-dependent nucleosome mobilization', EMBO Journal, 21(10), pp. 2430–2440. doi: 10.1093/emboj/21.10.2430.

Boyer, L. A., Latek, R. R. and Peterson, C. L. (2004) 'The SANT domain: A unique histone-tail-binding module?', Nature Reviews Molecular Cell Biology, 5(2), pp. 158–163. doi: 10.1038/nrm1314.

Brescia, P. et al. (2013) 'CD133 Is Essential for Glioblastoma Stem Cell Maintenance', pp. 857–869. doi: 10.1002/stem.1317.

Casanovas, O. et al. (2005) 'Drug resistance by evasion of antiangiogenic targeting of VEGF signaling in late-stage pancreatic islet tumors', 8(October), pp. 299–309. doi: 10.1016/j.ccr.2005.09.005.

Chu, X. et al. (2017) 'Genotranscriptomic meta-analysis of the CHD family chromatin remodelers in human cancers – initial evidence of an oncogenic role for CHD7', Molecular Oncology, 11(10), pp. 1348–1360. doi: 10.1002/1878-0261.12104.

Colbert, L. E. et al. (2014) 'CHD7 Expression Predicts Survival Outcomes in Patients with Resected Pancreatic Cancer', Cancer Research, 74(10), pp. 2677–2687. doi: 10.1158/0008-5472.CAN-13-1996.

Colin, C. et al. (2010) 'Cloning and characterization of a novel alternatively spliced transcript of the human CHD7 putative helicase', BMC Research Notes. BioMed Central Ltd, 3(1), p. 252. doi: 10.1186/1756-0500-3-252.

Daubresse, G. et al. (1999) 'The Drosophila kismet gene is related to chromatin-remodeling factors and is required for both segmentation and segment identity.', Development (Cambridge, England), 126(6), pp. 1175–1187.

Deaton, A. and Bird, A. (2011) 'CpG islands and the regulation of transcription', Genes & development, 25(10), pp. 1010–1022. doi: 10.1101/gad.2037511.1010.

Engelen, E. et al. (2011) 'Sox2 cooperates with Chd7 to regulate genes that are mutated in human syndromes', Nature Publishing Group, 43(6). doi: 10.1038/ng.825.

Feng, W. et al. (2013) 'The chromatin remodeler CHD7 regulates adult neurogenesis via activation of soxc transcription factors', Cell Stem Cell. doi: 10.1016/j.stem.2013.05.002.

Feng, W. et al. (2017) 'Chd7 is indispensable for mammalian brain development through activation of a neuronal differentiation programme', Nature Communications, 8. doi: 10.1038/ncomms14758.

Flanagan, J. F. et al. (2005) 'Double chromodomains cooperate to recognize the methylated histone H3 tail', Nature, 438(7071), pp. 1181–1185. doi: 10.1038/nature04290.

Fujita, K. et al. (2014) 'Roles of chromatin remodelers in maintenance mechanisms of multipotency of mouse trunk neural crest cells in the formation of neural crest-derived stem cells', MECHANISMS OF DEVELOPMENT. Elsevier Ireland Ltd, (May). doi: 10.1016/j.mod.2014.05.001.

Gusyatiner, O. and Hegi, M. E. (2017) 'Monika Hegi 2017 review Gliomas epigenetics.pdf'.

Hall, J. A. and Georgel, P. T. (2007) 'CHD proteins: a diverse family with strong ties', Biochemistry and Cell Biology, 85(4), pp. 497–508. doi: 10.1139/O07-072.

Han, J. et al. (2015) 'TGF-β signaling and its targeting for glioma treatment', 5(3), pp. 945–955.

Hatanpaa, K. J. et al. (2010) 'Epidermal Growth Factor Receptor in Glioma: Signal Transduction, Neuropathology, Imaging, and Radioresistance', Neoplasia, 12(9), pp. 675–684. doi: 10.1593/neo.10688.

He, D. et al. (2016) 'Chd7 cooperates with Sox10 and regulates the onset of CNS myelination and remyelination', Nature Neuroscience. Nature Publishing Group, 19(5), pp. 678–689. doi: 10.1038/nn.4258.

Hegi, M. E. et al. (2005) 'MGMT Gene Silencing and Benefit from Temozolomide in Glioblastoma', New England Journal of Medicine, 352(10), pp. 997–1003. doi: 10.1056/NEJMoa043331.

Heintzman, N. D. et al. (2007) 'Distinct and predictive chromatin signatures of transcriptional promoters and enhancers in the human genome.', Nature genetics, 39(3), pp. 311–8. doi: 10.1038/ng1966.

Hitoshi, N., Ken-ichi, Y. and Jun-ichi, M. (1991) 'Efficient selection for high-expression transfectants with a novel eukaryotic vector', Gene, 108(2), pp. 193–199. doi: 10.1016/0378-1119(91)90434-D.

Ho, L. and Crabtree, G. R. (2010) 'Chromatin remodelling during development.', Nature, 463(7280), pp. 474–84. doi: 10.1038/nature08911.

Hurd, E. A. et al. (2007) 'Loss of Chd7 function in gene-trapped reporter mice is embryonic lethal and associated with severe defects in multiple developing tissues', Mammalian Genome, 18(2), pp. 94–104. doi: 10.1007/s00335-006-0107-6.

Huse, J. T., Holland, E. and Deangelis, L. M. (2013) 'ME64CH05-DeAngelis Glioblastoma: Molecular Analysis and Clinical Implications', Annu. Rev. Med, 64, pp. 59–70. doi: 10.1146/annurev-med-100711-143028.

Inda, M. del M., Bonavia, R. and Seoane, J. (2014) 'Glioblastoma multiforme:A look inside its heterogeneous nature', Cancers, 6(1), pp. 226–239. doi: 10.3390/cancers6010226.

Jones, K. M. et al. (2015) 'CHD7 maintains neural stem cell quiescence and prevents premature stem cell depletion in the adult hippocampus', Stem Cells. doi: 10.1002/stem.1822.

Jongmans, M. C. J. et al. (2009) 'CHD7 mutations in patients initially diagnosed with Kallmann syndrome - The clinical overlap with CHARGE syndrome', Clinical Genetics, 75(1), pp. 65–71. doi: 10.1111/j.1399-0004.2008.01107.x.

Kim, H. G. et al. (2008) 'Mutations in CHD7, Encoding a Chromatin-Remodeling Protein, Cause Idiopathic Hypogonadotropic Hypogonadism and Kallmann Syndrome', American Journal of Human Genetics, 83(4), pp. 511–519. doi: 10.1016/j.ajhg.2008.09.005.

Kim, M. S. et al. (2011) 'Genetic and expressional alterations of CHD genes in gastric and colorectal cancers', Histopathology, 58(5), pp. 660–668. doi: 10.1111/j.1365-2559.2011.03819.x.

Kita, Y., Nishiyama, M. and Nakayama, K. I. (2012) 'Identification of CHD7 S as a novel splicing variant of CHD7 with functions similar and antagonistic to those of the full-length CHD7 L', Genes to Cells, 17(7), pp. 536–547. doi: 10.1111/j.1365-2443.2012.01606.x.

Korc, M. and Friesel, R. E. (2009) 'The role of fibroblast growth factors in tumor growth.', Current cancer drug targets, 9(5), pp. 639–51. doi: 10.2174/156800909789057006.

Layman, W. S. et al. (2009) 'Defects in neural stem cell proliferation and olfaction in Chd7 deficient mice indicate a mechanism for hyposmia in human CHARGE syndrome', Human Molecular Genetics, 18(11), pp. 1909–1923. doi: 10.1093/hmg/ddp112.

Layman, W. S., Hurd, E. A. and Martin, D. M. (2010) 'Chromodomain Proteins in Development: Lessons from CHARGE Syndrome', Clinical Genetics, 78(1), pp. 11–20. doi: 10.1111/j.1399-0004.2010.01446.x.Chromodomain.

Li, B., Carey, M. and Workman, J. L. (2007) 'The Role of Chromatin during Transcription', Cell, 128(4), pp. 707–719. doi: 10.1016/j.cell.2007.01.015.

Liao, Y., Smyth, G. K. and Shi, W. (2013) 'The Subread aligner: Fast, accurate and scalable read mapping by seed-and-vote', Nucleic Acids Research, 41(10). doi: 10.1093/nar/gkt214.

Louis, D. N. et al. (2007) 'The 2007 WHO classification of tumours of the central nervous system', Acta Neuropathologica. doi: 10.1007/s00401-007-0243-4.

Louis, D. N. et al. (2016) 'The 2016 World Health Organization Classification of Tumors of the Central Nervous System: a summary', Acta Neuropathologica. Springer Berlin Heidelberg, 131(6), pp. 803–820. doi: 10.1007/s00401-016-1545-1.

Mao, H. et al. (2013) 'Deregulated Signaling Pathways in Glioblastoma Multiforme: Molecular Mechanisms and Therapeutic Targets', Cancer investigation, 30(1), pp. 48–56. doi: 10.3109/07357907.2011.630050.Deregulated.

Marfella, C. G. A. and Imbalzano, A. N. (2007) 'NIH Public Access', 27(4), pp. 339–351. doi: 10.1016/j.neuron.2009.10.017.A.

Martin, D. M. (2010) 'Chromatin remodeling in development and disease: Focus on CHD7', PLoS Genetics, 6(7), pp. 1–4. doi: 10.1371/journal.pgen.1001010.

Massagué, J. (2008) 'Review TGF β in Cancer', (Figure 1), pp. 215–230. doi: 10.1016/j.cell.2008.07.001.

Micucci, J. A. et al. (2014) 'CHD7 and retinoic acid signaling cooperate to regulate neural stem cell and inner ear development in mouse models of CHARGE syndrome', Human Molecular Genetics, 23(2), pp. 434–448. doi: 10.1093/hmg/ddt435.

Noushmehr, H. et al. (2011) 'NIH Public Access', 17(5), pp. 510–522. doi: 10.1016/j.ccr.2010.03.017.Identification.

Oba-Shinjo, S. M. et al. (2005) 'Identification of novel differentially expressed genes in human astrocytomas by cDNA representational difference analysis', Molecular Brain Research, 140(1–2), pp. 25–33. doi: 10.1016/j.molbrainres.2005.06.015.

Ohta, S. et al. (2016) 'CHD7 promotes proliferation of neural stem cells mediated by MIF', Molecular Brain. Molecular Brain, pp. 1–12. doi: 10.1186/s13041-016-0275-6.

Okuno, H. et al. (2017) 'CHARGE syndrome modeling using patient-iPSCs reveals defective migration of neural crest cells harboring CHD7 mutations', eLife, 28, pp. 1–26. doi: doi: 10.7554/eLife.21114.

Ostrom, Q. T. et al. (2017) 'CBTRUS Statistical Report: Primary brain and other central nervous system tumors diagnosed in the United States in 2010–2014', Neuro-Oncology, 19(suppl_5), pp. v1–v88. doi: 10.1093/neuonc/nox158.

Patten, S. A. et al. (2012) 'Role of Chd7 in zebrafish: A model for CHARGE syndrome', PLoS ONE, 7(2). doi: 10.1371/journal.pone.0031650.

Pleasance, E. D. et al. (2010) 'A small-cell lung cancer genome with complex signatures of tobacco exposure', Nature, 463(7278), pp. 184–190. doi: 10.1038/nature08629.

Ran, F. A. et al. (2013) 'Genome engineering using the CRISPR-Cas9 system.', Nature protocols, 8(11), pp. 2281–308. doi: 10.1038/nprot.2013.143.

Reifenberger, G. et al. (2016) 'Advances in the molecular genetics of gliomas — implications for classification and therapy', Nature Reviews Clinical Oncology. Nature Publishing Group, 14(7), pp. 434–452. doi: 10.1038/nrclinonc.2016.204.

Robinson, M. D., McCarthy, D. J. and Smyth, G. K. (2009) 'edgeR: A Bioconductor package for differential expression analysis of digital gene expression data', Bioinformatics, 26(1), pp. 139–140. doi: 10.1093/bioinformatics/btp616.

Sandmann, T. et al. (2015) 'Patients with proneural glioblastoma may derive overall survival benefit from the addition of bevacizumab to first-line radiotherapy and temozolomide: Retrospective analysis of the AVAglio trial', Journal of Clinical Oncology, 33(25), pp. 2735–2744. doi: 10.1200/JCO.2015.61.5005.

Savagner, P., Yamada, K. M. and Thiery, J. P. (1997) 'The Zinc-Finger Protein Slug Causes DesmosomeDissociation, an Initial and Necessary Step forGrowth Factor–induced Epithelial–Mesenchymal Transition', 137(6), pp. 1–17. doi: 10.1083/jcb.137.6.1403.

Scanlan, M. J. et al. (2002) 'Cancer-related serological recognition of human colon cancer: identification of potential diagnostic and immunotherapeutic targets.', Cancer research, 62(14), pp. 4041–7. Available at: http://www.ncbi.nlm.nih.gov/pubmed/12124339.

Schneider, R. et al. (2004) 'Histone H3 lysine 4 methylation patterns in higher eukaryotic genes', Nature Cell Biology, 6(1), pp. 73–77. doi: 10.1038/ncb1076.

Schnetz, M. P. et al. (2009) 'Genomic distribution of CHD7 on chromatin tracks H3K4 methylation patterns', Genome Research. doi: 10.1101/gr.086983.108.

Schnetz, M. P. et al. (2010) 'CHD7 targets active gene enhancer elements to modulate ES cell-specific gene expression', PLoS Genetics. doi: 10.1371/journal.pgen.1001023.

Schulz, Y. et al. (2014) 'CHD7, the gene mutated in CHARGE syndrome, regulates genes involved in neural crest cell guidance', Human Genetics, 133(8), pp. 997–1009. doi: 10.1007/s00439-014-1444-2.

Seystahl, K., Wick, W. and Weller, M. (2016) 'Therapeutic options in recurrent glioblastoma-An update', Critical Reviews in Oncology/Hematology. Elsevier Ireland Ltd, 99, pp. 389–408. doi: 10.1016/j.critrevonc.2016.01.018.

Soeda, A. et al. (2015) 'The evidence of glioblastoma heterogeneity', Scientific Reports, 5, p. 7979. doi: 10.1038/srep07979.

Srinivasan, S., Dorighi, K. M. and Tamkun, J. W. (2008) 'Drosophila Kismet regulates histone H3 lysine 27 methylation and early elongation by RNA polymerase II', PLoS Genetics, 4(10). doi: 10.1371/journal.pgen.1000217.

Szopa, W. et al. (2017) 'Diagnostic and Therapeutic Biomarkers in Glioblastoma : Current Status and Future Perspectives'. Hindawi Publishing Corporation, 2017. doi: 10.1155/2017/8013575.

Tabatabai, G. et al. (2007) 'Synergistic antiglioma activity of radiotherapy and enzastaurin', Annals of Neurology, 61(2), pp. 153–161. doi: 10.1002/ana.21057.

Tabatabai, G. and Weller, M. (2011) 'Glioblastoma stem cells', Cell and Tissue Research. doi: 10.1007/s00441-010-1123-0.

Tahara, T. et al. (2014) 'Colorectal carcinomas with CpG island methylator phenotype 1 frequently contain mutations in chromatin regulators', Gastroenterology. Elsevier Ltd, 146(2). doi: 10.1053/j.gastro.2013.10.060.

Takada, I. et al. (2007) 'A histone lysine methyltransferase activated by non-canonical Wnt signalling suppresses PPAR-γ transactivation', Nature Cell Biology, 9(11), pp. 1273–1285. doi: 10.1038/ncb1647.

Tavares, S. et al. (2017) 'Actin stress fiber organization promotes cell stiffening and proliferation of pre-invasive breast cancer cells', Nature Communications, 8(May). doi: 10.1038/ncomms15237.

Thon, N., Kreth, S. and Kreth, F.-W. (2013) 'Personalized treatment strategies in glioblastoma: MGMT promoter methylation status.', OncoTargets and therapy, 6, pp. 1363–72. doi: 10.2147/OTT.S50208.

Trombetta-Lima, M. et al. (2015) 'Isolation and characterization of novel RECK tumor suppressor gene splice variants', Oncotarget, 6(32). doi: 10.18632/oncotarget.5305.

Verhaak, R. G. W. et al. (2010) 'Integrated Genomic Analysis Identifies Clinically Relevant Subtypes of Glioblastoma Characterized by Abnormalities in PDGFRA, IDH1, EGFR, and NF1', Cancer Cell. doi: 10.1016/j.ccr.2009.12.020.

Vignali, M. et al. (2000) 'ATP-Dependent Chromatin-Remodeling Complexes', Molecular and Cellular Biology , 20(6), pp. 1899–1910. doi: 10.1128/MCB.20.6.1899-1910.2000.

Vissers L M, L. E. et al. (2004) 'Mutations in a new member of the chromodomain gene family cause CHARGE syndrome'. doi: 10.1038/ng1407.

Weiler, M. et al. (2013) 'mTOR target NDRG1 confers MGMT-dependent resistance to alkylating chemotherapy', Proceedings of the National Academy of Sciences, 111(1), pp. 409–414. doi: 10.1073/pnas.1314469111.

Weller, M. et al. (2014) 'EANO guideline for the diagnosis and treatment of anaplastic gliomas and glioblastoma', The Lancet Oncology, 15(9), pp. 395–403. doi: 10.1016/S1470-2045(14)70011-7.

Weller, M. et al. (2015) 'Glioma', Nature Reviews Disease Primers, (July), p. 15017. doi: 10.1038/nrdp.2015.17.

Wincent, J. et al. (2008) 'CHD7 mutation spectrum in 28 Swedish patients diagnosed with CHARGE syndrome', Clinical Genetics, 74(1), pp. 31–38. doi: 10.1111/j.1399-0004.2008.01014.x.

Yan, H., Parsons, W. and Jin, G. (2009) 'Mutations in Gliomas', The New England Journal of Medicine, 360(8), pp. 765–773. doi: 10.1007/s00428-009-0805-z.

Yaniv, M. (2014) 'Chromatin remodeling: From transcription to cancer', Cancer Genetics. doi: 10.1016/j.cancergen.2014.03.006.

Yu, T. et al. (2013) 'Deregulated FGF and homeotic gene expression underlies cerebellar vermis hypoplasia in CHARGE syndrome', eLife, 2013(2), pp. 1–15. doi: 10.7554/eLife.01305.

CURRICULUM VITAE

Name: Raquel Arminda Carvalho Machado

Place and birth date: Viçosa, 23/03/1987

Education

since 08/2013   **USP – University of São Paulo, Brazil**

PhD student – Major: Biochemistry

Period abroad: 02/2015 – 11/2015

UZH – University of Zurich, Switzerland

Laboratory of Neurooncology – University Hospital Zurich

Supervisor: Prof. Dr. Michael Weller

02/2011-12/2012   **ETH Zurich, Department of Biology, Switzerland**

Master of Science – Major: Cell Biology

03/2005-07/2010   **UFV – Federal University of Viçosa (MG), Brazil**

Combined degree graduation: Lic. and B.Sc. Biological Sciences

Work Experience and Supplementary Training

Since 08/2013   **PhD Student at the University of São Paulo, Brazil**

Department of Biochemistry

Molecular and Cell Therapy Center (NUCEL)

Supervisor: Prof. Dr. Mari Cleide Sogayar

PhD Project: Role of the CHD7 chromatin remodeler protein in human brain tumor cells.

08/2011-06/2013   **Master Student at ETH Zurich, Switzerland**

Department of Cell Biology

Supervisor: Sebastian Jessberger

Master Thesis Project – "Reprogramming adult hippocampal neural stem/progenitor cells and their potential remyelination capacity"

01/2010-05/2010   **Internship as Student Researcher, Germany**

Leibniz-Institut für Naturstoff-Forschung und Infektionsbiologie e.V. Hans-Knöll-Institut Jena

Project – "Regulation of *Aspergillus fumigatus* secondary metabolism genes"

10/2008-12/2008   **Student Researcher, IAESTE Internship Program, DAAD Scholarship**

Landwirtschaftliches Technologiezentrum Augustenberg, Germany

Theory and practice in the areas of seed testing with special respect to variety with electrophoresis

08/2007-07/2008   **Student Researcher, Federal University of Viçosa, Brazil**

Department of General Biology

Institutional Program for Scientific Initiation Scholarships (PIBIC/CNPq)

Project – "Morphological and ultrastructural study of the reproductive female system of the lizard *Hemidactylus mabouia*"

List of publications

Schneider H, Szabo E, **Machado RA**, Broggini-Tenzer A, Walter A, Lobell M, Heldmann D, Süssmeier F, Grünewald S, Weller M. Novel TIE-2 Inhibitor BAY-826 Displays In Vivo Efficacy in Experimental Syngeneic Murine Glioma Models. *Journal of Neurochemistry*. 140:170-182 (2016).

Braun SMG, Pilz GA, **Machado RAC**, Moss J, Becher B, Toni N & Jessberger S. Directed differentiation of hippocampal neural stem/progenitor cells into oligodendrocytes enhances remyelination in the adult brain after injury. *Cell Reports*. 11, 1679-85 (2015).

Simon M.G. Braun, **Raquel A.C. Machado** & Sebastian Jessberger. Temporal control of virus-mediated transgene expression in newborn cells in the adult brain. *Stem Cell Reports*. 1, 114–122 (2014).

Marlen Knobloch, Simon M.G. Braun, Luis Zurkirchen, Carolin von Schoultz, Nicola Zamboni, Marcos J. Araùzo-Bravo, Werner J. Kovacs, Özlem Karalay, Ueli Suter**, Raquel A.C. Machado**, Marta Roccio, Matthias P. Lutolf, Clay F. Semenkovich & Sebastian Jessberger. Metabolic control of adult neural stem/progenitor cell activity by FASNdependent Lipogenesis. *Nature*. 493, 226–230 (2013).

Additional Activities

07/2016-08/2017   Tutor of undergraduate students:

Thiago Marchini: *Deletion of an intergenic lncRNA by CRISPR/Cas9 editing system and its application in functional genomics research.*

Bárbara Rodrigues: *Molecular Cloning of the CHD7 Chromatin Remodeling Promoter Region.*

Bruno Oliveira: *Role of CHD7 on chondrocyte differentiation of human mesenchymal stem cells.*

08/2014-12/2014   Lab Teaching Assistant, University of São Paulo, Brazil

Assistant student in "Metabolism and Molecular Biology"

02/2011-05/2011   Lab Teaching Assistant, ETH Zürich, Switzerland

Assistant student in "Grundlagen der Biologie I" Biochemistry

PCR experiment: Taq DNA Polymerase activity assay

08/2006-12/2009   Department of General Biology, UFV

CNPq Scholarship - Tutor in Cytology, Histology and Embryology

Languages

Portuguese (native speaker) - English (advanced) - German (good)